HDL-CR-82-158-1

April 1983

Integrated Component Fluidic Servovalves and Position Control Systems

by D. N. Wormley and K-M. Lee

Prepared by

Massachusetts Institute of Technology
Department of Mechanical Engineering
Cambridge, MA 02139

Under contract

DAAK21-79-C-0158

U.S. Army Electronics Research and Development Command
Harry Diamond Laboratories
Adelphi, MD 20783

UNCLASSIFIED

SECURITY CLASSIFICATION OF THIS PAGE (When Data Entered)

REPORT DOCUMENTATION PAGE		READ INSTRUCTIONS BEFORE COMPLETING FORM
1. REPORT NUMBER HDL-CR-82-158-1	2. GOVT ACCESSION NO. AD-A127362	3. RECIPIENT'S CATALOG NUMBER
4. TITLE (and Subtitle) Integrated Component Fluidic Servovalves and Position Control Systems		5. TYPE OF REPORT & PERIOD COVERED Contractor Report Final 1979-1982 6. PERFORMING ORG. REPORT NUMBER
7. AUTHOR(s) D. N. Wormley K-M Lee (HDL Contact: James Joyce)		8. CONTRACT OR GRANT NUMBER(s) DAAK21-79-C-0158
9. PERFORMING ORGANIZATION NAME AND ADDRESS Massachusetts Institute of Technology Department of Mechanical Engineering Cambridge, MA 02139		10. PROGRAM ELEMENT, PROJECT, TASK AREA & WORK UNIT NUMBERS Program Ele: 6.11.02.A HDL Project: A44934
11. CONTROLLING OFFICE NAME AND ADDRESS Harry Diamond Laboratories 2800 Powder Mill Road Adelphi, MD 20783		12. REPORT DATE April 1983 13. NUMBER OF PAGES 84
14. MONITORING AGENCY NAME & ADDRESS(if different from Controlling Office)		15. SECURITY CLASS. (of this report) UNCLASSIFIED 15a. DECLASSIFICATION/DOWNGRADING SCHEDULE

16. DISTRIBUTION STATEMENT (of this Report)

Approved for public release; distribution unlimited.

17. DISTRIBUTION STATEMENT (of the abstract entered in Block 20, if different from Report)

18. SUPPLEMENTARY NOTES

DRCMS Code: 611102.H.440011
DA Project: 1L161102AH44

19. KEY WORDS (Continue on reverse side if necessary and identify by block number)

Servovalve
Laminar proportional amplifier
Fluidic gain block
Position control system

20. ABSTRACT (Continue on reverse side if necessary and identify by block number)

The operating characteristics of fluidic laminar proportional amplifiers (LPA's) operating on hydraulic oil have been determined as a function of pressure and temperature. The useful operating range of these elements has been defined for application in multistage gain blocks and summing amplifiers.

An operational servovalve constructed from LPA's has been developed and coupled with a fluidic position feedback transducer, summing amplifier and ram to construct a closed loop posi-

DD FORM 1 JAN 73 1473 EDITION OF 1 NOV 65 IS OBSOLETE 1

UNCLASSIFIED

SECURITY CLASSIFICATION OF THIS PAGE (When Data Entered)

20. Abstract (Cont'd)

tion control system. Static and dynamic experimental evaluation of the servosystem has shown that its performance is comparable to that of a servo employing electrohydraulic components.

This development effort has demonstrated the capability to develop high performance, closed loop servo components from standard, integrated component fluidic elements.

CONTENTS

FIGURES

TABLES

1. INTRODUCTION

Hydraulic control systems are widely used in applications where high force levels, fast response and high power to weight ratios are required. Aerodynamic control surface actuators, machine tool actuators, mobile equipment control systems and marine control systems frequently employ closed loop hydraulic control systems. Important performance criteria for these systems include maximum force and velocity capabilities, accuracy, repeatability, reliability, maintainability and cost.

The primary power modulation elements in high performance hydraulic systems are servovalves. In position and velocity control systems servovalves are utilized extensively as indicated in figure 1. Also shown in the figure are typical pressure-flow output characteristics of commercial sliding spool servovalves. Servovalves with linear flow gains and high pressure gains are desired to achieve accuracy and overcome actuator and load stiction.

Electrohydraulic servovalves consisting typically of a torque motor, a first stage flapper nozzle or jet-pipe valve and a final stage sliding spool valve are the dominant type of valves employed in high performance hydraulic systems.[1] In these valves the electromechanical interface and the sliding mechanical elements contribute to valve cost, sensitivity to contamination and sensitivity to failure due to radiation.

The high reliability, insensitivity to extreme environments and low cost associated with no moving part fluidic elements and the potential for weight and size reduction in comparison to conventional valves are attractive features for servovalves. In addition, the implementation of a closed loop control system employing only fluid and mechanical elements offers potential for reduction of sensitivity to radiation and increased reliability with the elimination of electro-mechanical interfaces. In systems where these attributes are important and where the quiescent power drain associated with open-center fluid valves can be accommodated, fluidic servovalves and pure fluid-mechanical control systems have high application potential.

The application potential of pure fluid servovalves and control systems

---

[1] R. Deadwyler, Two Stage Servovalve Development Using a First-Stage Fluidic Amplifier, Harry Diamond Laboratories, HDL-TM-80-21 (July 1980).

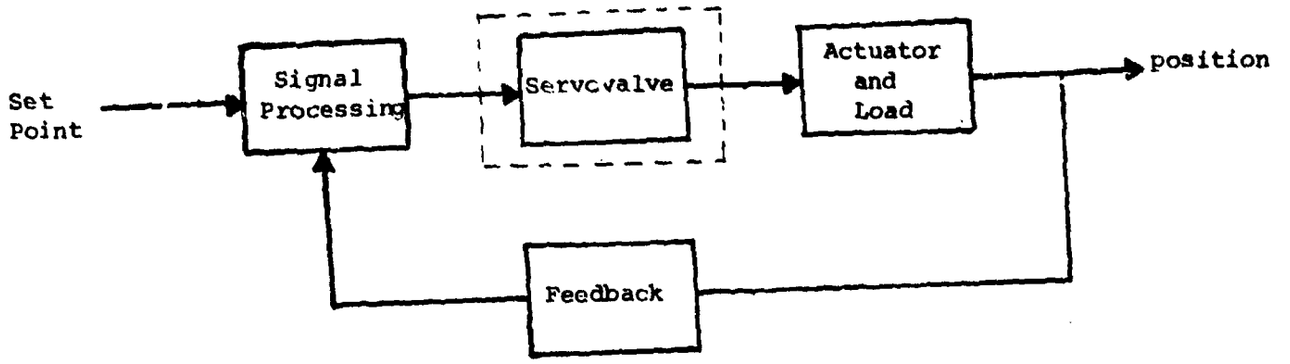

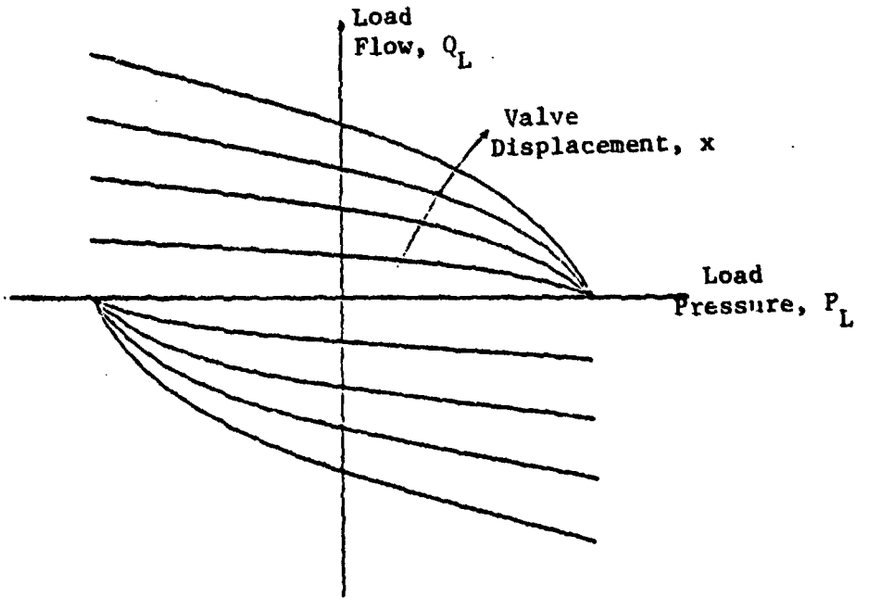

Figure 1. Closed loop position servo and servovalve output characteristics.

motivated a study[2] in which a pure fluid servovalve was constructed using laminar proportional amplifiers (LPA's) in a breadboard configuration. In the present study, development of pure fluid servovalves and servosystems has continued. Servovalves constructed from standard C format laminates[3] and interconnecting elements have been developed to reduce packaging volume and weight, provide a basis for standardization and to improve valve dynamic response. The static and dynamic characteristics of the C format LPA elements individually and integrated into the servovalve have been measured including performance sensitivity to temperature. Finally the servovalve has been employed in a closed loop position control system which includes an actuator and fluidic position transducer for evaluation.

Two aspects of the influence of temperature are particularly addressed in this study, namely, the static characteristic performance and the laminar operating range of the LPA as a function of supply conditions.

In all tests described in this report, hydraulic oil Univis J-43 has been used. The properties and specifications of the fluid are summarized in table 1 and the kinematic viscosity as a function of temperature is shown in figure 2 in the range from 20°F to 140°F. Univis J-43 changes in viscosity over this typical temperature range. An exponential curve fit of the form:

$$\nu_o = \nu_o e^{-\lambda(T-T_o)} \qquad (1)$$

where

ν = kinematic viscosity at temperature T,

ν_o = kinematic viscosity at reference temperature, T_o

λ = viscosity - temperature coefficient,

may be used to approximate the kinematic viscosity of the hydraulic oil Univis J-43 as a function of temperature

with λ = 0.02862 1/°C [0.0159 1/°F]

and ν_o = 21.78 cSt. evaluated at 25°C [77°F]

The exponential curve of equation (1) is a good approximation to the fluid viscosity as shown in figure 2.

---

[2]D.N. Wormley, D. Lee, and K-M Lee, Development of a Fluidic, Hydraulic Servovalve, HDL-CR-81-216-1, Harry Diamond Laboratories (February 1981).

[3]M.F. Cycon and D.J. Schaffer, Design Guide for Laminar Flow Fluidic Amplifiers and Sensors, HDL-CR-28-288-1, Harry Diamond Laboratories (April 1982).

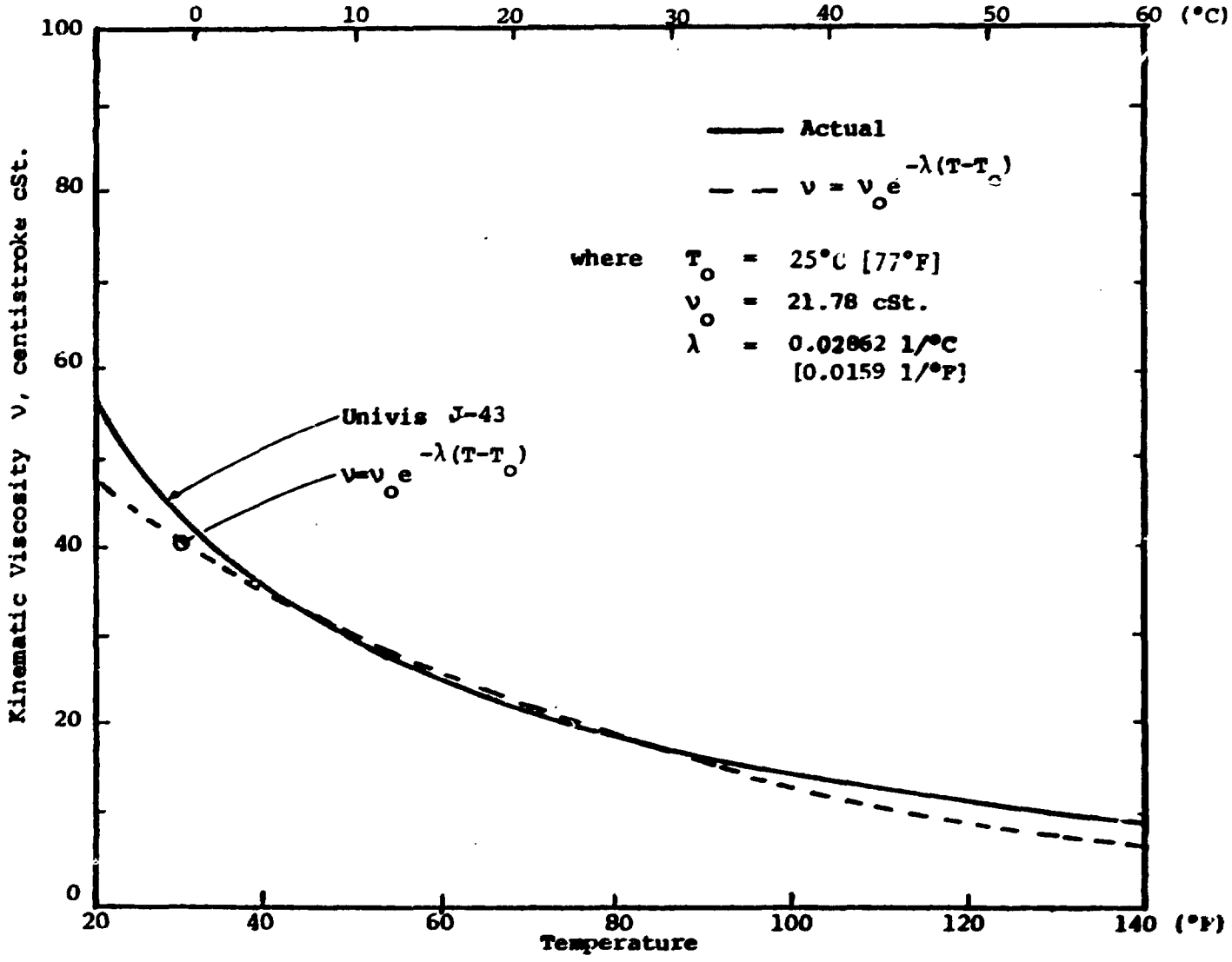

Figure 2. Kinematic viscosity as a function of temperature.

TABLE 1 HYDRAULIC OIL UNIVIS J-43 SPECIFICATION

Specific gravity: 0.8607

Temperature (°C)	Kinematic Viscosity (cSt.)
100	5.2
54	10.3
40	14.9
-18	102.7
-40	495.5
-54	2332.

2. FLUIDIC INTEGRATED COMPONENTS

Fluidic C format integrated components are basic elements in the servovalve. The primary elements are the LPA and the channel resistance which are shown in figure 3. The secondary elements are vents, exhausts, spacers, transfers, base plate, input and valve manifolds. The primary elements are standardized in design and manufacturing and are thus well documented and have repeatable characteristics.

2.1 Laminar Proportional Amplifier

Laminar proportional amplifiers have been designed to operate in the laminar flow regime. The detailed geometry of a typical HDL integrated component laminar proportional amplifier with a summary of LPA characteristic dimensions are illustrated in figure 4.

The LPA performance is influenced by the temperature of the operating fluid through its influence on the fluid viscosity.

The analytical design procedures which predict the performance of the laminar proportional amplifier based on the characteristic dimensions and the supply conditions have been discussed by Drzewiecki et al.[4] The

[4] T.M. Drzewiecki, D.N. Wormley and F.M. Manion, Computer Aided Design Procedure for Laminar Fluidic Systems, Journal of Dynamic Systems, Measurement and Control, 97, Series G, No. 4 (December 1975).

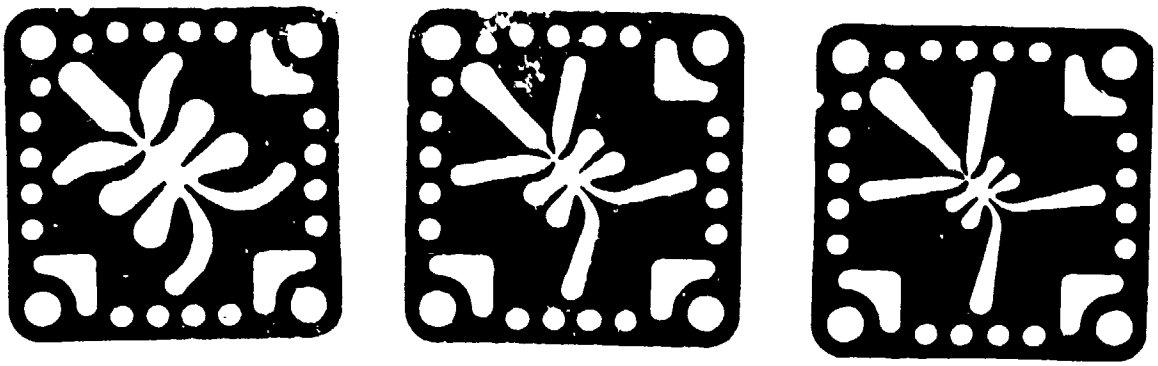

(a) laminar proportional amplifier (LPA)

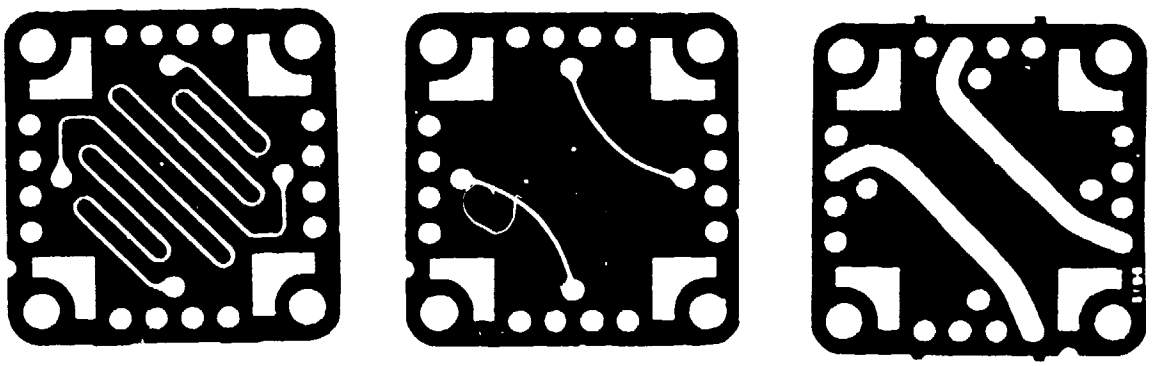

(b) linear channel resistance

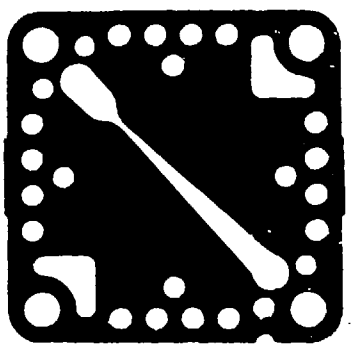

(c) nozzle or nonlinear resistance

Figure 3. Primary fluidic C format integrated components.

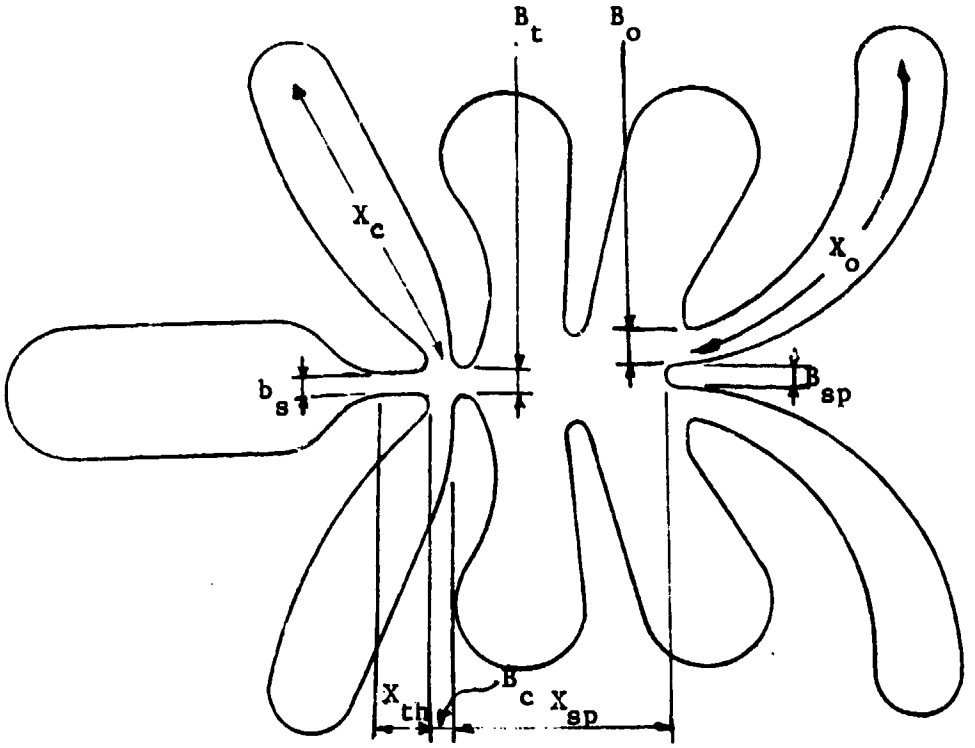

b_s	=	supply nozzle width
σ	=	aspect ratio, h/b_s
B_c	=	control port minimum width
B_o	=	outlet port minimum width
B_{sp}	=	splitter width
B_t	=	downstream control edges spacing
X_c	=	control port channel length
X_o	=	outlet port channel length
X_{th}	=	supply nozzle throat length
X_{sp}	=	supply nozzle - splitter distance

Capitalized parameters are normalized to b_s.

Figure 4. Silhouette for b_s = 0.5 mm LPA in C Format

LPA's with aspect ratios less than one are commonly used in the design of multistage gain blocks. However, limited experimental data are available for LPA's of aspect ratio less than one. The work described in this section provides data and correlations for gain block and servovalve design using LPA's in this range of aspect ratios.

The supply condition of an LPA may be characterized by the modified Reynolds number

$$N_R' = \frac{N_R}{\left(1 + \frac{1}{\sigma}\right)^2 \left(1 + X_{th}\right)}$$

where

$$N_R = \frac{b_s}{\nu} \sqrt{\frac{2P_s}{\rho}}$$

ρ = fluid density

P_s = supply pressure, gage

σ = nozzle aspect ratio, h/b_s

Experimental data have been collected from three different C format LPA configurations (HDL 63020, HDL 72010 and HDL 61505) with aspect ratios of σ = 0.667, 0.55 and 0.333 and supply nozzle throat widths of 0.75 mm, 0.5 mm and 0.375 mm respectively. The characteristic dimensions are shown in Table 2. The LPA's have been tested under blocked-load conditions over a temperature range of 5.5°C (42°F) to 48°C (118°F) and a pressure range of 35 kPa (5 psi) to 11,032 kPa (1600 psi). In all tests, the control bias pressures were adjusted to 5 percent of the supply pressure.

The analytical and experimentally measured blocked-load pressure gain are plotted against the modified Reynolds number in figure 5. The analytical model is based on the modified two-dimensional, incompressible, laminar jet deflection theory discussed by Drzewiecki et al.[4] The experimental gains were determined from the slope of the blocked-load characteristics at the null position.

---

[4] T.M. Drzewiecki, D.N. Wormley and F.M. Manion, Computer Aided Design Procedure for Laminar Fluidic Systems, Journal of Dynamic Systems, Measurement and Control, 97, Series G, No. 4 (December 1975).

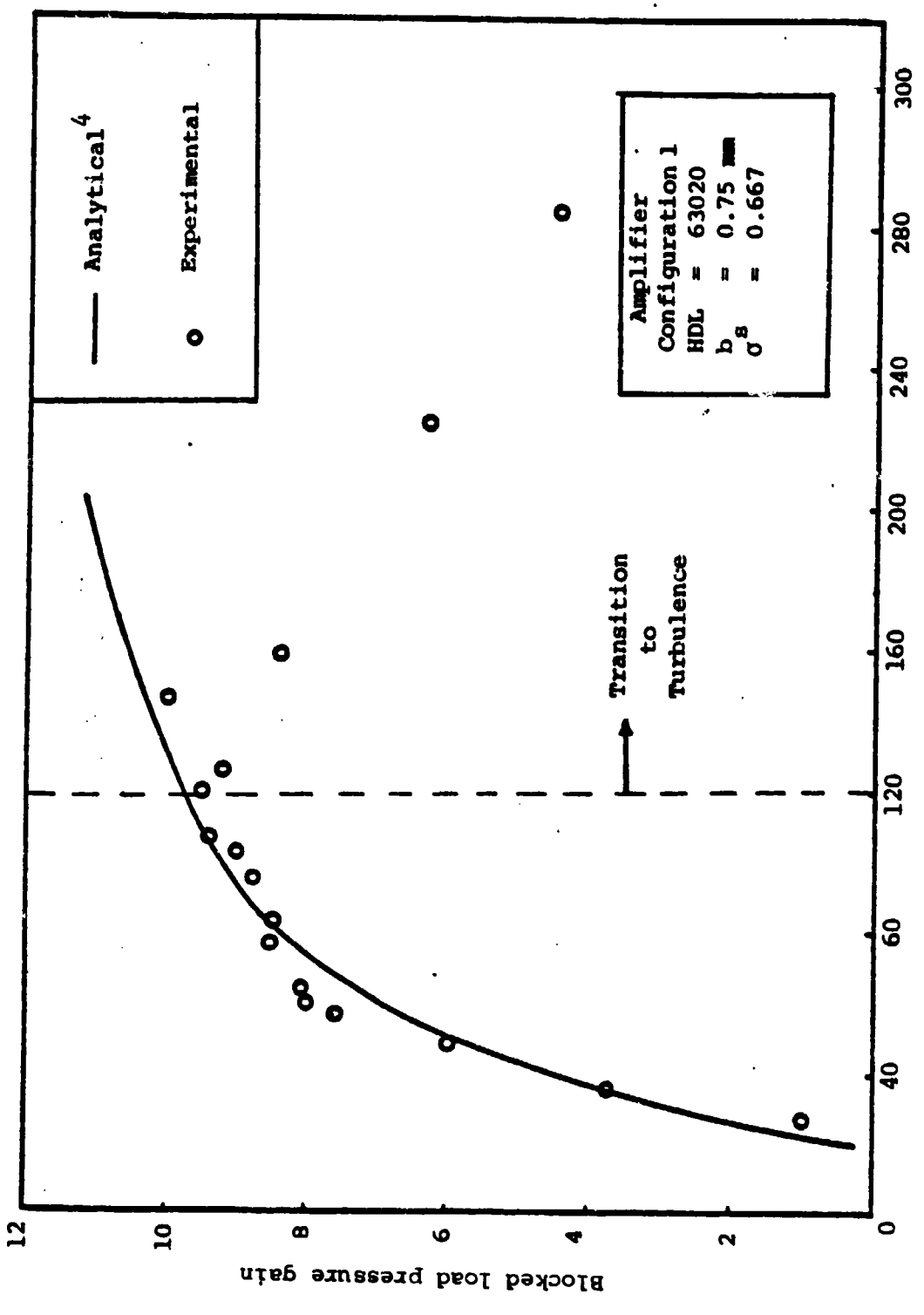

Figure 5. Comparison of theory and data of blocked load gain

TABLE 2 CHARACTERISTIC DIMENSIONS OF LPA's

HDL design	63020	72010	61505
b_s (mm)	0.75	0.5	0.375
	0.667	0.55	0.333
B_s	1.0	1.0	1.0
$\bar{B}_c$	3.08	4.0	4.733
x_c	8.875	13.312	21.
B_o	1.2	1.25	1.33
$\bar{B}_o$	2.667	2.875	3.6
X_o	14.875	16.56	22.08
B_t	1.25	1.125	1.167
B_{sp}	0.55	0.5	0.533
X_{th}	1.257	1.25	1.25
X_{sp}	8.0	8.0	8.0

The experimental data closely follow the analytical prediction up to $N_R' = 120$ beyond which transition-to-turbulence occurs and the theory based on laminar flow fails. In the turbulent flow regime, the flow noise increases, offset increases and the gain decreases. Therefore, the transition-to-turbulence establishes an upper design limit of operation for the LPA. In the laminar flow regime, the blocked-load pressure gain increases as the Reynolds number increases.

A guideline to determine the point of transition from laminar to turbulence for fluidic devices (when $X_{sp} = 8$ to 10) has been discussed by Drzewiecki et al.[5]

$$\frac{C_d N_R}{\left(1 + \frac{1}{\sigma}\right)^2} = 200 \qquad (2)$$

where C_d = volumetric discharge coefficient, $f(N_R')$ or the expression may be written as

[5] T.M. Drzewiecki and F.M. Manion, Fluerics 40: LJARS, The Laminar Jet Angular Rate Sensor, HDL-TM-79-7, Harry Diamond Laboratories (December 1979).

$$C_d N_R' \Big|_{tr.} = \frac{200}{1+X_{th}} . \tag{3}$$

For $X_{sp} \approx 8$ and $X_{th} = 1.25$, the point of transition from laminar to turbulence occurs at $N_R' \approx 120$.

The lower operating limit of the amplifier may be predicted from the information on the control edge clearance. The amplifier ceases to function if the jet cannot deflect. The distance from the control edge to the jet edge, based on the assumption that the jet spreads linearly, is given by Manion et al.[6]

$$B_v = \frac{1}{2}\left[B_t - 1 - \frac{B_c}{0.0278\ C_d^3 N_R / C_\theta}\right] \tag{4}$$

where

B_v = distance between control edge and jet edge

C_θ = momentum flux coefficient.

With $C_\theta \approx 1.32\ C_d^2$ and $B_v = 0$, the expression may be written as

$$C_d N_R' = \frac{47.5\ B_c}{\left(B_t - 1\right)\left(1+\frac{1}{\sigma}\right)^2\left(1+X_{th}\right)} . \tag{5}$$

The average value of $C_d N_R'$ for the three amplifier configurations is approximately equal to 10 and the point at which the LPA fails to function occurs at $N_R' \approx 22$.

The experimental data obtained for the blocked-load pressure gain of the three different LPA configurations are plotted in figure 6. The effect of the modified Reynolds number on the blocked-load pressure gain may be summarized by noting the four regions defined in the following paragraphs.

In region (1), $0 \leq N_R' < 40$, the blocked-load pressure gain is less than 50 percent of its maximum value. In all three different con-

---

[6] F.M. Manion and T.M. Drzewiecki, Analytical Design of Laminar Proportional Amplifiers, Proceedings of the HDL Fluidic State-of-the-Art Symposium, 1, Harry Diamond Laboratories (October 1974).

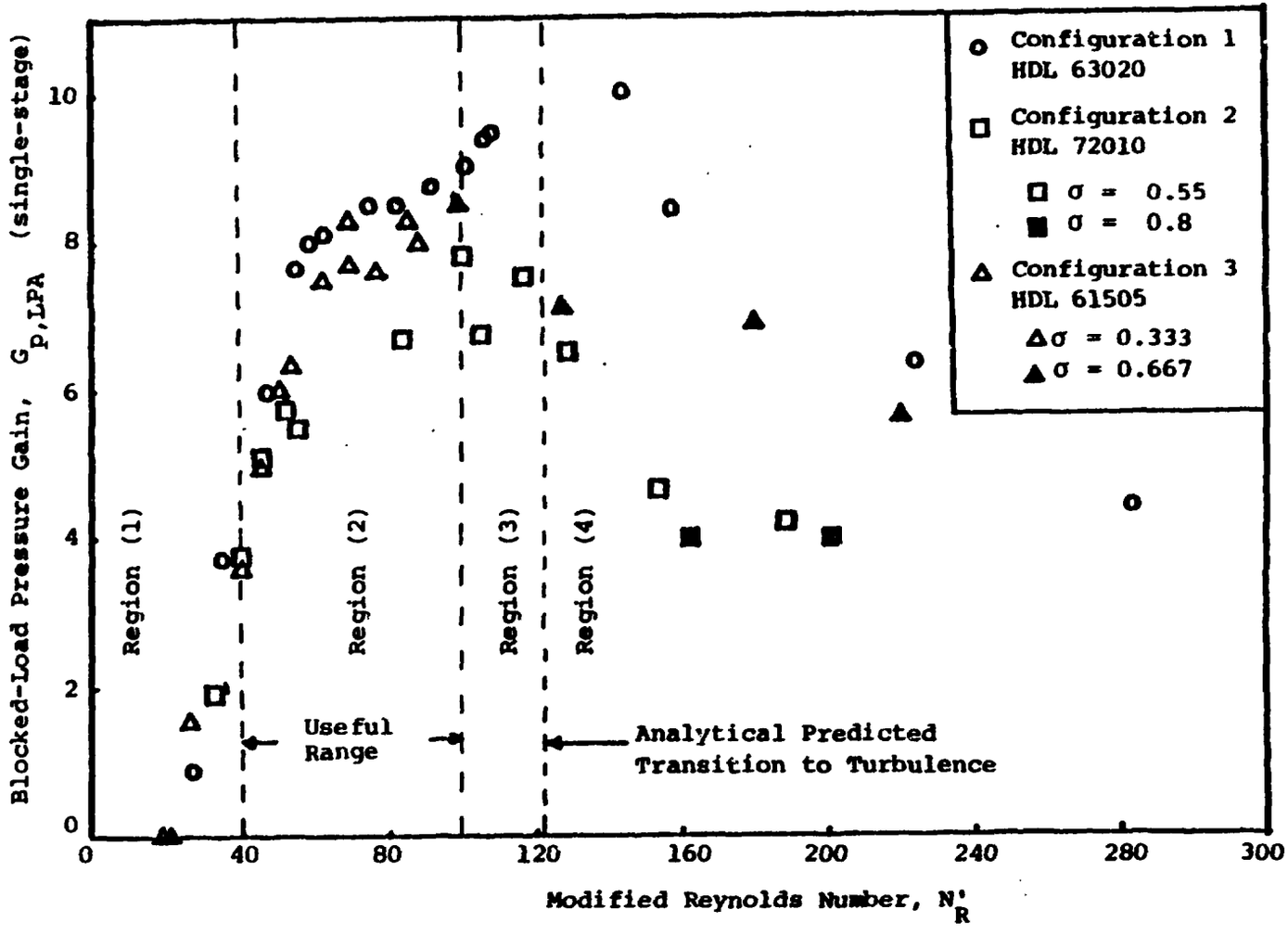

Figure 6. Experimental data illustrating the operating range of LPA.

figurations tested, the LPA gain is zero for $N_R' \leq 20$.

In region (2), $40 \leq N_R' \leq 100$, the typical LPA operating range is bounded by two limits, a lower limit below which the LPA gain is too low for use and an upper limit beyond which transition-to-turbulence occurs.

In region (3), $100 \leq N_R' < 120$, just before the analytical predicted point of transition-to-turbulence, the experimental data are scattered. This uncertainty suggests that the point of transition-to-turbulence is in this region.

In region (4), $N_R' \geq 120$, the blocked-load pressure gain decreases and noise increases since the LPA's are operated beyond the transition-to-turbulence.

2.2 Fluidic Channel Resistance

The channel resistor is one of the important elements in fluidic circuits. In general, the channel resistance may be represented as a laminar, fully-developed duct resistance. The channel resistance consists of a linear portion due to the fully developed viscous dissipative flow in the channel plus a nonlinear portion due to the entrance region pressure drop. A general expression for a channel resistance given by Drzewiecki[7] is

$$R = \frac{12\,\mu x}{(\bar{b}h)^2}\left[\sigma_c\left(1 + \frac{1}{\sigma_c^2}\right) + C\right] + \frac{0.475\rho Q}{(bh)^2} \qquad (6)$$

where

for $1 \leq \sigma_c \leq 2$, $\quad 0.35 \leq C \leq 0.5$;

for $\sigma_c > 2$, $\quad C = 0.5$,

x = channel length in the direction of flow,

$\bar{b}$ = average channel length,

b = minimum channel width,

Q = volumetric flow through duct,

σ_c = channel aspect ratio, $\frac{h}{\bar{b}}$

[7] T.M. Drzewiecki, Fluerics 37. A General Planar Nozzle Discharge Coefficient Representation, HDL-TM-74-5, Harry Diamond Laboratories, (1974).

μ = absolute fluid viscosity,

C = empirical constant.

For the case where the channel length is much longer than the entrance length, the nonlinear term may be neglected. An analytical study on the hydrodynamic entrance length for incompressible flow in rectangular ducts has been performed by Han.[8] The experiments to verify the analysis of Han for aspect ratios of 5 and 2 have been performed by Sparrow et al.[9]. The results of these studies to determine the entrance length may be summarized as

$$L_e = 0.055\left(\frac{\sigma_c}{1+\sigma_c}\right)^2 N_{R_c} \qquad \text{for } \sigma_c = 5,$$

$$L_e = 0.127\left(\frac{\sigma_c}{1+\sigma_c}\right)^2 N_{R_c} \qquad \text{for } \sigma_c = 2,$$

where

L_e = normalized entrance length, $\ell e/b$

N_{R_c} = channel Reynolds number, referred to b.

For flow between parallel-plates, Schlichting[10] has derived an expression for the entrance length as

$$\frac{L_e}{\sigma_c^2 N_{R_c}} = 0.04 \qquad \text{for } b >> h.$$

If the assumption of fully developed flow is justified and the entrance length can be neglected, the flow can be described by Poiseuille flow between parallel plates and the expression for the resistance may be stated as

$$R_c = \frac{12\mu x}{bh^3} \qquad \text{for } b >> h. \qquad (7)$$

---

[8] L.S. Han, Hydrodynamic Entrance Lengths for Incompressible Flow in Rectangular Ducts, Journal of Applied Mechanics, 27, Trans. ASME (1960).

[9] E.M. Sparrow, C.W. Hixon and G. Shavitt, Experiments on Laminar Flow Development in Rectangular Ducts, Journal of Basic Engineering, Trans. ASME (March 1976).

[10] M. Schlichting, Boundary Layer Theory, McGraw-Hill, New York, New York, (1960).

The standard nozzle, 5221A-20 shown in figure 3, has been used as a channel resistor in the design of the gain block. Since the channel length is much longer than the entrance length of the flow for a wide range of Reynolds numbers, the quasi-fully-developed assumption is justified, and equation (6) may be applied. Normalizing equation (6) to the linear portion, the expression for resistance is

$$\bar{R} = 1 + \frac{0.475}{12}\left(\frac{\bar{b}}{b}\right)^2 \frac{\left(\sigma + \frac{1}{\sigma} + 2\right)}{\left(\frac{h}{\bar{b}} + \frac{\bar{b}}{h} + C\right)} \cdot \frac{1 + X_{th}}{X} C_d N'_R \qquad (8)$$

where

$$\bar{R} = \frac{R}{\left[\frac{12\mu x}{(\bar{b}h)^2}\left(\frac{h}{\bar{b}} + \frac{\bar{b}}{h} + C\right)\right]} .$$

The nozzle resistance as a function of modified Reynolds numbers has been determined experimentally. The range of temperatures and the pressure drops across the nozzle are from 6°C to 48°C and from 5516kPa to 10170 kPa respectively. The experimentally determined nozzle resistance is compared with analytically predicted values using equation (8) as a function of modified Reynolds numbers in figure 7. The experimental data falls within 10 percent of the predictions in the range of N'_R tested.

3. FLUIDIC GAIN BLOCK AND SERVOVALVE

The fluidic servovalve consists of a multi-stage LPA gain block and a set of laminar flow resistors. The gain block is a basic power amplifier while the resistors are used to provide feedback and summing functions.

3.1 Gain Block Configuration and Characteristics

The analytical design of the fluidic gain block to predict the essential characteristics as a function of individual stage operating Reynolds number, control bias pressure and the detailed geometry of the LPA has been discussed by Manion et al.[4,11]

---

[4] T.M. Drzewiecki, D.N. Wormley and F.M. Manion, Computer-Aided Design Procedure for Laminar Fluidic Systems, Journal of Dynamic Systems, Measurement and Control, 97, Series G, No. 4 (December 1975).

[11] F.M. Manion and G. Mon, Fluerics 33: Design and Staging of Laminar Proportional Amplifiers, HDL-TR-1608, Harry Diamond Laboratories (September 1972).

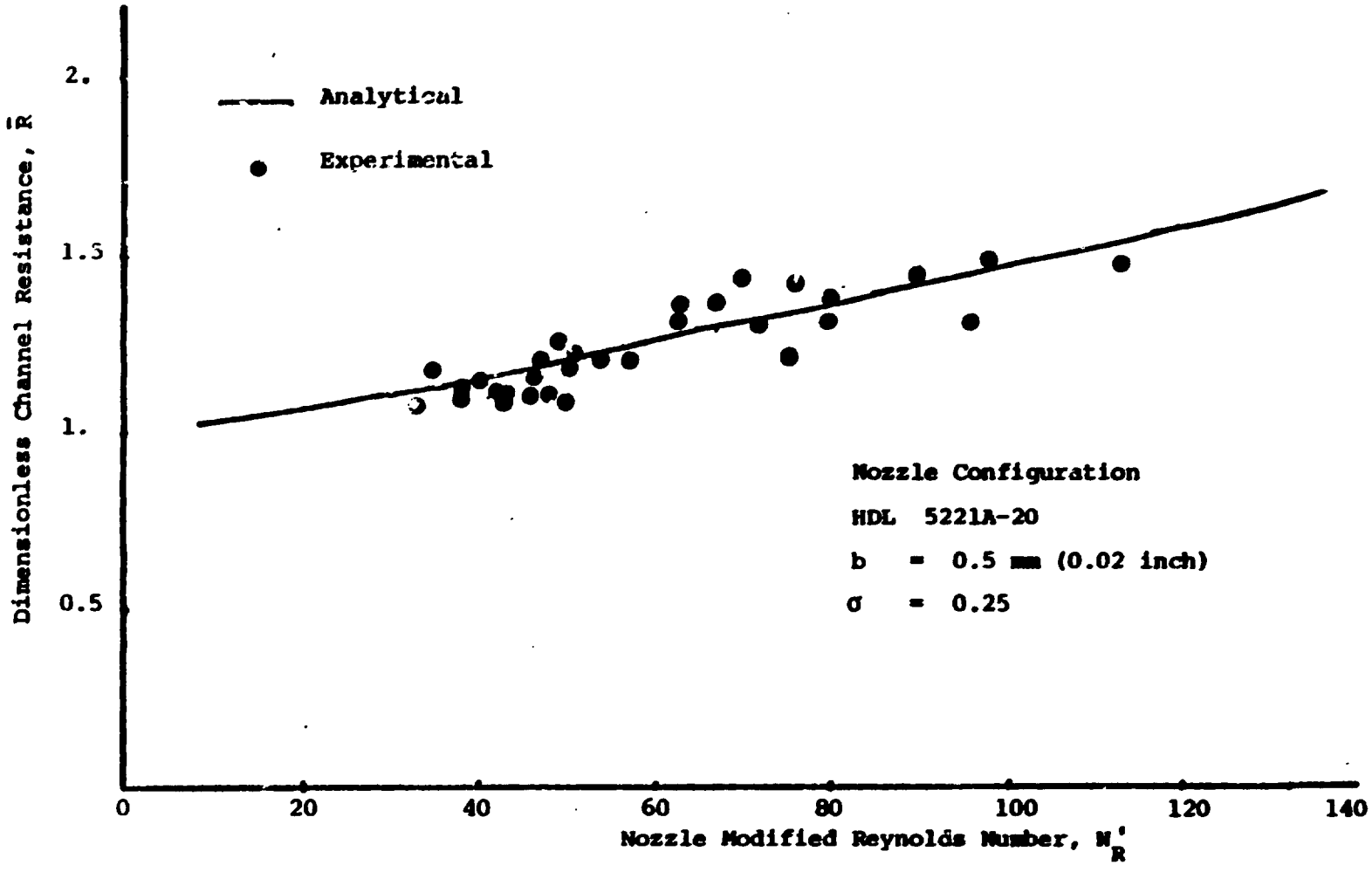

Figure 7. Comparison of analytical and experimental nozzle resistance.

The general design criteria of a gain block are as follows:

(1) Maximize the laminar operating range by matching the modified Reynolds numbers, of each stage:

$$N'_{R1} = N'_{R2} = N'_{R3}.$$

(2) Achieve 90° phase shift bandwidth requirement:

$$f_{90°} = \frac{\left(\frac{\pi}{2}\right)}{2\pi \sum_{i=1}^{3} \frac{4x_{sp}}{C_{di}\sqrt{\frac{2P_{si}}{\rho}}}}.$$

(3) Maximize the blocked-load pressure gain:

$$K_p = \frac{K_1 \cdot K_2 \cdot K_3}{\left(1 + \frac{R_{01}}{R_{i2}}\right)\left(1 + \frac{R_{02}}{R_{i3}}\right)}$$

where K_1, K_2 and K_3 are blocked-load pressure gain of 1st, 2nd and 3rd stages LPA respectively. R_{01} and R_{02} are output resistance of the 1st and 2nd stages and R_{i2} and R_{i3} are input resistance of the 2nd and 3rd stages.

(4) Maximize the input-to-output resistance ratio:

$$R_{i1}/R_{03}.$$

(5) Minimize the quiescent flow draw:

$$Q_s = \sum_{i=1}^{3} Q_{si},$$

where Q_{si} (i = 1,2,3) are supply flows of the 1st, 2nd and 3rd stages. An iterative design procedure is generally required to achieve a design which meets (if possible) the above design criteria.

The gain block shown in figure 8 has been designed using the guidelines cited above.

The supply pressure of the three stage gain block is connected directly to the final stage of the gain block. The first and second

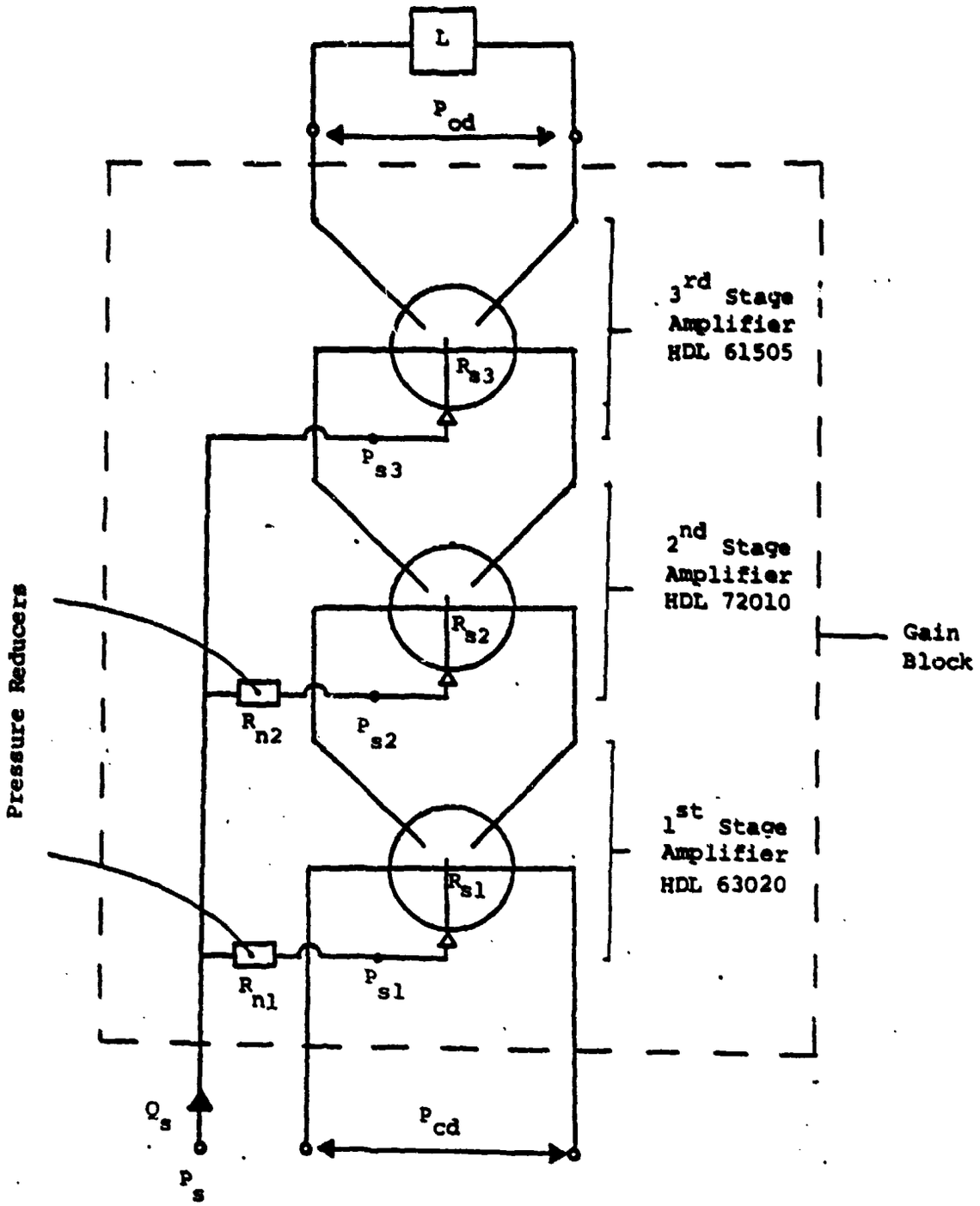

Figure 8. Gain block schematics.

stages are supplied by reducing the main pressure through the pressure reducers which are a number of nozzles in parallel.

The first and second stage supply pressures depend on the final stage supply condition with respect to the fluid properties. The supply pressure of i^{th} stage, P_{si} may be expressed as

$$\frac{P_{si}}{P_s} = \frac{1}{1 + \frac{m_i}{n_i} \frac{R_{ni}}{R_{si}}} \tag{9}$$

where

m_i = no. of LPA's in parallel of i^{th} stage,
n_i = no. of resistor nozzles in parallel of i^{th} stage,
R_{si} = LPA supply resistance of i^{th} stage,
R_{ni} = nozzle resistance of i^{th} stage.

As the nozzle resistance, R_{ni}, and the supply resistance, R_{si} are connected in series, the flow through R_{ni} and R_{si} are related by the continuity equation as

$$\frac{Q_{ni}}{Q_{si}} = \frac{m_i}{n_i} . \tag{10}$$

With equation (10), the ratio of the nozzle resistance, R_{ni}, to the supply resistance, R_{si}, may be expressed as

$$\frac{R_{ni}}{R_{si}} = \frac{24\, X_{ni}}{\bar{B}_{ni}^2} \left[\frac{\sigma_i}{H_{ni}^2}\right] \cdot \left[\frac{H_{ni}}{\bar{B}_{ni}} + \frac{\bar{B}_{ni}}{H_{ni}} + C\right] \cdot \frac{C_{di}}{N_{Ri}} + 0.95 \left[\frac{\sigma_i}{B_{ni} H_{ni}}\right]^2 \frac{m_i}{n_i} C_{di}^2 \tag{11}$$

where

σ_i = LPA aspect ratio,
X_{ni} = normalized nozzle length, x_{ni}/b_{si},
$\bar{B}_{ni}$ = normalized nozzle average channel length, $\bar{b}_{ni}/b_{si}$,
B_{ni} = normalized nozzle throat width, b_{ni}/b_{si},
H_{ni} = normalized nozzle height, h_{ni}/b_{si},

$$1 \leq \frac{H_{ni}}{\bar{B}_{ni}} \leq 2, \qquad 0.35 \leq C \leq 0.5; \qquad \frac{H_{ni}}{\bar{B}_{ni}} > 2, \; C = 0.5.$$

Subscript i refers to the i^{th} stage.

The Reynolds number of the first and second stage LPA may be related to that of the final stage as

$$N_{Ri} = \frac{b_{si}}{b_{sf}} \sqrt{\frac{P_{si}}{P_s}} N_{Rf} \tag{12}$$

where

b_{si} = LPA supply nozzle throat width, i^{th} stage,
b_{sf} = LPA supply nozzle throat width, final stage,
N_{Ri} = Reynolds number of i^{th} stage,
N_{Rf} = Reynolds number of final stage.

As the first and second stage supply pressures are an implicit function of the final stage Reynolds number, N_{Rf}, the first and second stage operating Reynolds numbers depend only on the final stage Reynolds number. In the following discussions, the gain block operating Reynolds number is referred to the operating Reynolds number of the final stage, N_{Rf}. The first and second stage Reynolds numbers can be related to the final stage by solving equations (9) through (12) simultaneously.

In the report by Wormley et al.[2] a hyperbolic tangent curve has been used to describe the nonlinear saturation characteristics of the gain block. The output pressure/flow characteristics of the gain block may be expressed as

$$\frac{Q_L}{Q_{Ls}} = \tanh \frac{P_{cd}}{P_{cds}} - \frac{P_{od}}{P_{ods}} \tag{13}$$

where

Q_L = output load flow,
P_{od} = amplifier output pressure differential,
P_{cd} = amplifier input pressure differential,

---

[2] D.N. Wormley, D. Lee, and K-M Lee, Development of a Fluidic, Hydraulic Servovalve, HDL-CR-81-216-1, Harry Diamond Laboratories (February 1981).

Q_{Ls} = saturation output load flow,

P_{ods} = saturation amplifier output pressure differential,

and where the saturation control pressure differential is defined as

$$P_{cds} = \frac{P_{ods}}{K_p} = \frac{Q_{Ls}}{K_q} \tag{14}$$

with the incremental amplifier static pressure gain K_p and flow gain, K_q defined as

$$K_p = \left.\frac{\partial P_{od}}{\partial P_{cd}}\right|_{Q_L = 0} \tag{15}$$

$$K_q = \left.\frac{\partial Q_L}{\partial P_{cd}}\right|_{P_{od} = 0} \tag{16}$$

A three-stage fluidic gainblock with a single supply pressure based on the standard packaging technique was constructed and tested. The construction schematic of the gain block is shown in figure 9. The stacking order is listed in appendix A. The characteristic dimensions of the amplifier laminates and the three stage amplifier parameters, measured with Univis J-43 at a temperature of 27°C, are summarized in table 3. The experimental output characteristics are displayed in figure 10. The comparison between the predicted and the experimentally measured characteristics displayed in figure 11 shows that the analytical model with hyperbolic tanh curve closely matches the experimental data.

3.2 Fluidic Servovalve Configuration and Characteristics

The conceptualization, analysis and design of a fluidic servovalve constructed from the gainblock and fluidic resistance elements in a breadboard configuration are described by Wormley et al.[2]. The flow feedback resistance in the case in which the net flow feedback is equal to zero can be eliminated. In order to minimize the loss of output flow due to feed-

[2] D.N. Wormley, D. Lee, and K-M. Lee, Development of a Fluidic, Hydraulic Servovalve, HDL-CR-81-216-1, Harry Diamond Laboratories (February 1981).

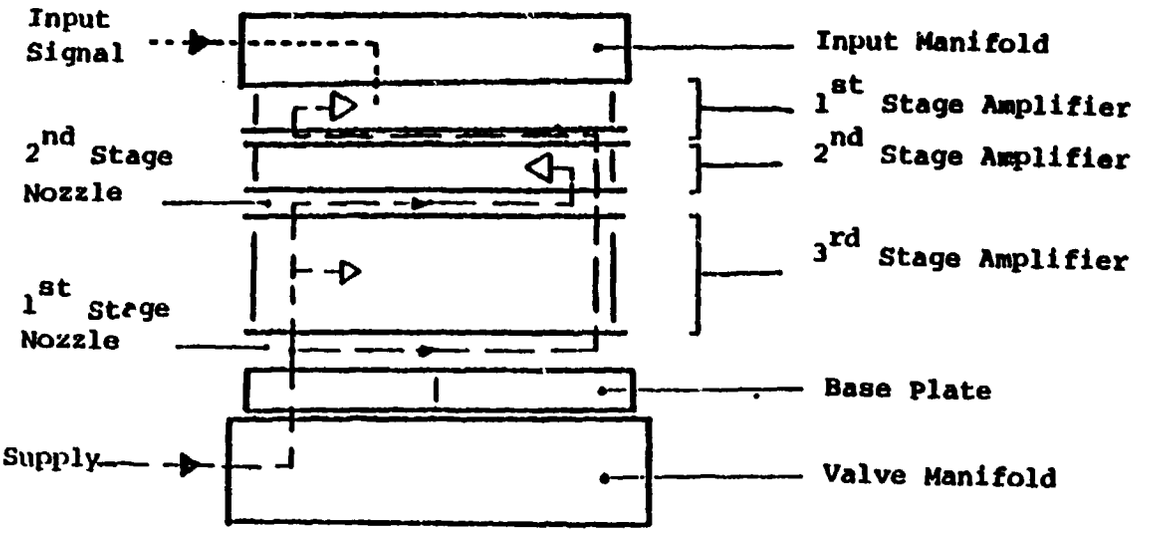

Figure 9. Gain block construction schematics.

TABLE 3 GAIN BLOCK CONFIGURATION AND INCREMENTAL PARAMETERS LAMINATE DESCRIPTION

Stage	Design	b_s (mm)	$\sigma = h/b_s$	Number of Sections
1	HDL 63020	0.75	0.667	2
2	HDL 72010	0.5	0.55	3
3	HDL 61505	0.375	0.333	6
EXPERIMENTAL DATA				
P_s	6895	kPa	1000	psi
P_{ods}	2551	kPa	370	psi
Q_{Ls}	8×10^{-6}	m^3/sec	0.5	cis
P_{cds}	8.72	kPa	35	in.H_2O
K_p	277			
K_q	8.6×10^{-7}	$m^3/sec/kPa$	0.35	cis/psi
R_a	5.80×10^{10}	$N-s/m^5$	140	psi/cis

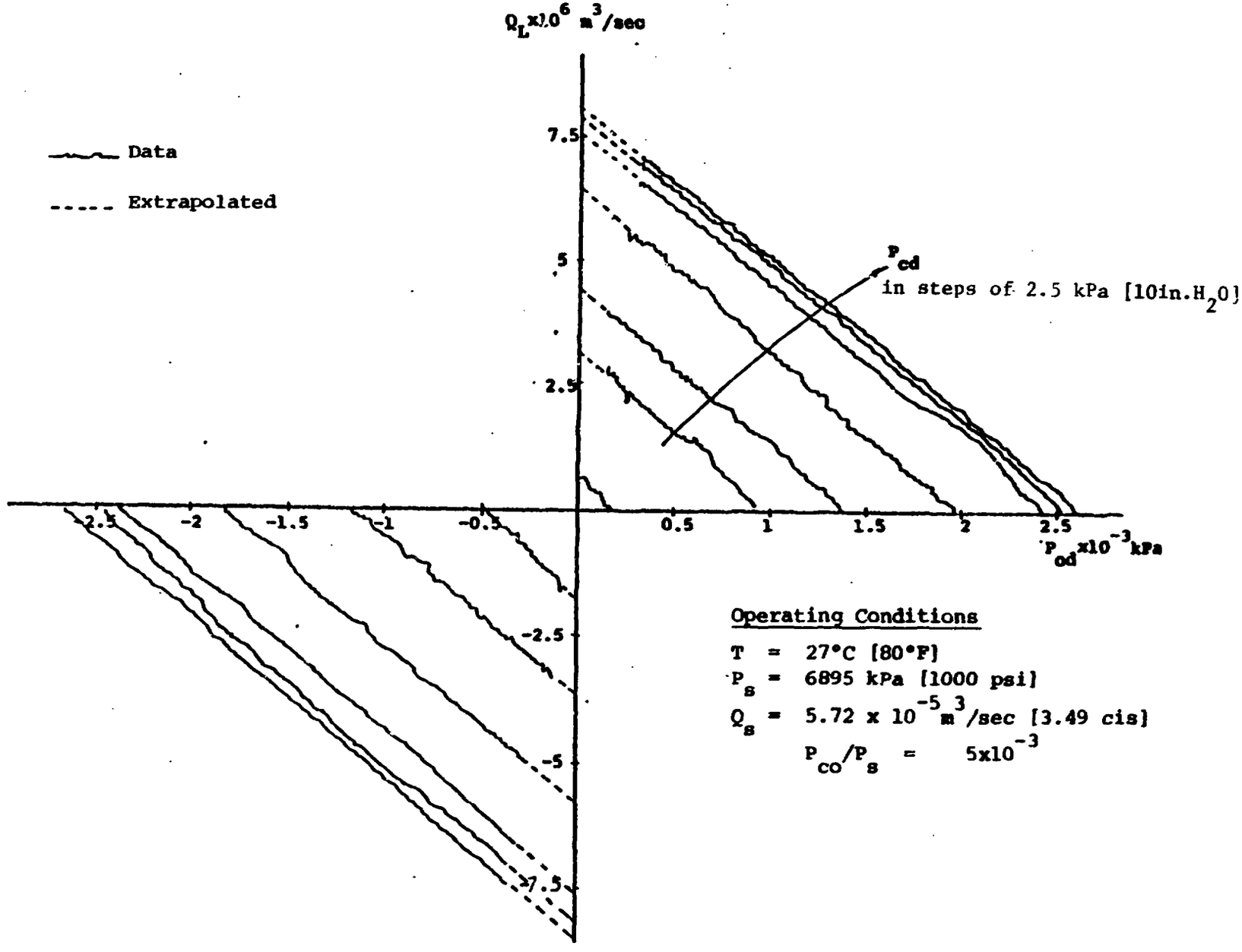

Figure 10. Experimental gain block output characteristics.

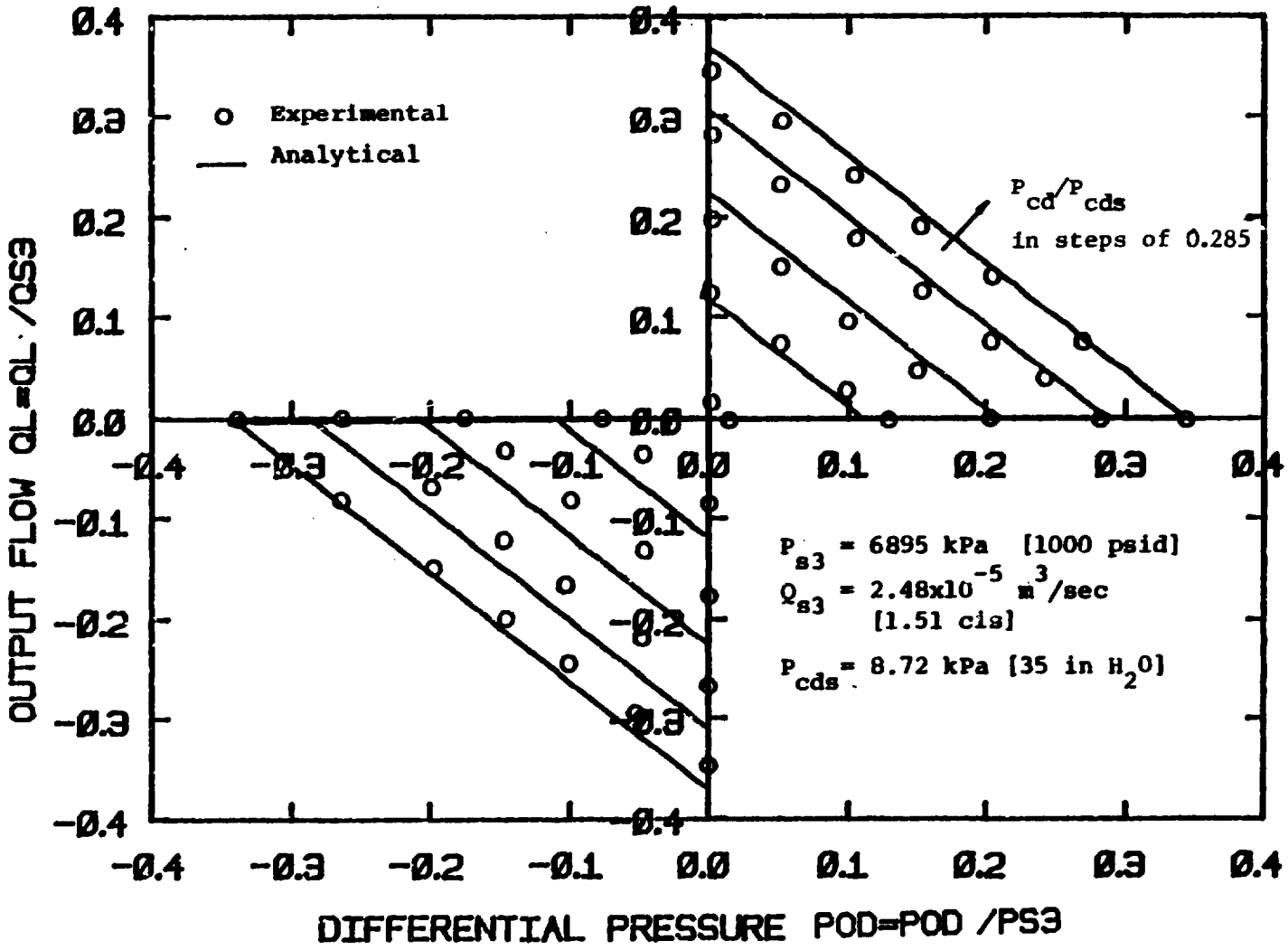

Figure 11. Comparison of computer-aid design prediction and experimental gain block output characteristics.

back and the complexity of the valve construction, the case of zero flow feedback is chosen for the performance evaluation. In this particular case, the resulting nonlinear normalized governing equation of the valve becomes

$$\frac{Q_L}{Q_{Ls}} + \frac{P_{od}}{P_{ods}} = \tanh\left[\alpha \frac{P_{id}}{P_{idm}} + \gamma \frac{P_{od}}{P_{ods}}\right] \tag{17}$$

where

P_{idm} = maximum input pressure differential

$$\alpha = \left(\frac{1}{1 + \frac{R_i}{R_a}}\right) \frac{P_{idm}}{P_{cds}} \quad \text{for } R_{fp} >> R_i \tag{18}$$

$$\gamma = \frac{R_i}{R_{fp}} \left(\frac{1}{1 + \frac{R_i}{R_a}}\right) K_p, \tag{19}$$

R_i = input resistance,

R_{fp} = pressure feedback resistance,

R_a = amplifier input deflection resistance.

The schematic drawing of the servovalve is shown in figure 12.

The fluidic servovalve steady state blocked-load pressure gain and no-load flow gain can be obtained from the linearized valve model as

$$G_{qs} = \left.\frac{\partial Q_L}{\partial P_{id}}\right|_{P_{od}=0} = \frac{K_q}{1 + \frac{R_i}{R_a}} \tag{20}$$

$$G_{ps} = \left.\frac{\partial P_L}{\partial P_{id}}\right|_{Q_L=0} = \frac{K_p}{(1-\gamma)\left(1 + \frac{R_i}{R_a}\right)}. \tag{21}$$

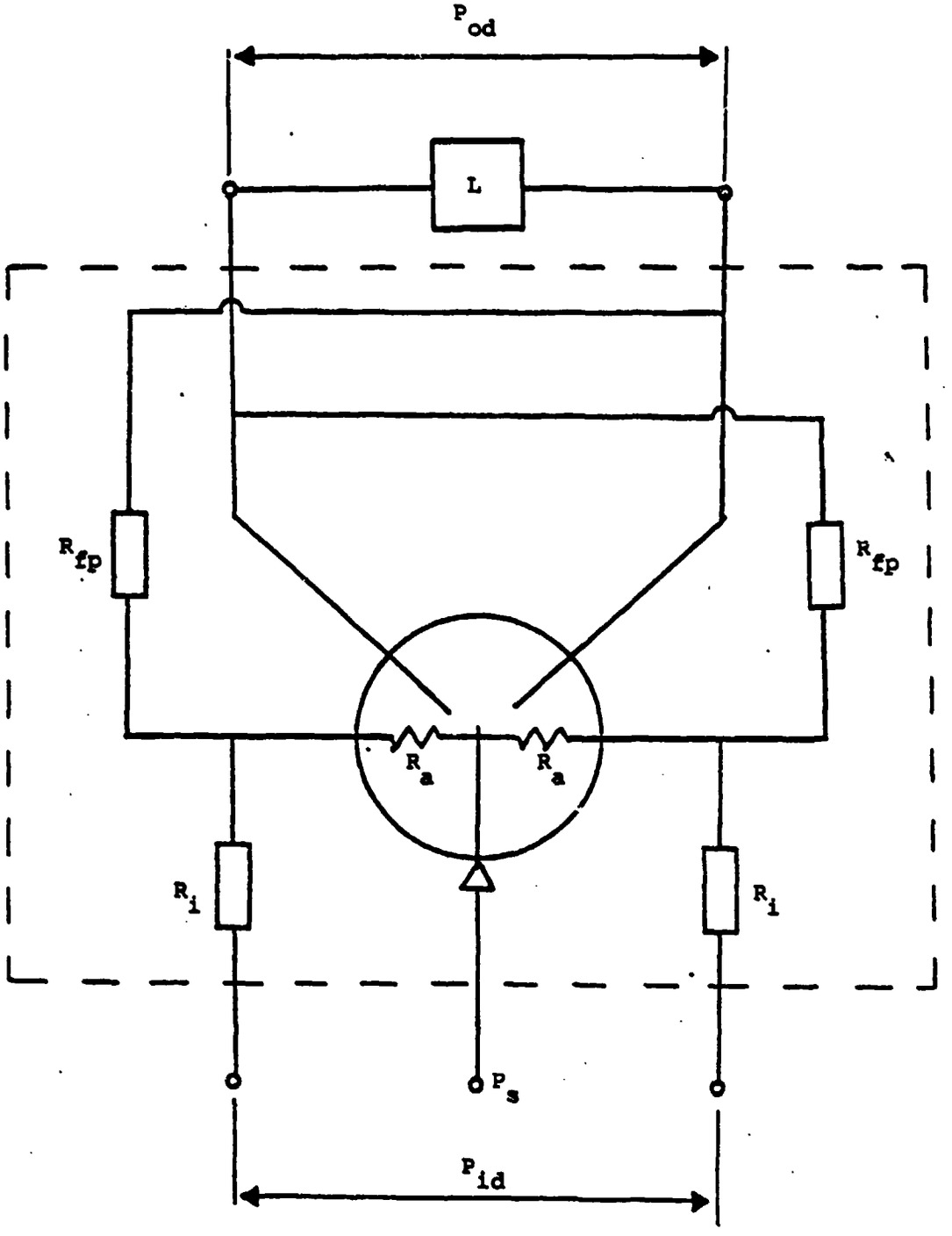

Figure 12. Servovalve schematic.

The steady state performance of the servovalve is characterized by the parameters α and γ. The valve parameter α indicates the flow gain linearity with respect to the maximum input pressure differential whereas the parameter γ provides information regarding the limit of servovalve stability.

As shown in equation (21), the servovalve pressure gain is sensitive to the valve parameter γ. The fluidic servovalve has a maximum pressure gain at γ equal to one and has a negative pressure gain for γ greater than one. The valve is unstable when the valve pressure gain curve has negative slope.

The effect of a variation in α is illustrated in figure 13. With $\gamma = 1$ to achieve maximum pressure gain, the servovalve flow gain becomes more non-linear as α is increased.

An integrated component fluidic servovalve has been constructed and tested. The gain block discussed in the preceeding section has been used in the servovalve design. Two HDL 5196 capillaries are connected in series to form an input resistor R_i. The pressure feedback resistor R_{fp} consists of four parallel HDL 5026 capillaries in series, with a HDL 5027 capillary. The experimentally measured resistances at the temperature of 27°C (80.6°F) are:

$$R_i = 4.42 \times 10^{10} \text{ N-s/m}^5 \quad (105 \text{ psi/cis}) \text{ and}$$

$$R_{fp} = 7.52 \times 10^{12} \text{ N-s/m}^5 \quad (17850 \text{ psi/cis}).$$

The servovalve construction schematic is shown in figure 14. The stacking order is summarized in appendix A.

The experimental data obtained at a temperature of 27°C and a supply pressure of 6895 kPa (1000 psi) showing the output characteristics are displayed in figure 15 and compared with the analytical prediction in figure 16. Apart from the offset, the analytical prediction fits the experimental characteristics well.

3.3 Temperature Effects and Compensation

For imcompressible flow, the working fluid temperature affects the Reynolds number, $N_R = (b_s/\nu)\sqrt{2P_s/\rho}$, through an influence on the fluid

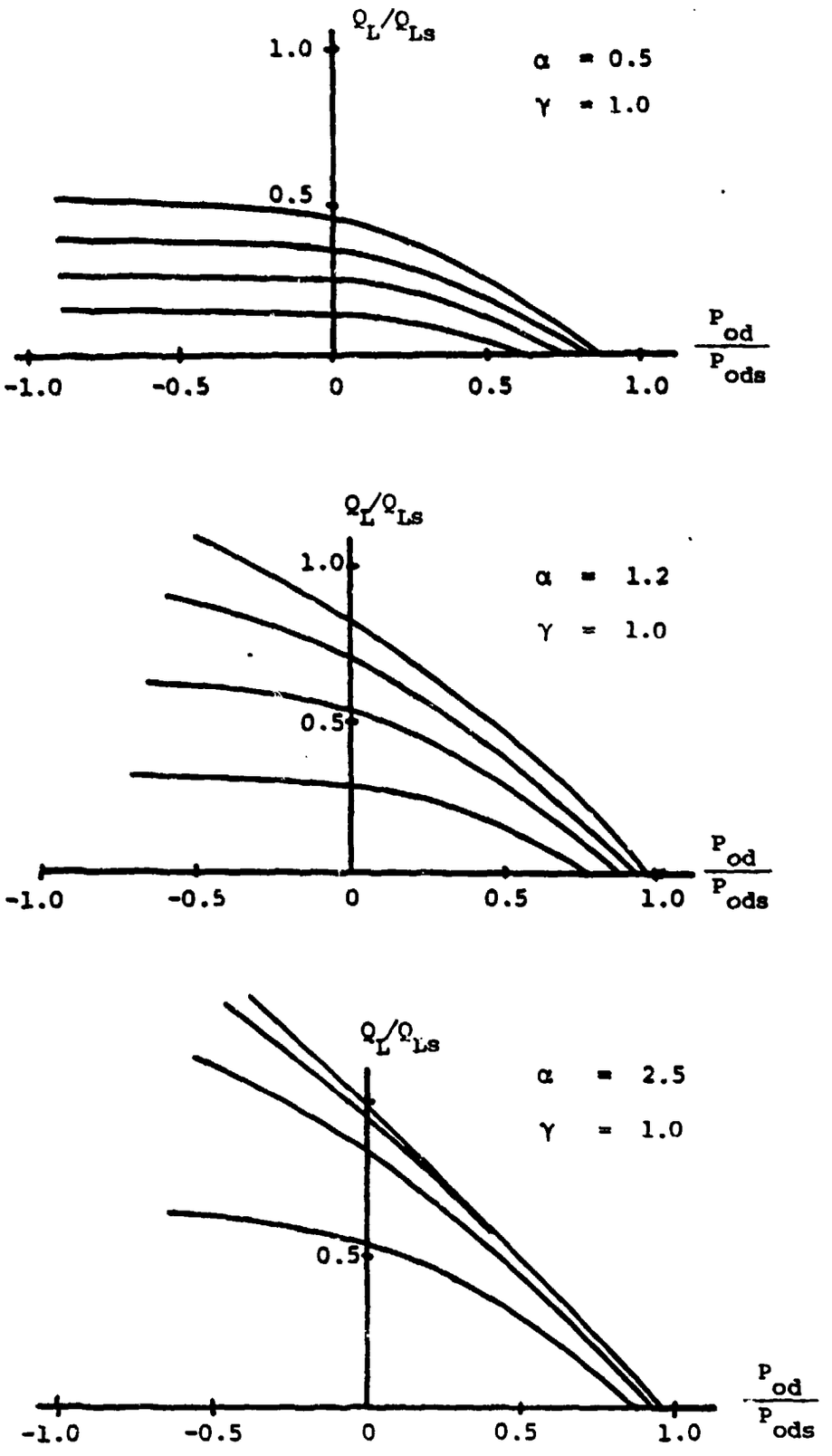

Figure 13. Effect of valve parameter α on Valve Characteristics.

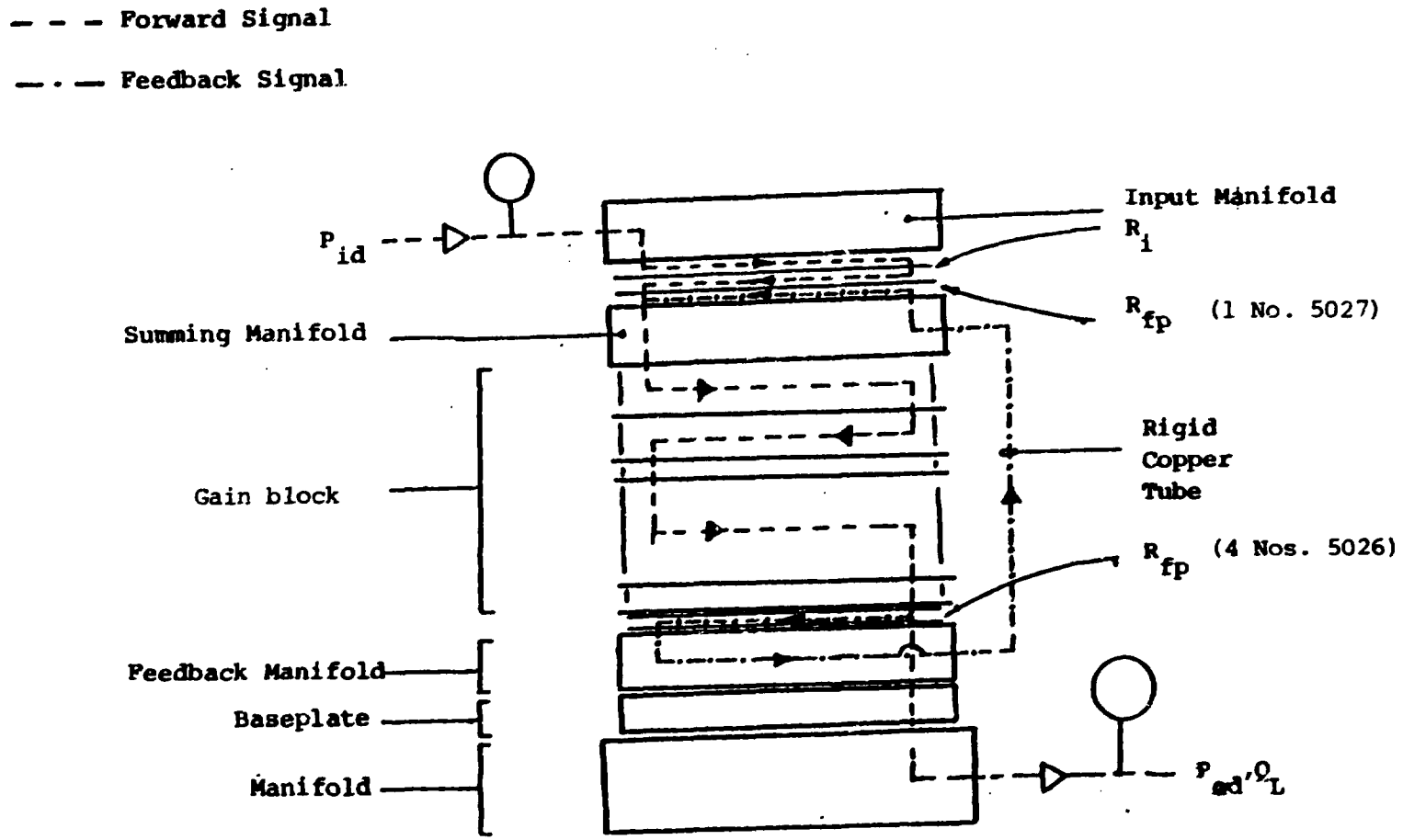

Figure 14. Servovalve construction schematics.

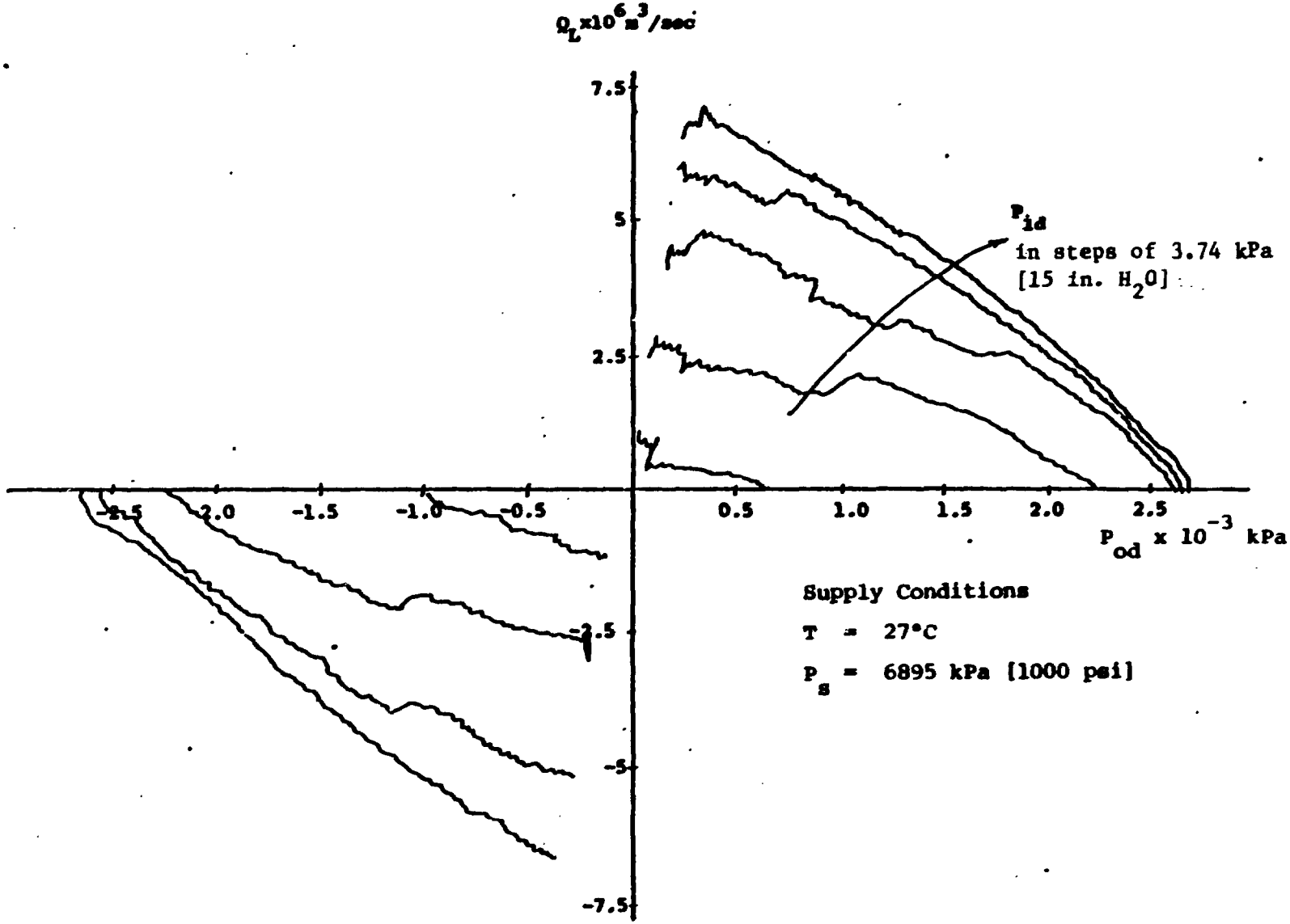

Figure 15. Experimental data of servovalve output characteristics.

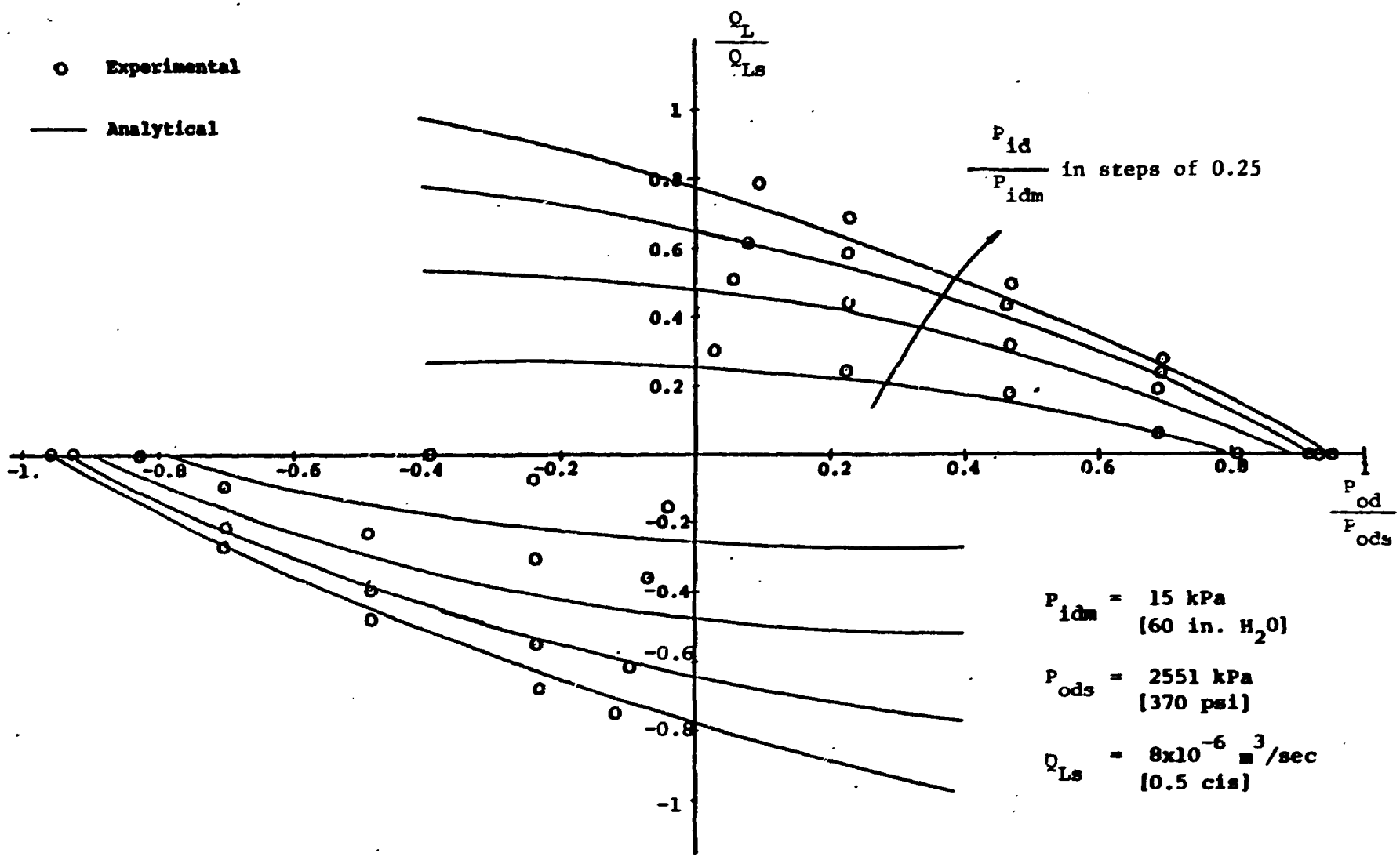

Figure 16. Comparison of experimental and analytical servovalve output characteristics.

viscosity. The effect of the change of operating Reynolds number on the blocked-load pressure gain of the LPA has been discussed in section 2.1.

The stability of the fluidic servovalve is primarily determined by the valve parameter γ which is a measure of the degree of positive pressure feedback. The value of γ can be increased by decreasing the pressure feedback resistance, or increasing the gain block pressure gain, K_p, or the value of input resistance to the point where γ is greater than one and the valve fails neutrally. The additional flow of the positive pressure feedback due to the increase in temperature tends to decrease the valve stability. On the other hand, if the positive feedback flow is reduced as a result of a decrease in temperature, the valve behaves as an amplifier with reduced feedback. To compensate for the temperature effects, the valve parameter γ must be kept at a desired constant value in the temperature range concerned. Since the ratio of two linear resistances is independent of fluid viscosity and the factor $1/(1 + R_i/R_a)$ is not significantly affected by temperature variations, the valve parameter γ is primarily dependent on the blocked-load pressure gain of the gain block, K_p.

The valve parameter α is proportional to the ratio of maximum input pressure differential, P_{idm}, to the saturation control pressure differential P_{cds}. The saturation control pressure differential, P_{cds}, decreases as the temperature increases. The maximum input pressure differential must be limited in order to keep the flow gain in a reasonable linear range. However, the linearity of the servovalve flow gain is maintained at the expense of the maximum input pressure differential, P_{idm}.

Since the gain block characteristic performance is primarily a function of final stage Reynolds number, this provides a means of temperature compensation by maintaining a constant operating Reynolds number, N_{Rf}. From the definition of the Reynolds number and the kinematic viscosity-temperature relation as written in equation (1), we have

$$\frac{N_{R_f}(T)}{N_{R_f}(T_o)} = \frac{\nu_o}{\nu}\sqrt{\frac{P_s(T)}{P_s(T_o)}} = e^{\lambda(T-T_o)}\sqrt{\frac{P_s(T)}{P_s(T_o)}} . \qquad (22)$$

If $N_{R_f}(T) = N_{R_f}(T_o)$ = constant, then

$$\frac{P_s(T)}{P_s(T_o)} = e^{-2\lambda(T-T_o)}. \tag{23}$$

Hence, the supply pressure must be varied directly proportional to the square of the fluid viscosity in order to maintain a constant Reynolds number. To decrease the high pressure required at the low temperature operating condition, the supply pressure is scheduled as a linear function of temperature, i.e.

$$\frac{P_s(T) - P_s(T_o)}{T - T_o} = \lambda_o. \tag{24}$$

The choice of λ_o depends on the temperature range considered and the maximum of safe supply pressure imposed by the hydraulic plant at the lowest temperature of interest. As an example, consider the following,

Reference temperature, $T_o = 25°C$ (77°F),

Reference pressure, $P_s(T_o) = 6895$ kPa (1000 psi),

Temperature range, $10°C < T < 50°C$, ($50°F \leq T \leq 122°F$),

Maximum supply pressure, $P_s\Big|_{max} = 11{,}032$ kPa (1600 psi),

It follows $\lambda_o = 275.8$ kPa/°C [22.2 psi/°F].

The experimental data for linearly compensated and uncompensated gain block and servovalve blocked-load pressure gain as a function of temperature are shown in figures 17 and 18. The temperature compensation based on the supply pressure scheduling significantly reduces the temperature sensitivity of both the gain block and servovalve pressure gain and successfully extends the operating range of the servovalve beyond the design temperature.

3.4 Dynamic Response

The fluidic servovalve dynamic model for small derivatives may be expressed as

$$Q_L(s) = G_q(s)P_{id}(s) - G_{qp}(s)P_{od}(s) \tag{25}$$

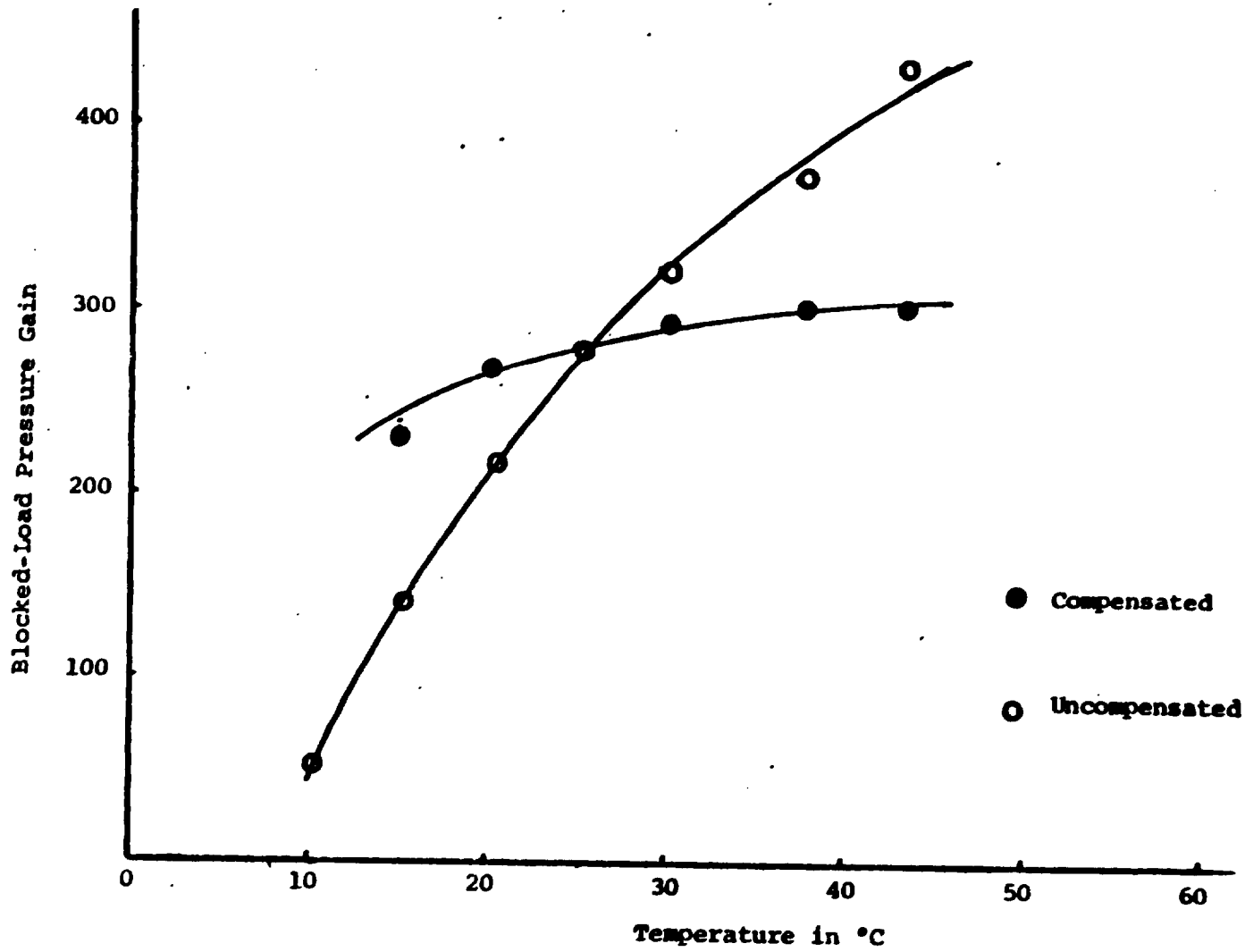

Figure 17. Gain block compensated and uncompensated blocked-load pressure gain.

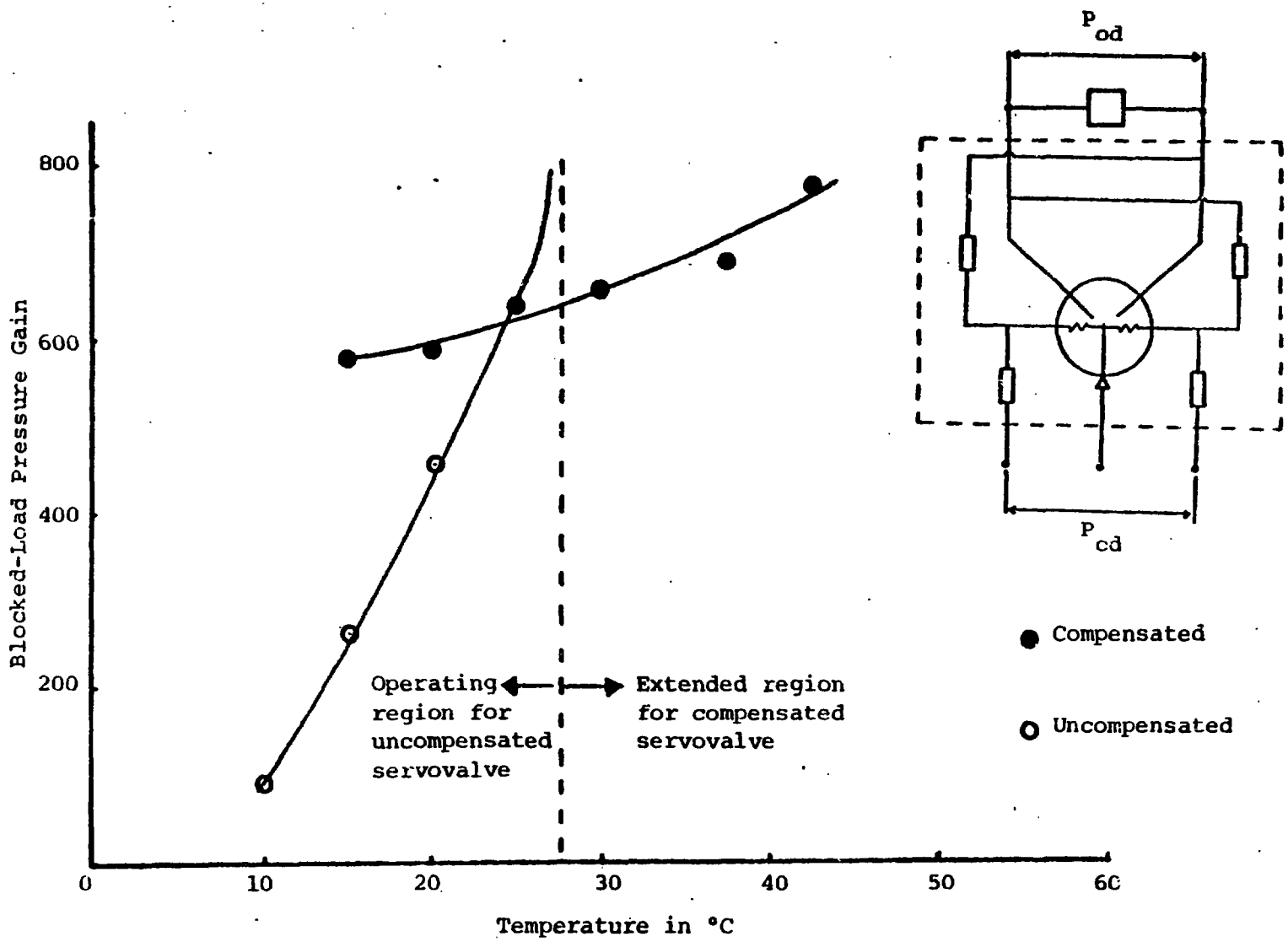

Figure 18. Fluidic servovalve compensated and uncompensated blocked-load pressure gain.

where $$G_q(s) = \left[\frac{\frac{1}{Z_i(s)}}{1 + \frac{1}{Z_a(s)}}\right] K_q(s), \quad (26)$$

$$G_{qp}(s) = G_p(s)[1 - \gamma(s)]K_{qp}(s). \quad (27)$$

$$G_p(s) = \frac{K_p(s)}{\left[1-\gamma(s)\right]\left[1 + \frac{Z_i(s)}{Z_a(s)}\right]}, \quad (28)$$

$$\gamma(s) = \frac{Z_i(s)}{Z_{fp}(s)} \cdot \frac{K_p(s)}{\left[1 + \frac{Z_i(s)}{Z_a(s)}\right]}, \quad (29)$$

s = Laplace operator.

The input $Z_i(s)$ and feedback $Z_{fp}(s)$ impedances consist of a resistance and inertance. The input deflection impedance of the gain block is $Z_a(s)$.

Two dynamic tests, flow frequency and pressure frequency response tests, have been conducted point by point on both the gain block and servovalve at a temperature of 27°C. The experimentally measured pressure and flow gain as a function of frequency are plotted in figures 19 and 20. The test data show that the flow gain of the valve reaches 90° phase shift at 80 Hz, the pressure gain reaches 90° phase shift at approximately 100 Hz and the experimentally measured pure delay time for both the pressure and flow gain is 1.1 ms.

The comparisons of the frequency response between the breadboard configuration and the integrated component fluidic servovalve are shown in figures 21 and 22. The elimination of the feedback line capacitance which is present in the breadboard configuration as described by Lee[12], leads to improved response in the integrated component fluidic servovalve. The data show that the pressure gain reaches 90° phase shift at 7 Hz for the bread-

[12] D. Lee, The Analytical and Experimental Development of a Fluidic Servovalve, Massachusetts Institute of Technology, Ph.D Thesis (April 1980).

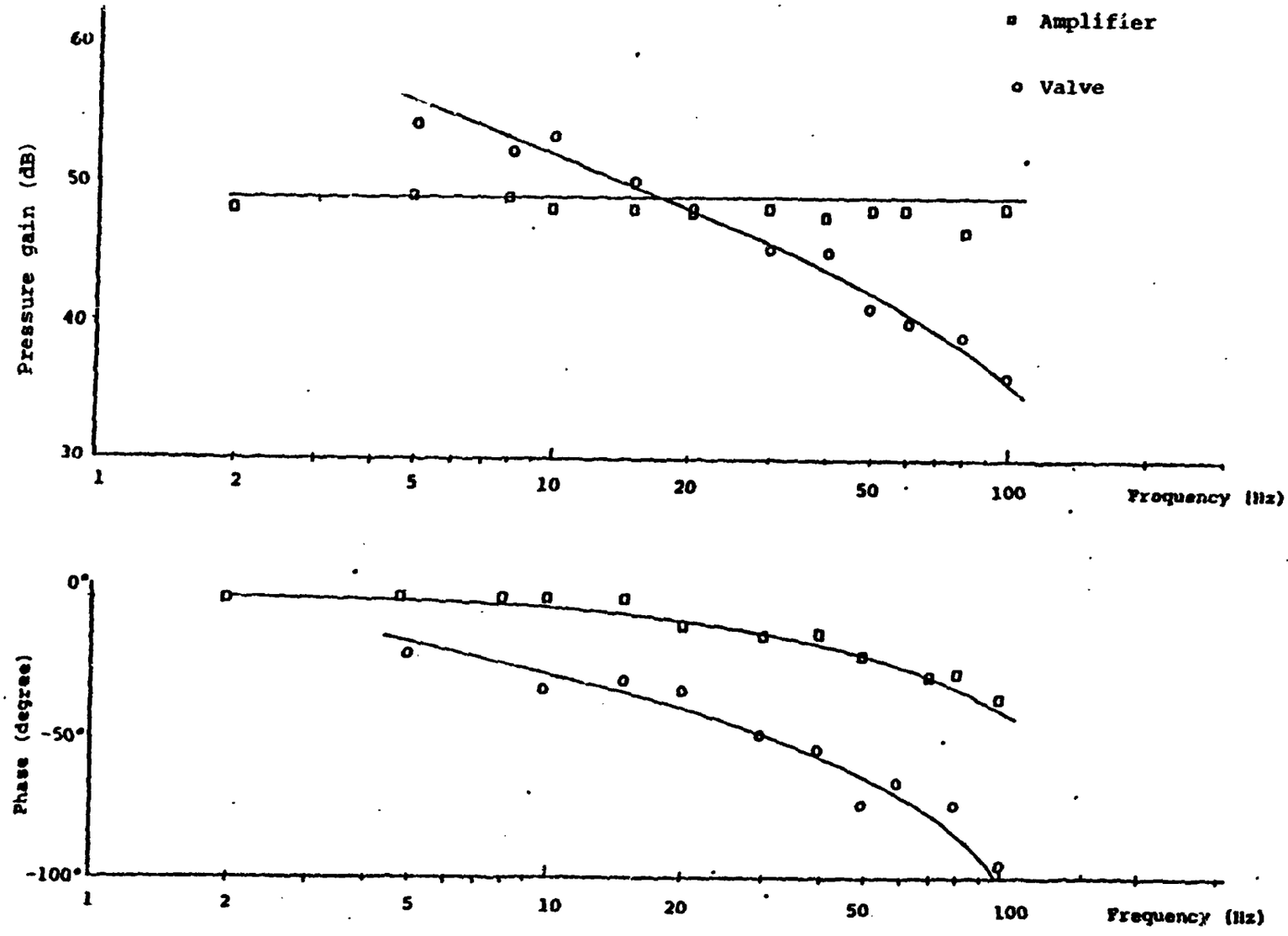

Figure 19. Gain block and servovalve blocked-load pressure gain.

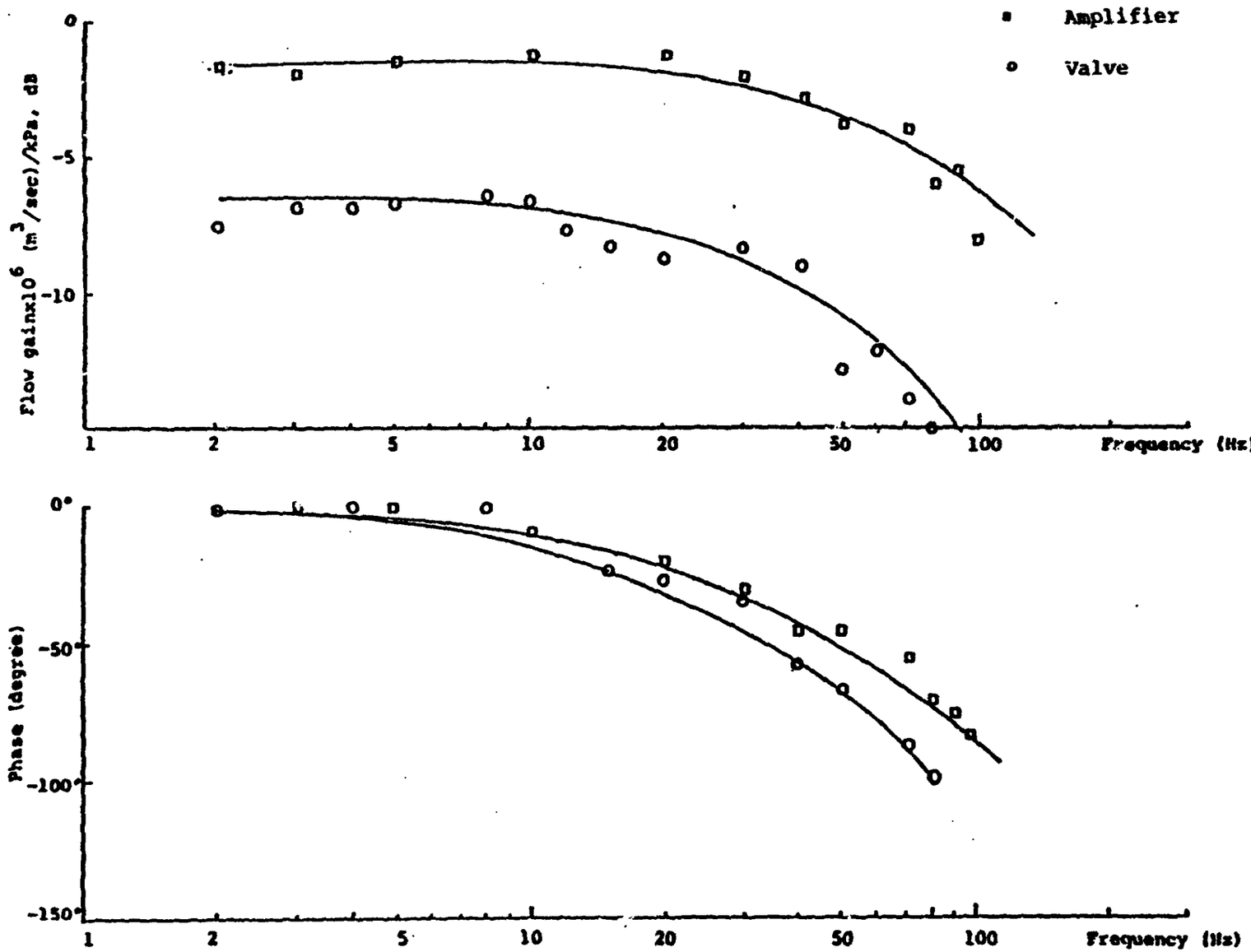

Figure 20. Gain block and servovalve no-load flow gain frequency response.

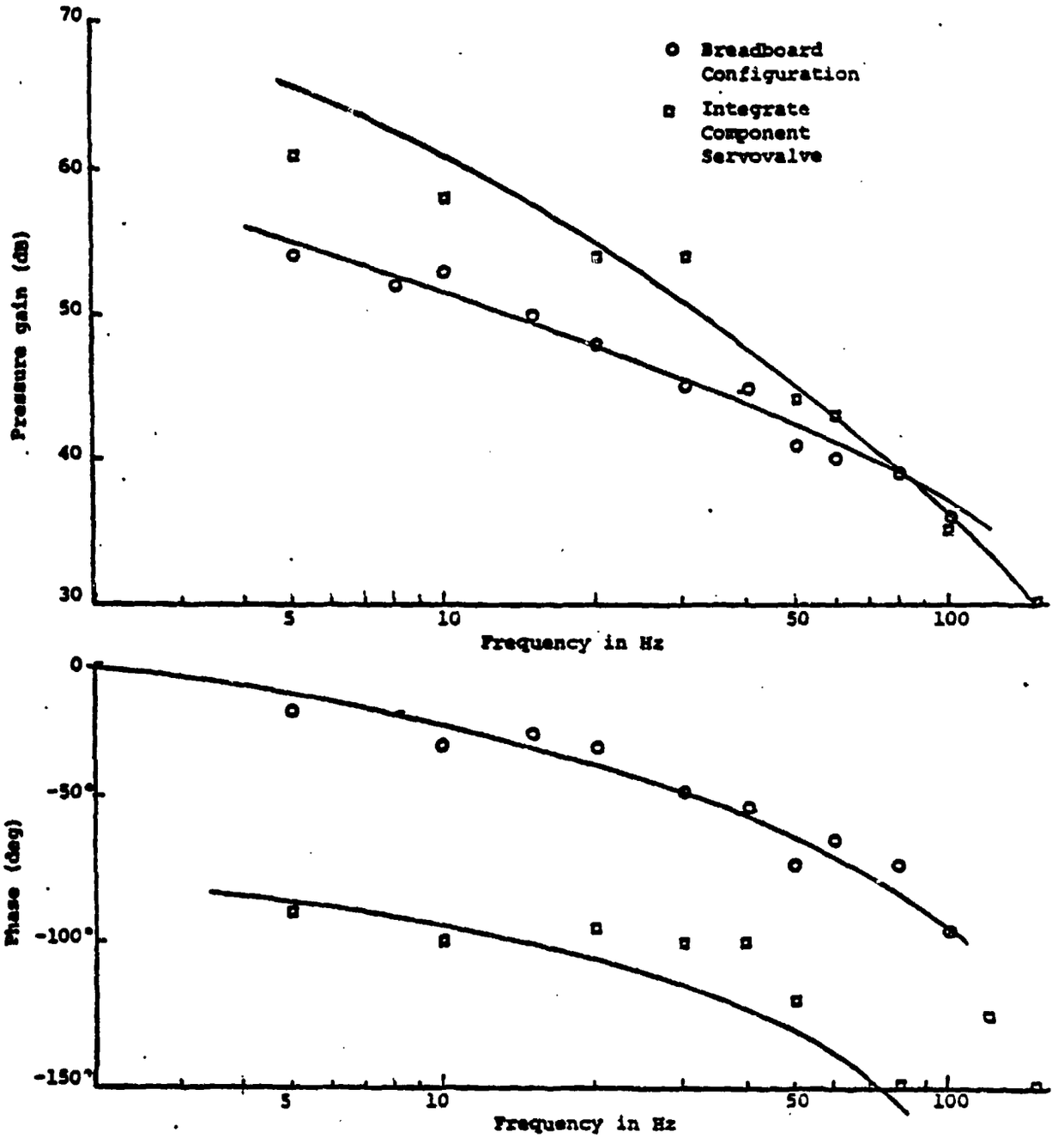

Figure 21. Comparison of blocked-load frequency response between integrated component servovalve and breadboard configuration servovalve.

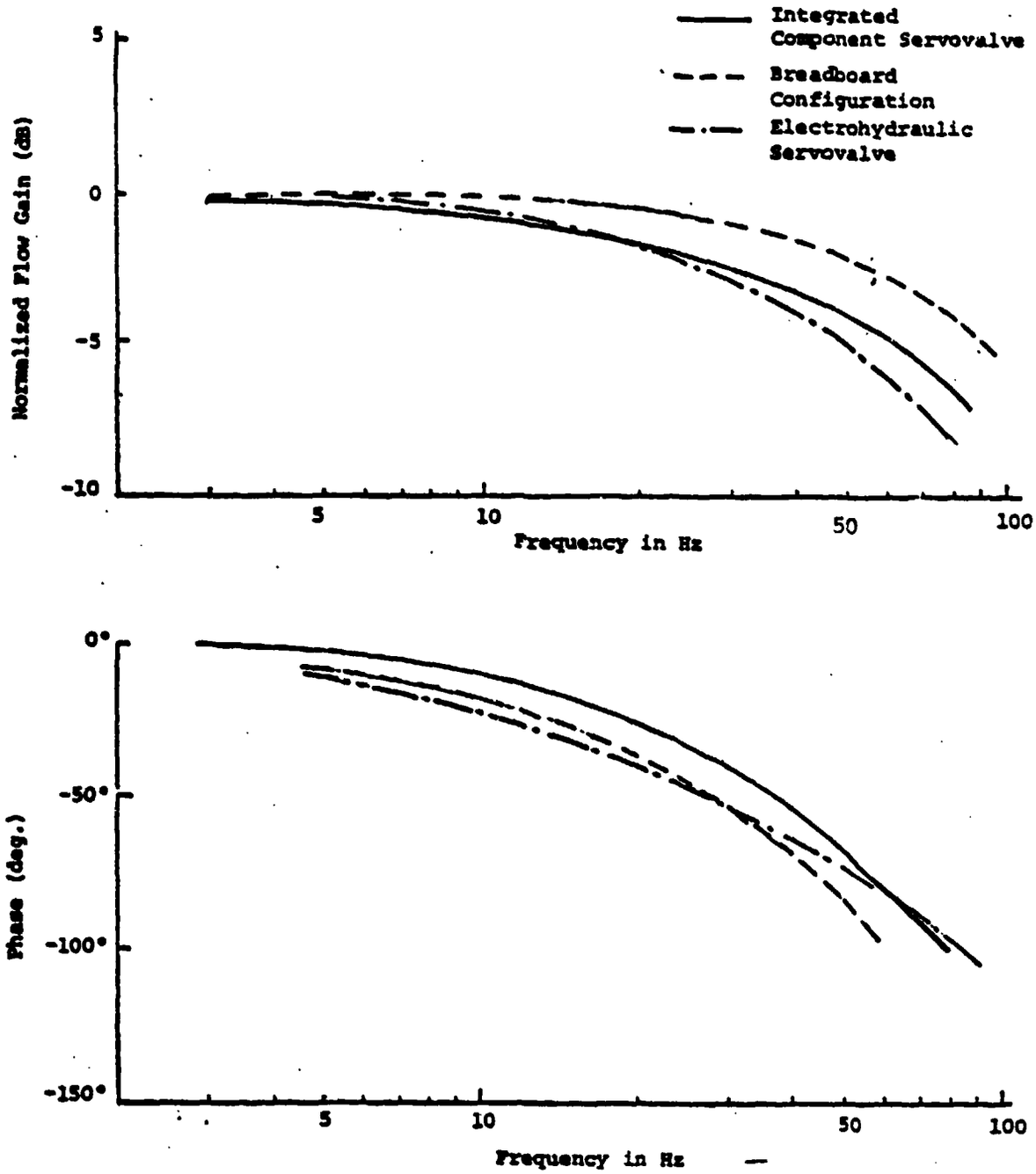

Figure 22. Comparison of no-load frequency response of integrated component servovalve, breadboard configuration and electrohydraulic servovalve.

board configuration and at 100 Hz for the integrated component configuration. figure 22 indicates that the flow gain reaches 90° phase shift at 60 Hz for the breadboard configuration and at 80 Hz for the integrated component configuration and electrohydraulic servovalve approximately. The comparison shows that a significant decrease in phase shift has been achieved and the dynamic performance of the fluidic servovalve is comparable to the electrohydraulic servovalve with standard packaging.

4. FLUIDIC POSITION SERVO

A closed-loop fluidic position servo has been constructed as shown in figure 23. An integrated component fluidic servovalve, similar to that discussed in the preceeding section, has been used as a power modulation element. A fluidic summing amplifier is also used to perform signal processing. In addition, a fluidic feedback transducer has been developed so that the mechanical displacement sensing is fedback in the form of a fluidic signal. The elements in the control system are described in the following paragraphs.

4.1 Fluidic Summer

The fluidic summer is shown in figure 23. For low frequency applications, the transfer function of the fluidic summer may be expressed as

$$K_s(s) = K_{ss} e^{-\tau_s s} \tag{30}$$

where

$$K_{ss} = \frac{G_{p,LPA}}{2 + \frac{R_1}{R_{as}}}, \tag{31}$$

$G_{p,LPA}$ = LPA blocked-load pressure gain,
R_1 = Summer input resistance,
R_{as} = LPA deflection resistance,
τ_s = LPA pure time delay.

4.2 Mechanical-Fluidic Displacement Transducer

The mechanical-fluidic displacement transducer is essentially a position feedback sensor in which the mechanical translational displacement is transformed into a fluidic signal. The electrical equivalent and the construction schematic are shown in figure 24. The displacement trans-

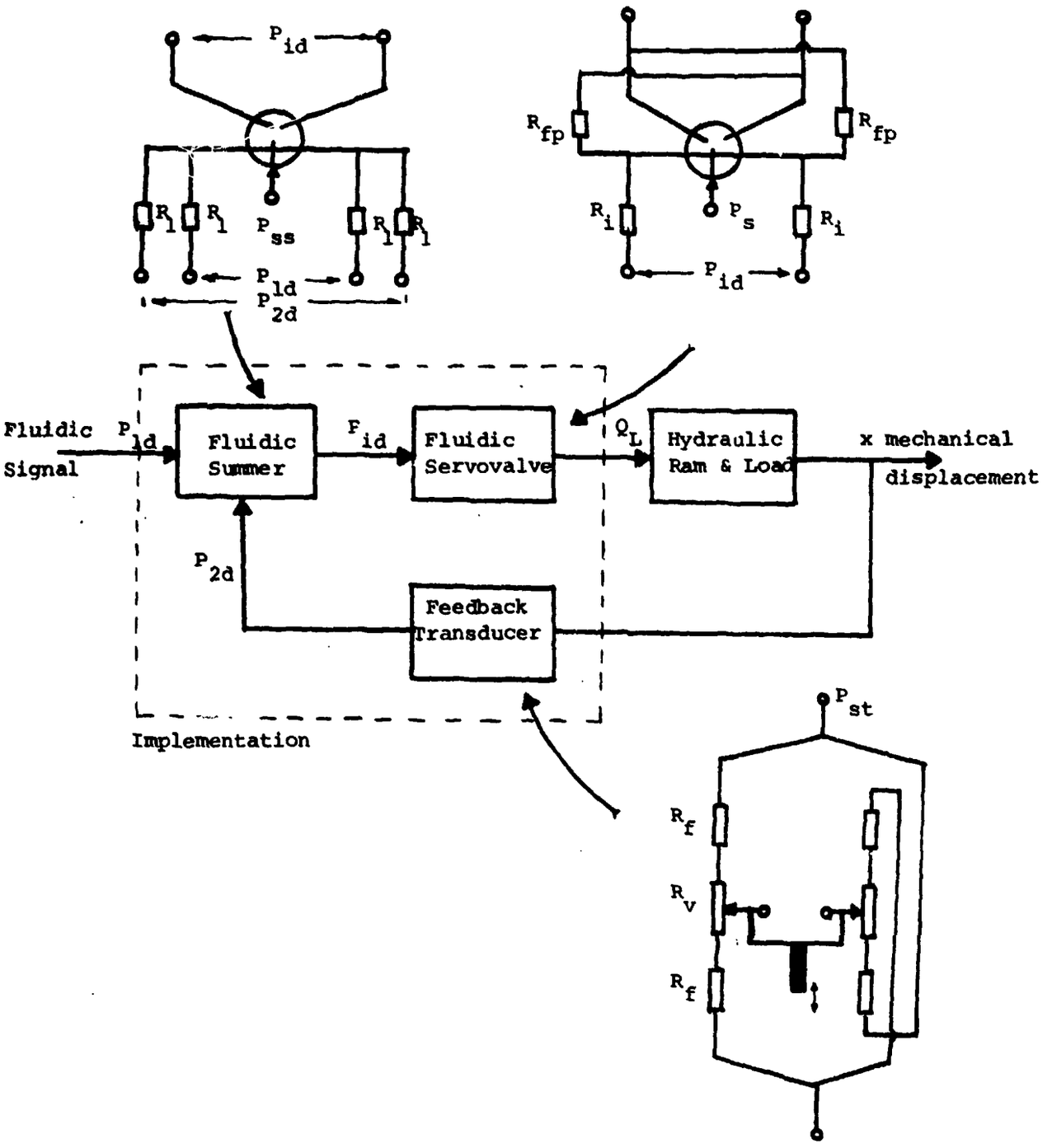

Figure 23. Fluidic position servo block diagram.

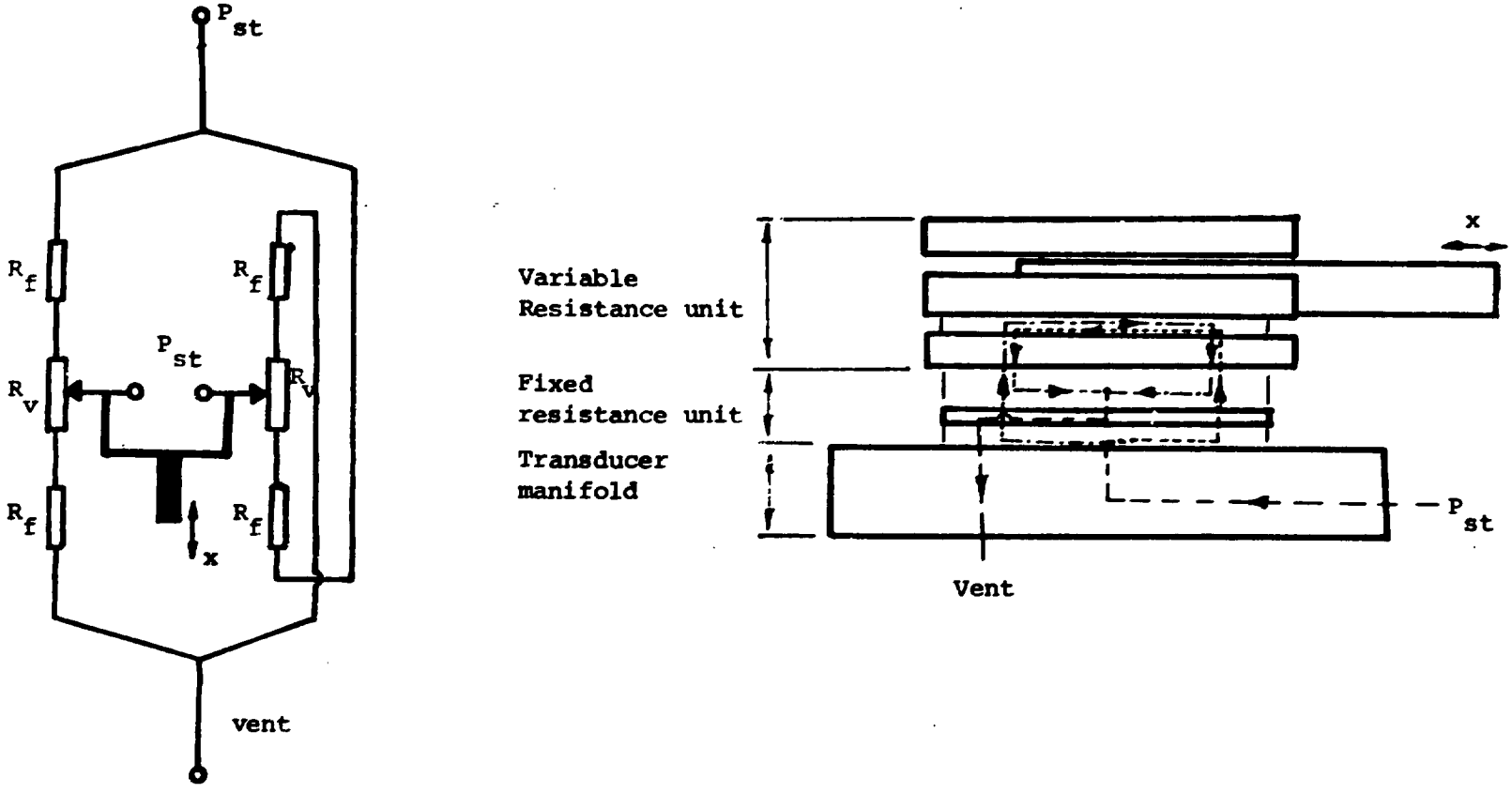

(a) Electricl equivalent (b) Construction schematics

Figure 24. Mechanical-fluidic displacement transducer schematics.

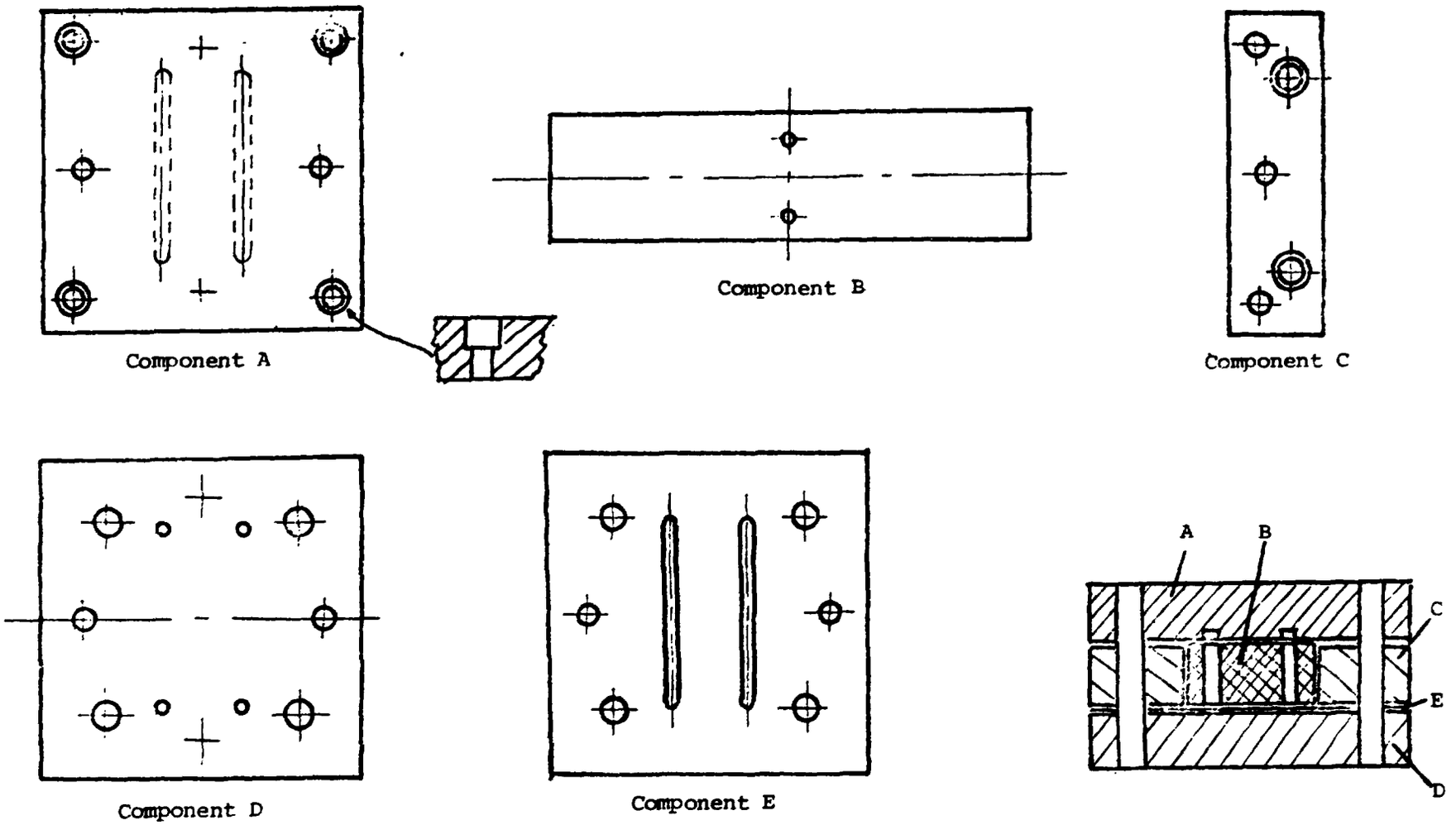

(c) Detail of variable resistance unit

Figure 24. Mechanical-fluidic displacement transducer schematic.

ducer may be considered as a fluidic resistance bridge. It consists of two pairs of fixed resistors and a pair of variable resistors.

The transducer sensitivity at blocked-load may be derived from circuit analysis

$$K_t(s) = \frac{P_{dt}(s)}{x(s)} = \frac{P_{st}}{x_m}\left[\frac{1}{1 + 2\dfrac{R_f + sL_f}{R_v + sL_v}}\right] \tag{32}$$

where

P_{dt} = output pressure differential of transducer,
P_{st} = supply pressure of transducer,
x = translational displacement,
x_m = half stoke,
R_f, R_v = fixed and variable resistance, respectively,
L_f, L_v = fixed and variable inertance, respectively.

The resistance and inertance of the channel resistance are

$$R_c = \frac{12\mu x}{bh^3} \qquad \text{for } b \gg h,$$

$$L_c = \frac{\rho x}{bh}, \tag{33}$$

and the time constant of the channel resistance, τ_c, may be expressed as

$$\tau_c = \frac{L_c}{R_c} = \frac{h^2}{12\nu}. \tag{34}$$

If equal channel heights are chosen for both fixed and variable resistances, the transfer function of the mechanical-fluidic displacement transducer may be simplified from equations (32) and (34) as

$$K_t(s) = \left(\frac{1}{1 + 2\dfrac{R_f}{R_v}}\right)\frac{P_{st}}{x_m} \tag{35}$$

and the dynamics of the transducer may be neglected.

4.3 Fluidic Servovalve

The characteristic performance of the fluidic servovalve has been discussed in section 3.2. In the application of the fluidic servovalve in

the position servo system, the output flow/pressure characteristics must be designed to meet the particular ram and load requirements. The actuator and load described as part of the position servo by Lee[13] has been used in this study so that a step response between the fluidic position servo and a conventional electrohydraulic position servo may be compared directly.

From the characteristics of the fluidic servovalve and the parameters of the actuator and load, the dimensionless group

$$\frac{G_{qp} d}{A_r^2} << 1$$

and the time constant,

$$\frac{m}{d} \leq 1 \text{ second}$$

may be calculated

where

$G_{qp}(s) = G_q(s)/G_p(s)$

d = damping coefficient

A_r = area of ram,

m = mass of load.

As a result of the high pressure gain and small load mass and friction, the load dynamics for this particular system can be neglected and the dynamic flow gain of the servovalve is the dominant valve performance parameter. The experimentally determined flow gain from section 3.4 is

$$G_q(s) = \frac{Q_L(s)}{P_{id}(s)} = \frac{G_{qs} e^{-\tau_v s}}{(1 + \tau_q s)} \qquad (36)$$

where

G_{qs} = steady state servovalve flow gain,

τ_v = pure time delay of the servovalve,

τ_q = first order time constant.

4.4 Closed-Loop Fluidic Position Servo

With the dynamic characteristic performance of the fluidic summer, fluidic feedback transducer and fluidic servovalve predicted in sections

4.1, 4.2 and 4.3 respectively, the fluidic position servo can be represented by the block diagram shown in figure 25. The open loop transfer function of position servo may be expressed as

$$GH(s) = \frac{Ke^{-\tau s}}{s(1+\tau_q s)} \qquad (37)$$

where

$$K = \frac{K_t \cdot K_{ss} \cdot G_{qs}}{A_r},$$

$$\tau = \tau_v + \tau_s.$$

The dynamic performance of the closed-loop position servo may be expressed in terms of two dimensionless parameters, namely, the normalized gain $K\tau$, and the normalized characteristic time constant τ/τ_q and may be analyzed by Root Locus analysis. Normalized gain for zero damping, which indicates the limit of closed-loop stability, and normalized gain for critical damping, which corresponds to a step response with no overshoot, are of particular interest. $K\tau$ corresponding to $\xi = 0$ and $\xi = 1$ are plotted as a function of τ/τ_q in figure 25. For simplicity and as a first-order guide in selecting the combination of $K\tau$ and τ/τ_q, the damping ratio ξ and normalized natural frequency, $\omega_n\tau$ are plotted against the normalized $K\tau$ with τ/τ_q as a parameter in figure 26.

4.5 Implementation

A fluidic position servo has been constructed and tested. The construction is shown in figure 27. A flapper-nozzle valve with an electrical torque motor has been used as a fluidic signal generator.

The gain block, used in the servo is a modified form of the gain block described in section 3 in which the steady state flow gain has been increased and the transport time delay has been reduced with no change in blocked-load pressure gain at the design temperature of 25°C. The increase of the no-load flow gain provides improved servo frequency response and has been achieved by increasing the number of sections in parallel in the final stage and by operating the servovalve at a higher supply pressure whereas the decrease of the pure time delay is achieved by using LPA's with smaller nozzle throat width ($x_{sp}/b_s = 8$) for first and second stages. The

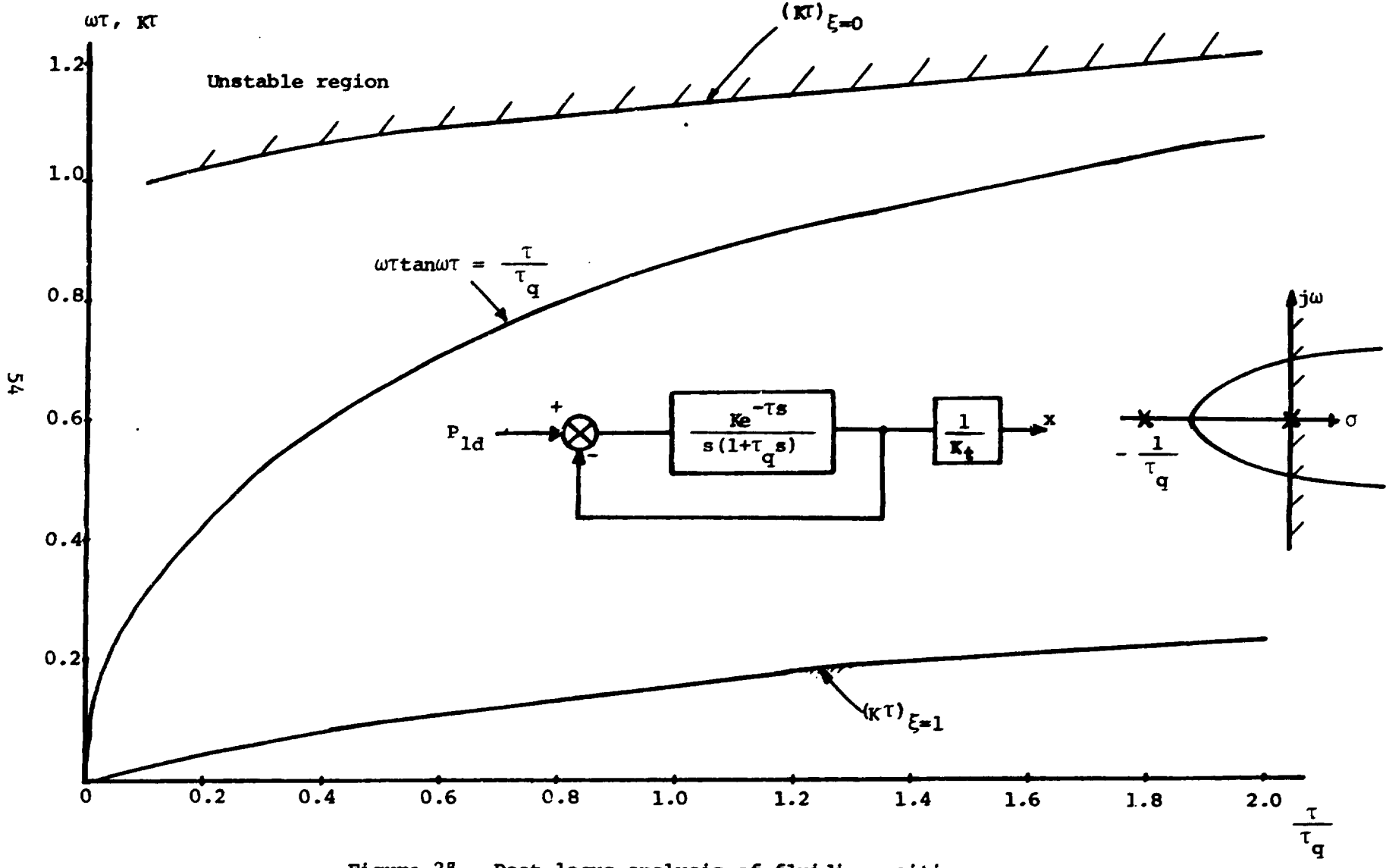

Figure 23. Root locus analysis of fluidic position servo.

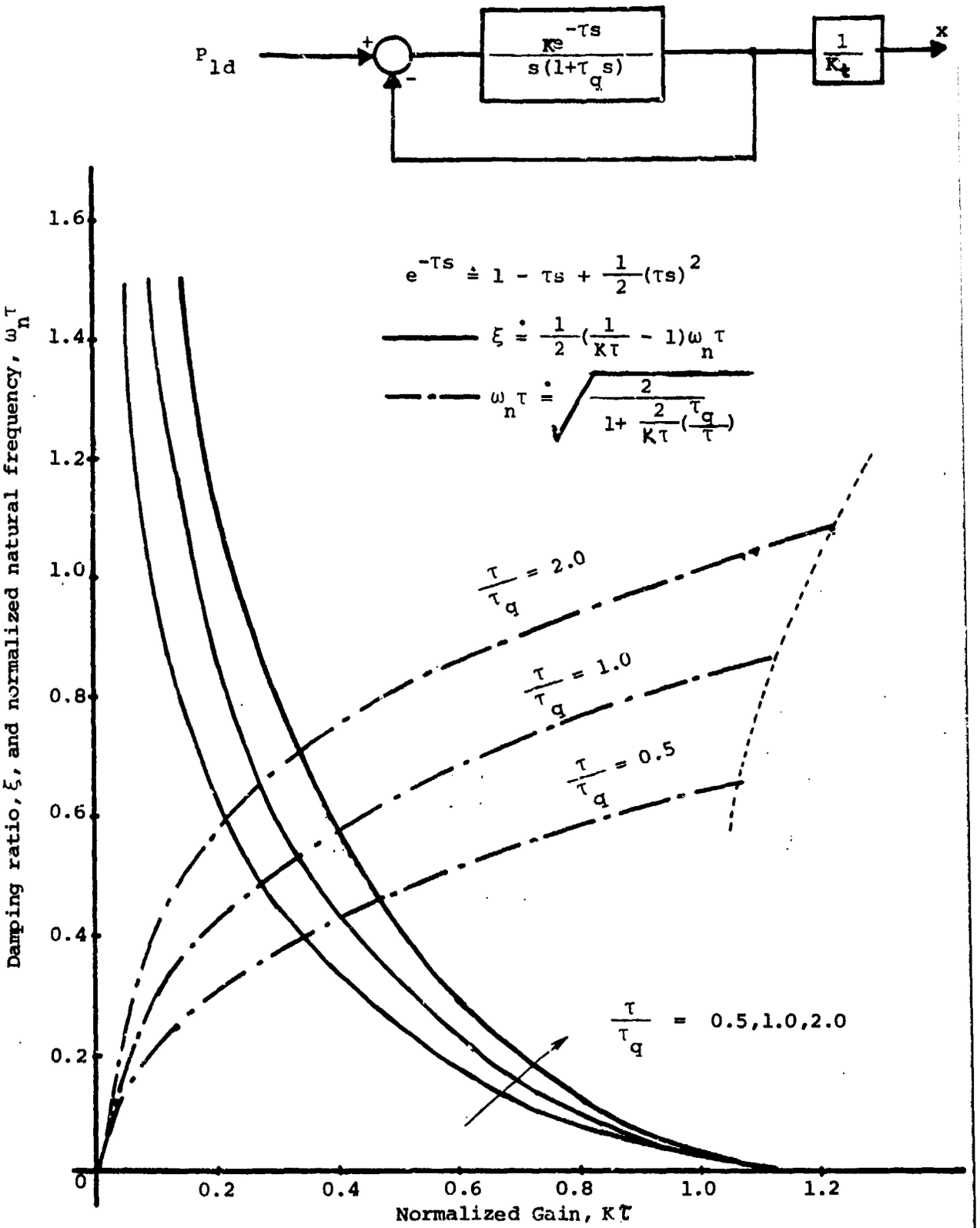

Figure 26. ξ and $\omega_n\tau$ of fluidic position servo.

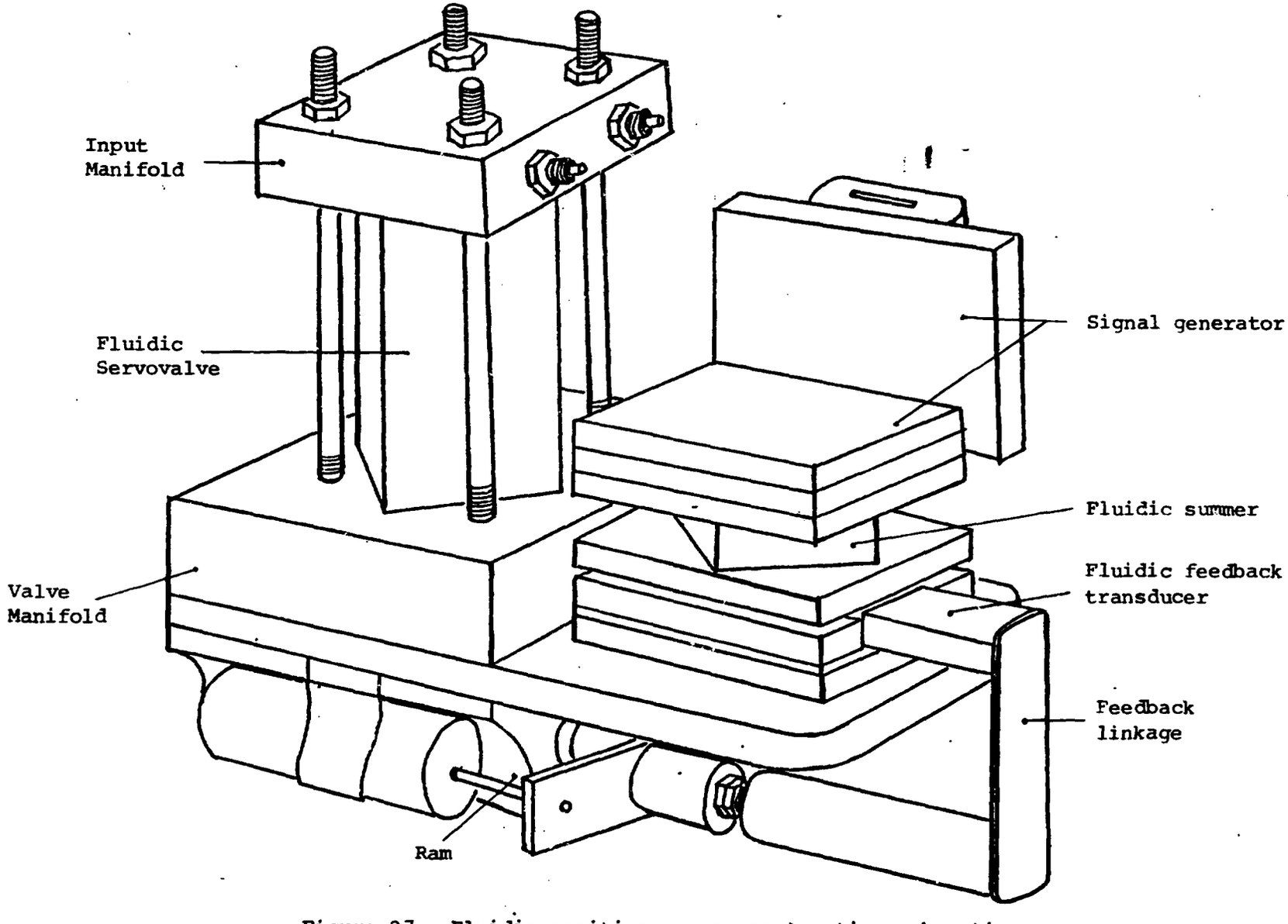

Figure 27. Fluidic position servo construction schematics.

increase in first and second stage gain, resulting from the higher aspect ratio, is designed to offset the additional pressure drop. Hence, K_p has not been varied significantly. The same input and feedback resistors as described in section 3.2 have been used to construct the servovalve.

The fluidic servo components are summarized in table 4. The components have been tested individually for both static and dynamic performance. The data are presented in figures 28 through 33 for the fluidic summer, displacement transducer and servovalve respectively. As shown in table 5, in which the essential servo component parameters are summarized, the servovalve flow gain has been increased by a factor of 2.2 and the pure time delay has been successfully reduced from 1.1 ms to 0.65 ms in comparison to the value of section 3. The displacement transducer exhibits a linear characteristic throughout the entire stroke tested in a blocked load condition and significantly solves the mechanical-to-fluidic interface problems encountered in the previous investigations.[13]

The fluidic position servo response has been calculated based on responses to step inputs. The experimental data, in figure 34 show that the fluidic position servo design with 5 percent overshoot exhibits performance comparable to the commercial electrohydraulic position servo and a significant improvement over the hydraulic position servo described by Lee and Wormley.[13]

Figure 35 compares the experimental and analytical step responses for the fluidic position servo. The preliminary analytical pure time delay based on the sum of LPA transport time lags in both the fluid in summer and servovalve is observed to be smaller than the measured time delay of the servo. Since the dynamic responses of the components have been measured individiaully, the additional time delay may be attributed to the interconnections between the components of the fluidic position servo.

5. SUMMARY AND CONCLUSIONS

The characteristic performance of HDL fluidic integrated components essential for servovalve design have been evaluated as a function of supply

---

[13] D. Lee and D.N. Wormley, Multistage Hydraulic Summing and Signal Processing Amplifiers and Fluidic Input Servovalve Development, Harry Diamond Laboratories, HDL-CR-76-233-1 (1976).

TABLE 4 FLUIDIC POSITION SERVO COMPONENT CONFIGURATION

FLUIDIC SUMMER		
LPA design 81505	σ = 1.666	b_s = 0.375 mm
N'_R = 90, $G_{p,LPA}$	10.5	
R_{as}	1.45×10^{11} N-s/m^5	350 psi/cis
Input resistance, R_1	6.863×10^{9} N-s/m^5	16.5 psi/cis

MECHANICAL-FLUIDIC DISPLACEMENT TRANSDUCER		
Variable resistance, R_v	2.03×10^{10} N-s/m^5	49 psi/cis
Fixed resistance, R_f	1.491×10^{10} N-s/m^5	36 psi/cis

FLUIDIC SERVOVALVE *

Amplifier

Stage	LPA	σ	No. of sections
1	x1505	1.000	5
2	x61505	0.667	4
3	x61505	0.333	12

Pressure Reducer

Stage	Nozzle	No. of sections
1	5221A-20	6
2	5221A-20	8
3	direct supply	—

*Supply pressure, P_s = 10.343 kPa (1500 psi)

TABLE 5 VALUES OF PARAMETERS OF FLUIDIC POSITION SERVO

ACTUATOR			
Area,	A_r	432 mm^2	0.67 in^2
Volume (single side)	V	8.19×10^3 mm^3	0.5 in^3
Oil Bulk Modulus,	β	1.38×10^6 kPa	2×10^5 psi
LOAD			
Mass,	m	16.65 kg	0.095 lb-s^2/in
Damping constant,	d	29.6 N-s/m	0.169 lb-s/in
FLUIDIC SUMMER			
Steady state gain,	K_{ss}	5	
Pure time delay,	τ_s	0.35 ms	
MECHANICAL-FLUIDIC DISPLACEMENT TRANSDUCER			
Transducer sensitivity,	K_t	11 kPa/mm	40.5 psi/in
FLUIDIC SERVOVALVE			
Steady state flow gain,	G_{qs}	1.207×10^{-9} m^5/N-s	0.5 cis/psi
Pure time delay,	τ_v	0.65 ms	
1^{st} order time constant,	τ_q	5.3 ms	

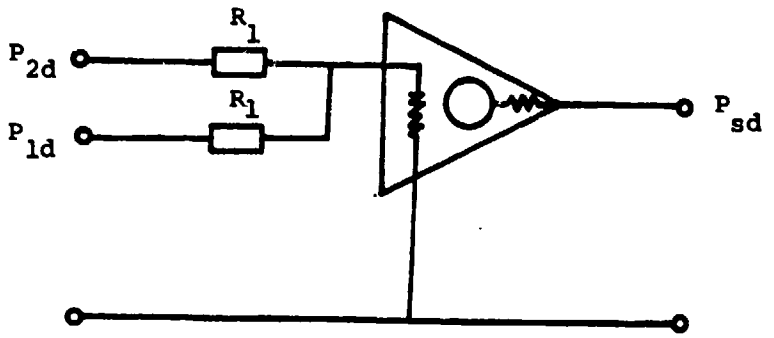

Fluidic Summer Schematic

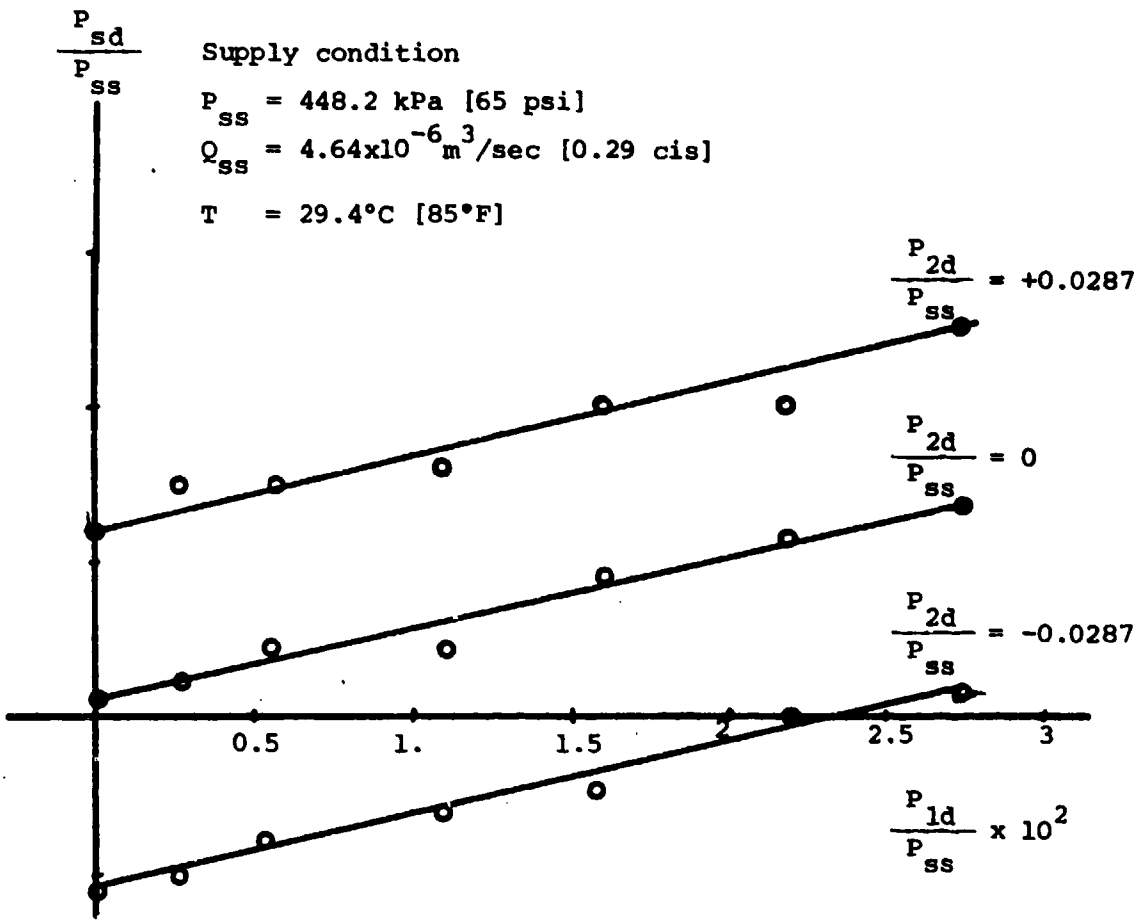

Figure 28. Fluidic summer schematic and static characteristics.

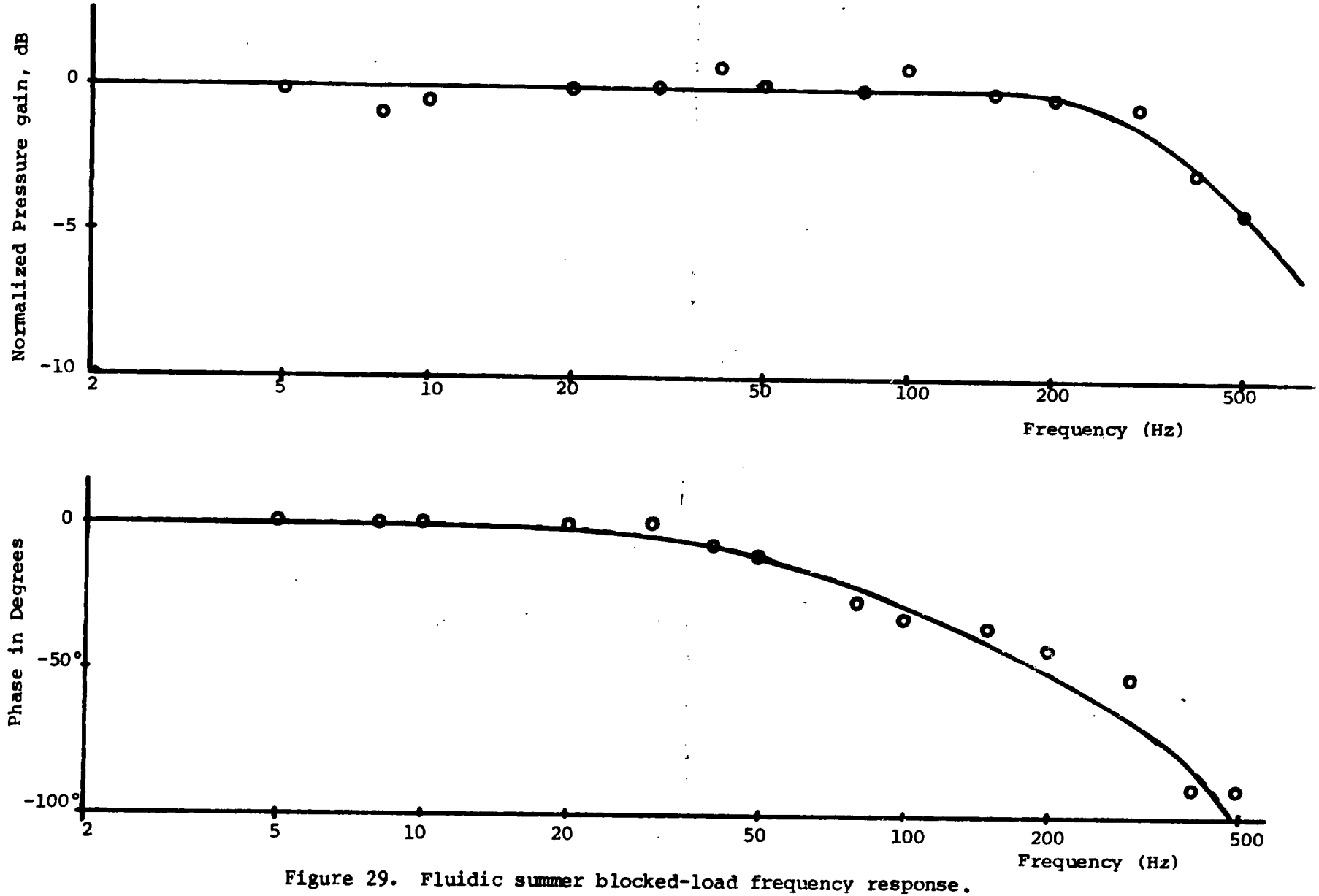

Figure 29. Fluidic summer blocked-load frequency response.

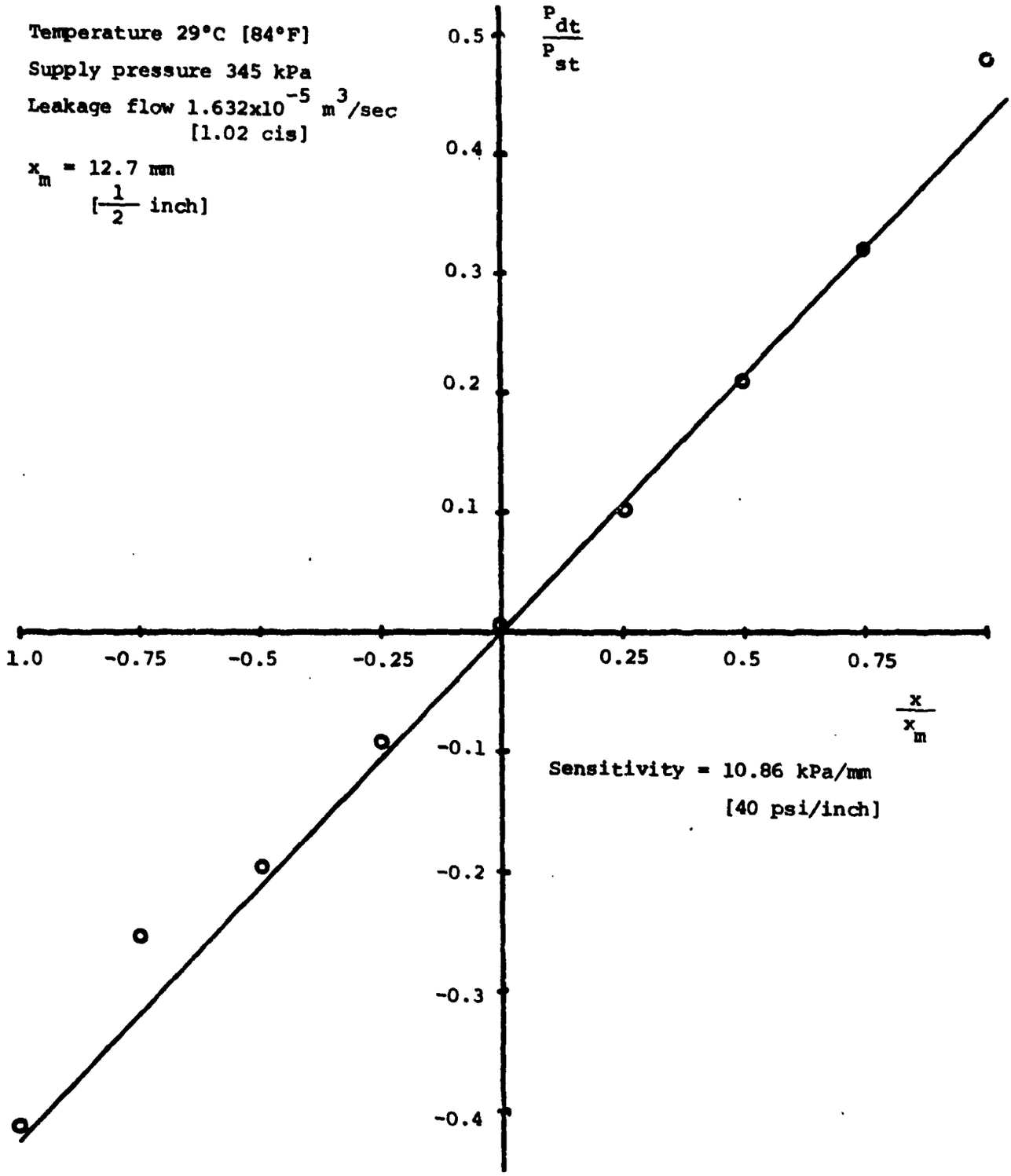

Figure 30. Displacement transducer blocked-load static characteristics.

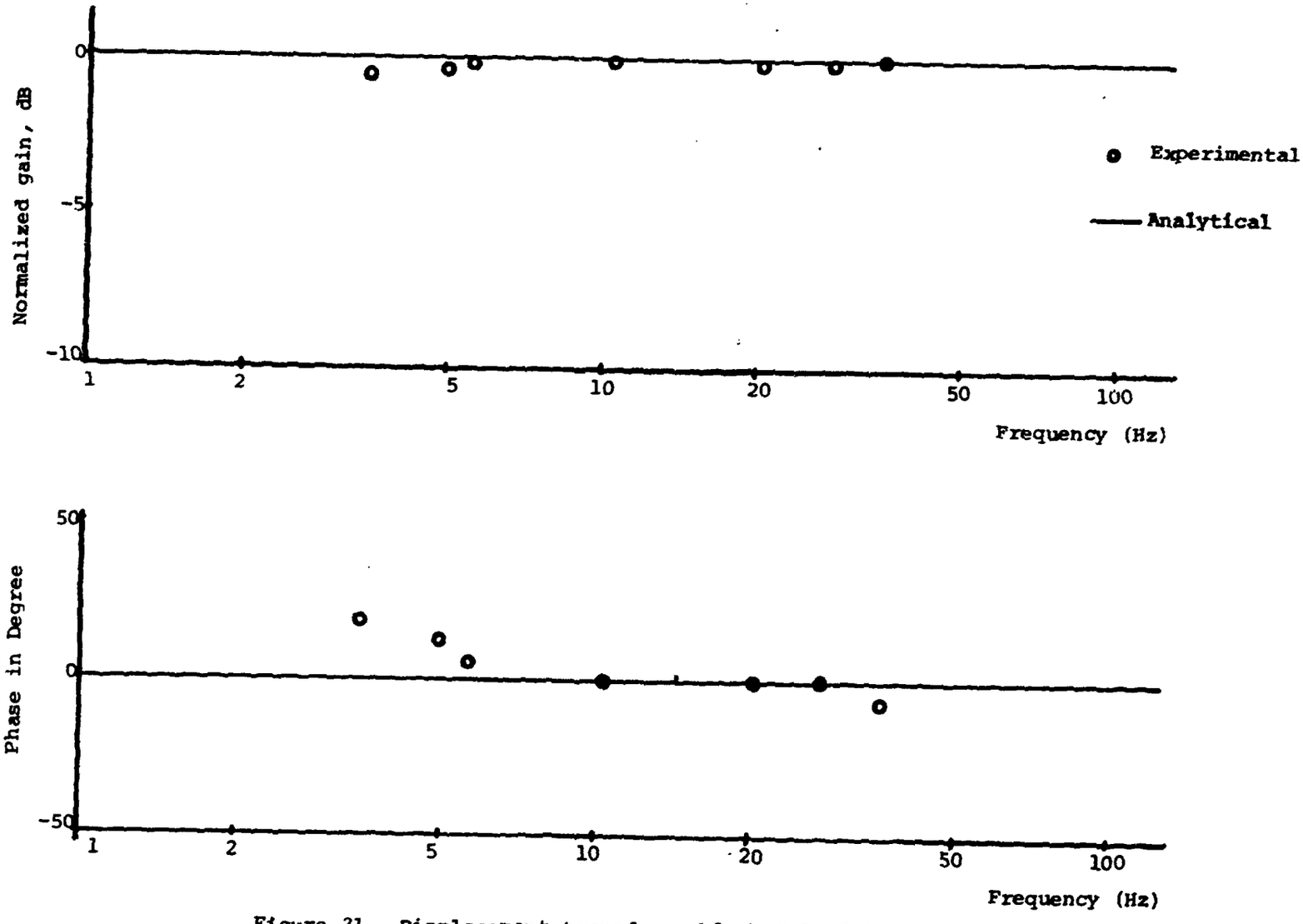

Figure 31. Displacement transducer blocked-load frequency response.

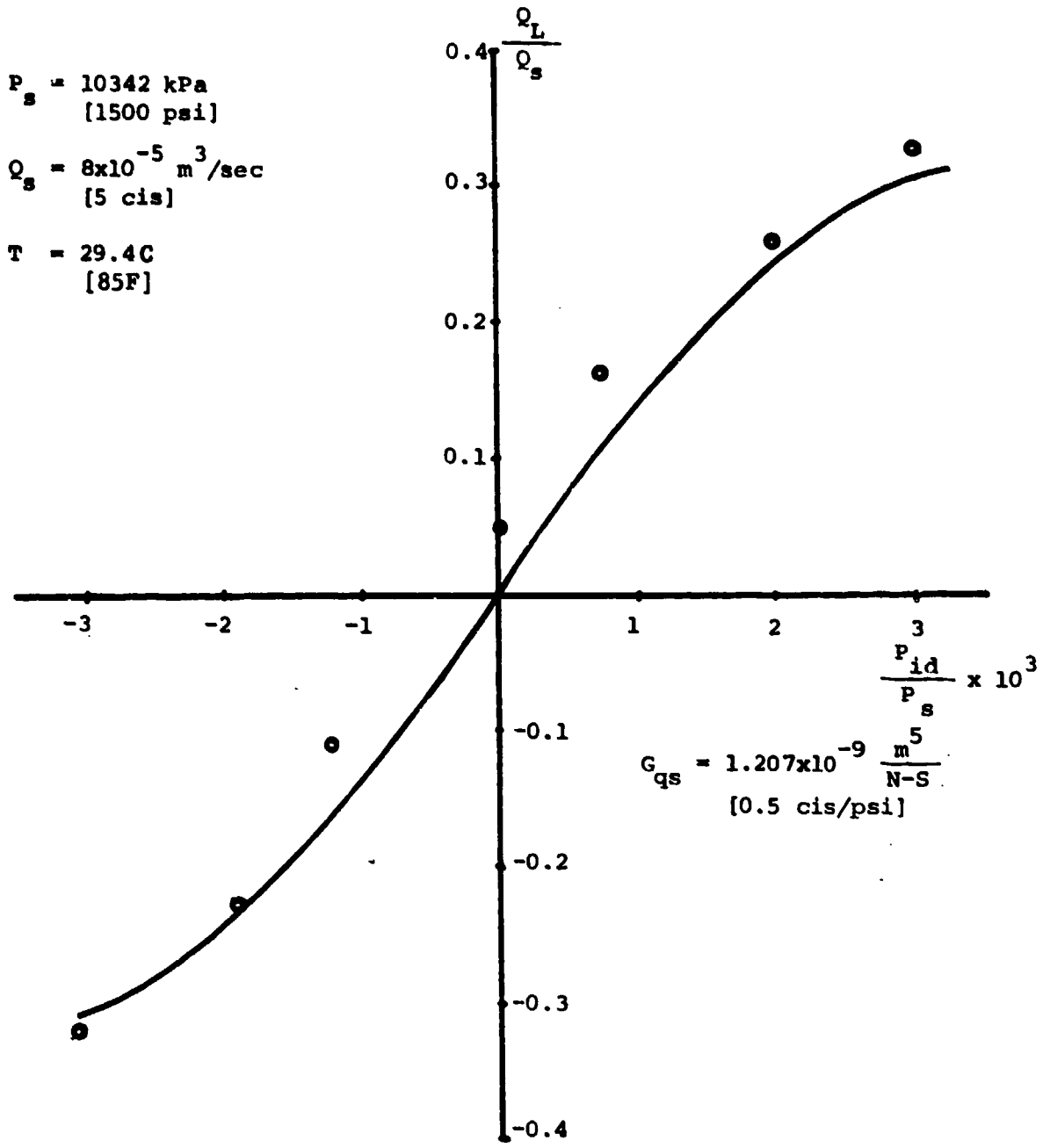

Figure 32. Fluidic servovalve no-load static characteristics.

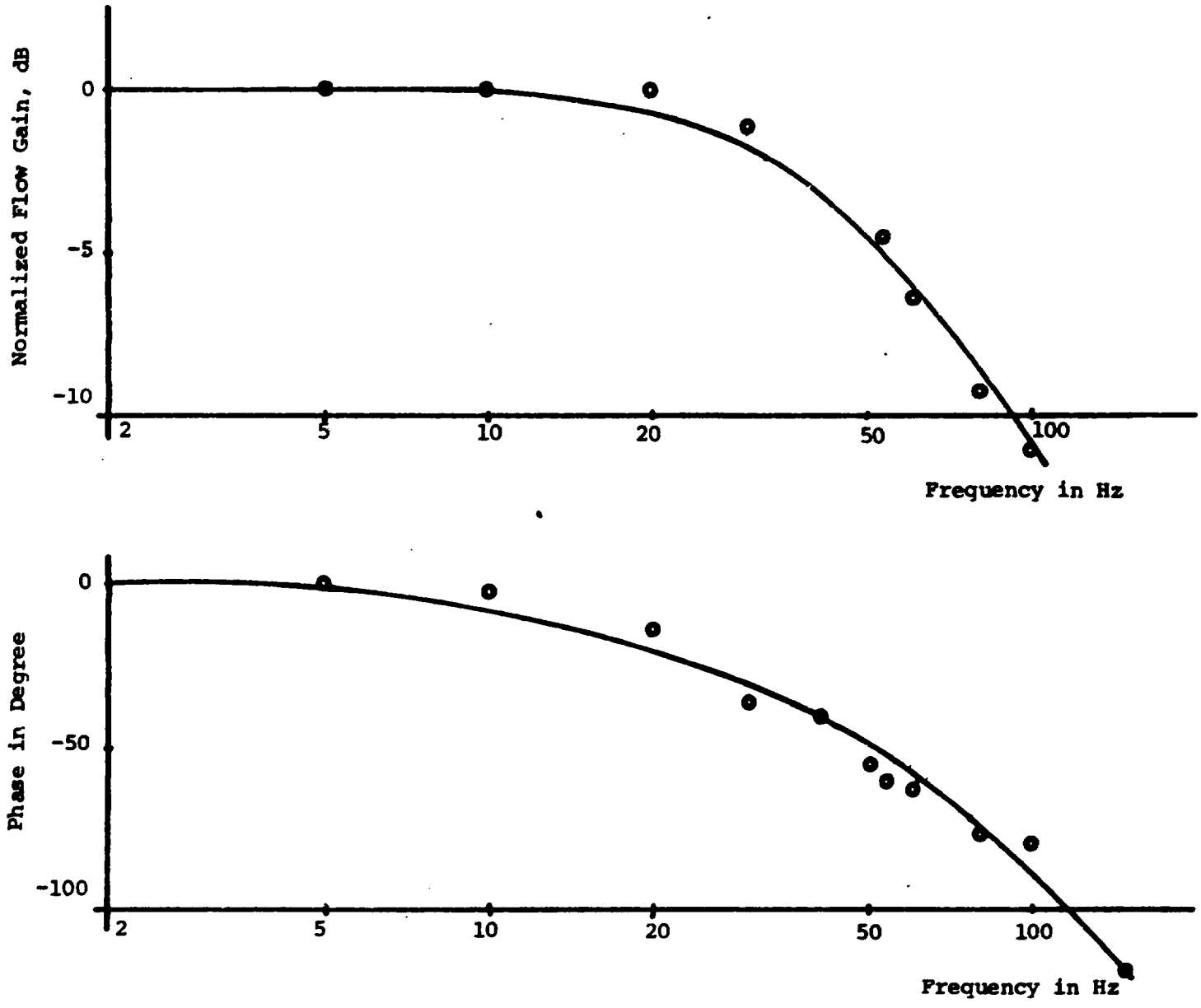

Figure 33. Fluidic servovalve no-load frequency response.

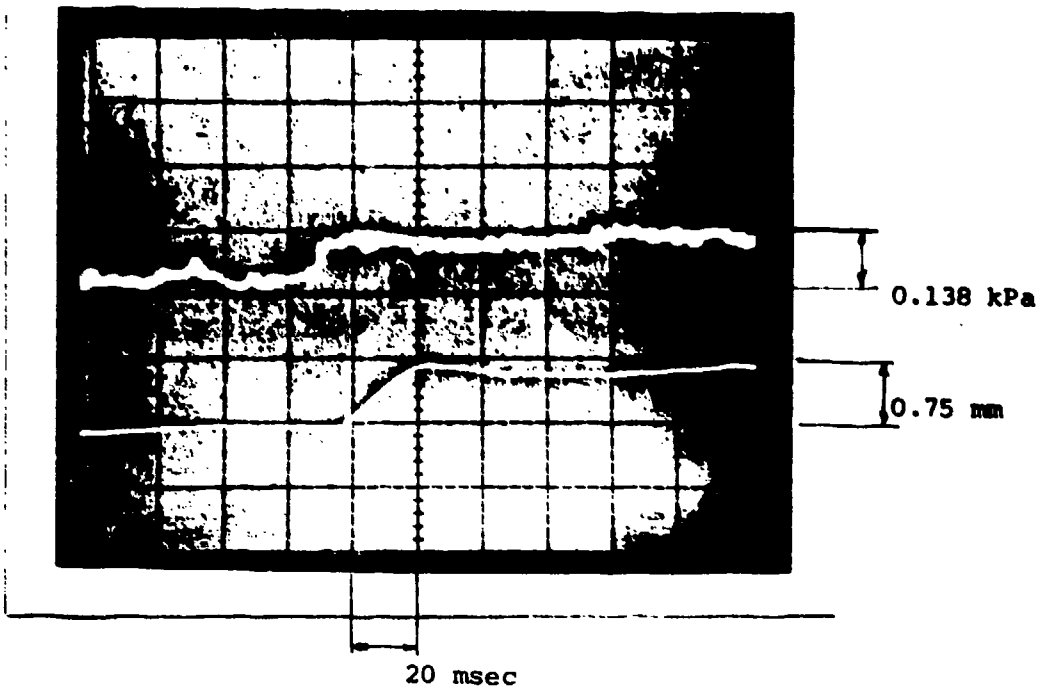

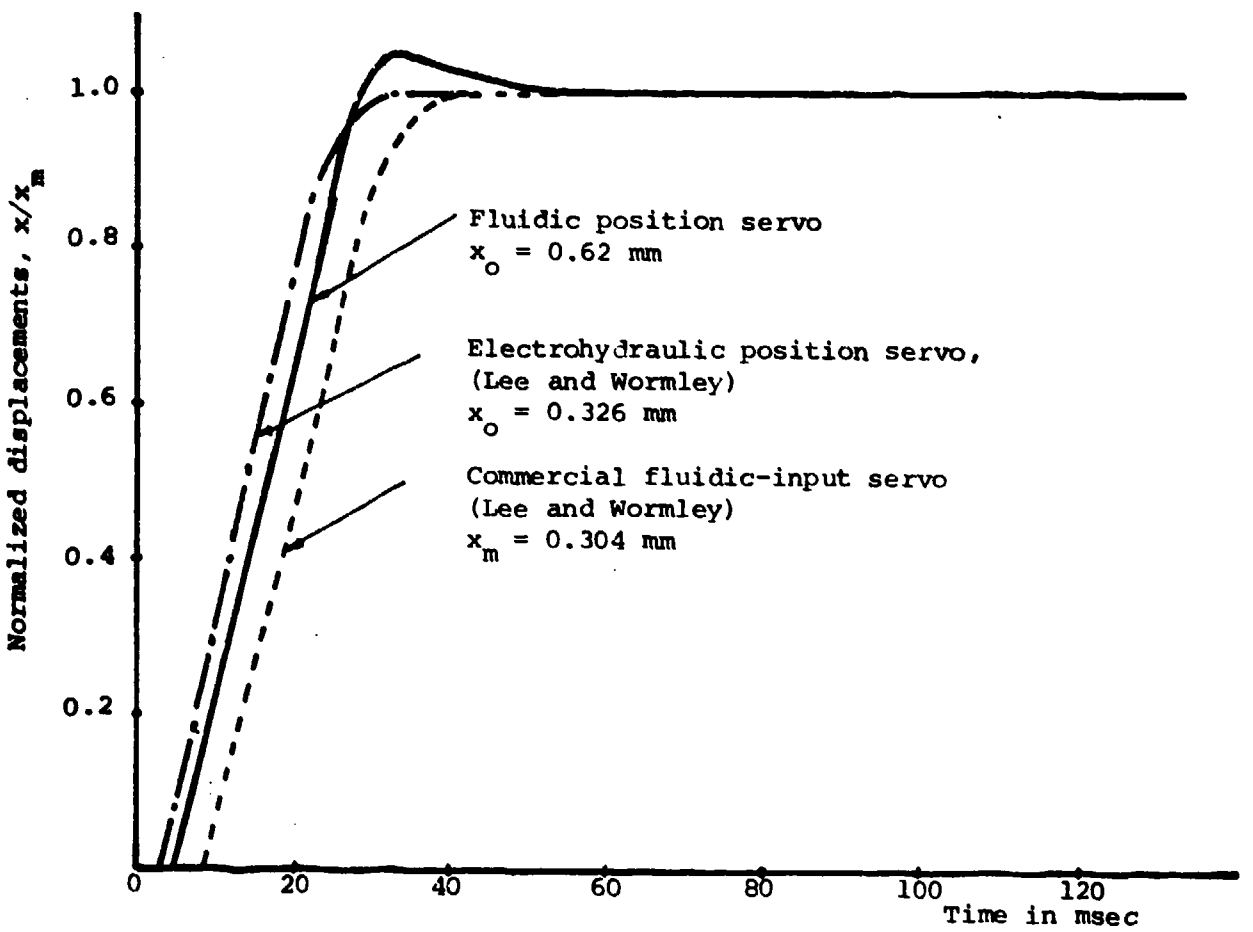

Figure 34. Comparison of step response between fluidic and commercial position servo.

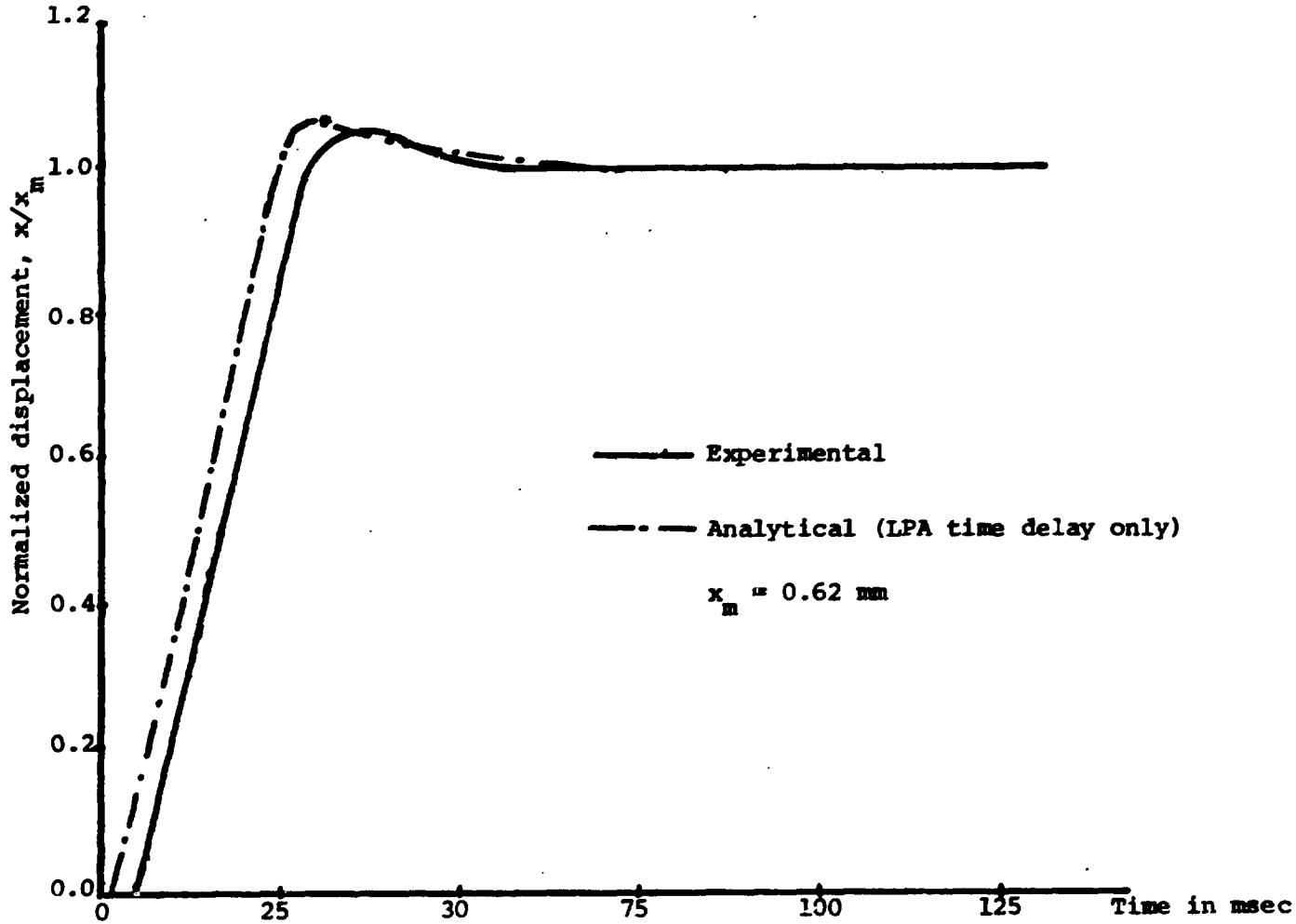

Figure 35. Comparison of experimental and analytical step response of fluidic position servo.

pressure and temperature which are characterized in terms of the modified Reynolds number. The point of transition-to-turbulence of three standard LPA configurations namely, HDL 63020, HDL 72010 and HDL 61505 occurs between modified Reynolds numbers of 100 and 120. The useful operating range of LPA's has been determined through the experimental program to be $40 \leq N_R' \leq 100$.

The relationship between the supply conditions of the individual stages and that of the final stage of the gain block has been derived and verified experimentally. Compensated fluidic gain blocks and servovalves are sensitive to temperature variation at constant supply pressure. The temperature compensation technique, based on the supply pressure scheduling to maintain an approximately constant final stage modified Reynolds number, significantly suppresses the temperature sensitivity of the blocked-load pressure gain of the gain block and servovalve.

The fluidic gain block, summing amplifier and feedback transducer have been used with an actuator and load mass to construct a closed loop position control systems. Static and dynamic tests of the servosystem have shown its performance comparable to an electrohydraulic servoloop. This development effort has demonstrated the capability to develop high performance position servo components from standard integrated component fluidic elements and to interconnect the components into a closed loop servo with performance comparable to high performance electrohydraulic commercial components.

In the current fluidic servo, the maximum load pressure differential and flow gain of the servovalve are primarily limited by the LPA characteristics. Future effort is merited to optimize the LPA design to achieve high pressure recovery, to reduce the ratio of quiescent to maximum load flow and to further minimize the overall power-to-weight ratio.

APPENDIX A. --GAIN BLOCK AND SERVOVALVE CONSTRUCTION DETAILS

In this appendix the gain block stacking order is summarized as given in tables A-1 and A-2 with the components shown in figure A-1.

TABLE A-1 GAIN BLOCK STACKING ORDER DESCRIPTIONS

Stacking Order	HDL Part No.	HDL Orientation	Quantity	Description
Valve Baseplate				
1	5018	C	(*)	
2	5047	G		
3	5221A-20	H	6 pairs	First Stage Pressure Reducer
4	5040	F		
5	5221A-20	H	3 pairs	
6	5018	H		
7	5200	C		
8	5200	H		
9	5021	F		
10	5216	F	2	Third Stage Amplifier and Vent Assembly
11	5339A	F	6 sections	
12	61505	F		
13	5339A	F		
14	5216	F	2	
15	5040	E	7 pairs	Second State Pressure Reducer
16	5221A-20	C		
17	5018	F	2 pairs	
18	5221A-20	C		
19	5021	C		
20	5046	B		
21	5021	D		
22	5216	C	2	
23	5216	H	2	
24	5046	D		
25	5018	A		
26	5046	B		
27	5046			
28	5239	H	3 sections	Second State Amplifier and Vent Assembly
29	5137	H		
30	72010	H		
31	5137	C		
32	5237	C		
33	5216	H		
34	5021	A		
35	5200	H		
36	5200	C		
37	5047	D		

*1 unless otherwise stated

TABLE A-1 (Cont.)

GAIN BLOCK STACKING ORDER AND DESCRIPTIONS

Stacking Order	HDL Part No.	HDL Orientation	Quantity	Description
38	5239	D	2	
39	5018	H		
40	5216	F	2	
41	5237	F		
42	5236	F		
43	63020	F		
44	5236	F		
45	5237	F		
46	5216	A		First Stage
47	5237	A		Amplifier
48	5236	A		and
49	63020	F		Vent
50	5236	F		Assembly
51	5237	F		
52	5216	F	2	
56	5046	E		
Input manifold				

TABLE A-2

SERVOVALVE STACKING ORDER AND DESCRIPTIONS

Stacking Order	Part No.	Orientation	Quantity	Description
Supply/output manifold baseplate				
1.	SP5			
2.	SP3			feedback mainfold
3.	HDL 5043			
4.	HDL 5026		4 pairs	feedback resistors
5.	HDL 5040			
6.	3 stage amplifier Refer to amplifier stacking order (1-56)			
7.	SP2			summing manifold
8.	HDL 5040			
9.	HDL 5027			feedback resistors
10.	HDL 5112		2	
11.	HDL 5196			input resistance
12.	HDL 5040			
13.	SP4			
14.	HDL 5040			
15.	HDL 5196			input resistor
16.	HDL 5040			
17.	HDL 5112		2	input manifold

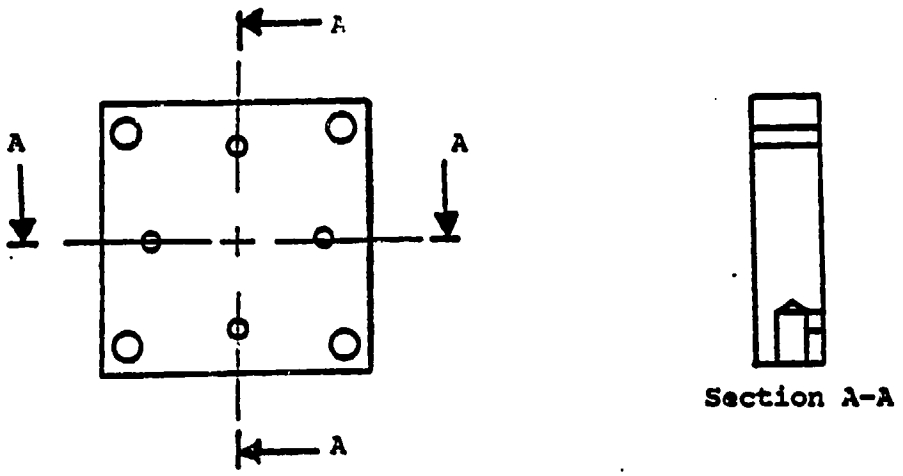

SP2 Summing Manifold (including cover)

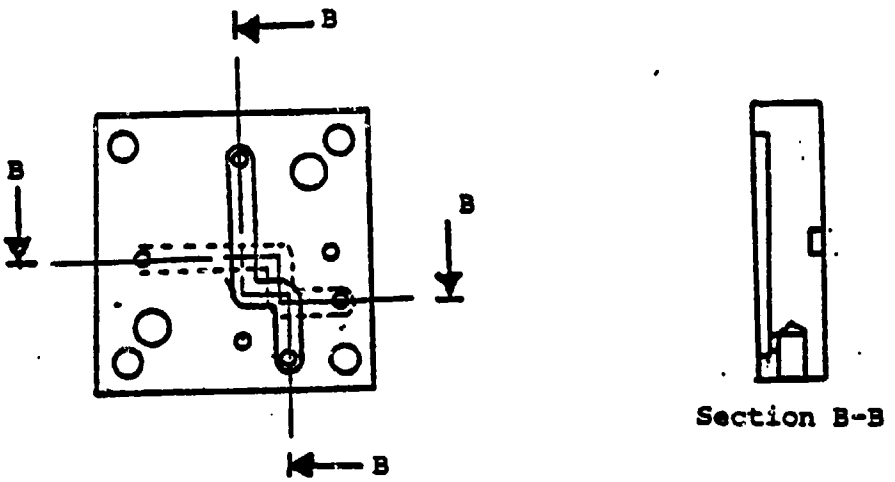

SP3 Feedback Manifold

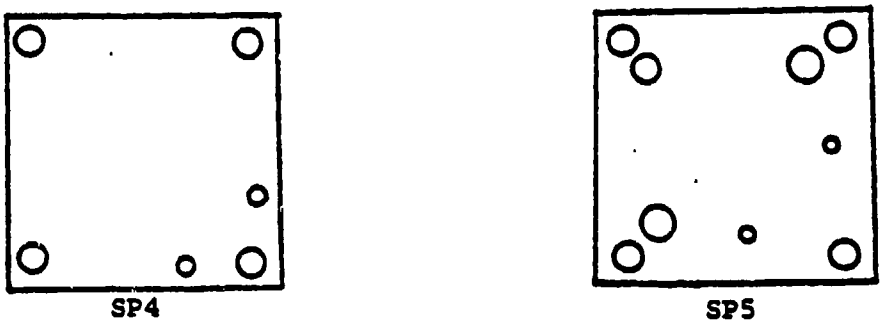

Figure A-1. Servovalve components descriptions.

NOMENCLATURE

A_r	ram area
B_c	LPA control port minimum width
$\bar{B}_c$	LPA average control port channel width
B_{ni}	normalized nozzle throat width, b_n/b_{si} of i^{th} stage
B_o	LPA outlet port minimum width
$\bar{B}_o$	LPA average outlet port channel width
B_{sp}	LPA splitter width
B_t	LPA downstream control edges space
B_v	LPA jet-control edge space
$\bar{B}_{ni}$	normalized nozzle average channel width, $\bar{b}_n/b_{si}$
C	empirical constant in channel resistance model
C_d	discharge coefficient
C_{di}	discharge coefficient of i^{th} stage LPA
C_θ	momentum flux coefficient
G_p	servovalve blocked-load pressure gain
G_{ps}	servovalve blocked-load pressure gain at steady state
$G_{p,LPA}$	LPA blocked-load pressure gain
G_q	servovalve no-load flow gain
G_{qs}	servovalve no-load flow gain at steady state
G_{qp}	servovalve output admittance
H_{ni}	normalized nozzle height, h_n/b_{si}
K	fluidic servo open-loop steady state gain
K_i	i^{th} stage LPA blocked-load pressure gain, i=1,2,3
K_p	gain block blocked-load pressure gain
K_q	gain block no-load flow gain
K_s	fluidic summer gain
K_{ss}	fluidic summer steady state gain
K_t	displacement transducer sensitivity
L_e	normalized entry length, $\ell e/b$
L_c	channel fluid inertance
L_f	transducer fixed channel fluid inertance
L_v	transducer variable channel fluid inertance
N_R	Reynolds number
N_{Rc}	channel Reynolds number
N_{Rf}	gain block final stage Reynolds number

N_{Ri}	gain block i^{th} stage Reynolds number
N'_R	LPA modified Reynolds number
N'_{Rf}	gain block final stage modified Reynolds number
N'_{Ri}	gain block i^{th} stage modified Reynolds number
P_{cd}	control pressure differential
P_{cds}	saturation control pressure differential
P_{co}	bias control pressure
P_{dt}	output pressure differential of transducer
P_{id}	input pressure differential
P_{idm}	maximum input pressure differential
P_L	defined in figure 1
P_{od}	output pressure differential
P_{ods}	saturation output pressure differential
P_s	main supply pressure
P_{sd}	defined in figure 28
P_{si}	supply pressure of i^{th} stage, i = 1,2,3
P_{ss}	supply pressure of summer
P_{st}	supply pressure of transducer
P_{1d}	input 1 of summer
P_{2d}	input 2 of summer
Q	volumetric flow rate
Q_L	load flow
Q_{Ls}	saturation load flow
Q_{ni}	flow through i^{th} stage nozzle
Q_s	supply flow
Q_{si}	supply flow of i^{th} stage LPA
R	channel resistance
$\bar{R}$	normalized resistance defined in equation (8)
R_a	gain block input deflection resistance
R_{as}	LPA input resistance for summer
R_f	fixed resistance in transducer
R_{fp}	servovalve feedback resistance
R_i	servovalve input resistance
R_{i1}	1^{st} stage input resistance
R_{i2}	2^{nd} stage input resistance
R_{i3}	3^{rd} stage input resistance

R_{ni}	nozzle resistance of i^{th} stage
R_{01}	1^{st} state output resistance
R_{02}	2^{nd} stage output resistance
R_{03}	3^{rd} stage output resistance
R_{si}	supply resistance of i^{th} stage
R_v	variable resistance in transducer
R_1	summer input resistance
T	temperature
T_o	reference temperature
X	channel length
X_c	LPA control port channel length
X_{ni}	normalized nozzle channel length of i^{th} stage
X_o	LPA outlet port channel length
X_{sp}	LPA supply nozzle-splitter distance
X_{th}	LPA supply nozzle throat length
Z_a	gain block input complex impedance
Z_i	servovalve input complex impedance
Z_{fp}	servovalve feedback complex impedance

Lower Case Letter

b	channel width
$\bar{b}$	average channel width
b_s	LPA supply nozzle throat width
b_{sf}	final state LPA supply nozzle throat width
b_{si}	i^{th} stage LPA supply nozzle throat width
d	damping coefficient
f	frequency
h	channel height
ℓ_e	entry length
m	mass
m_i	number of LPA in parallel in i^{th} stage
n_i	number of nozzles in parallel in i^{th} stage
S	Laplace transform operator
x	valve input in section 1
	channel length in section 2
	displacement in section 4
x_m	half stroke, maximum travel

x_{sp}	dimensional LPA supply nozzle-splitter distance

Greek Letter

α	servovalve parameter, defined in equation (18)
β	bulk modulus, table 5
γ	servovalve parameter, defined in equation (19)
λ	viscosity-temperature coefficient
λ_o	defined in equation (24)
μ	absolute viscosity of oil
ν	kinematic viscosity of oil
ν_o	kinematic viscosity at reference temperature
ξ	damping ratio
ρ	density
σ	aspect ratio
σ_c	channel aspect ratio, $h/\bar{b}$
σ_i	aspect ratio of i^{th} stage
τ	total time delay of fluidic servo
τ_c	defined in equation (34)
τ_q	1^{st} order time constant of $G_q(s)$
τ_s	time delay of summer
τ_v	time delay of servovalve
ω_n	natural frequency

Subscripts

tr.	transition
90°	90° phase shift

DISTRIBUTION

ADMINISTRATOR
DEFENSE TECHNICAL INFORMATION CENTER
ATTN DTIC-DDA (12 COPIES)
CAMERON STATION, BUILDING 5
ALEXANDRIA, VA 22314

COMMANDER
US ARMY RSCH & STD GP (EUR)
ATTN CHIEF, PHYSICS & MATH BRANCH
FPO NEW YORK 09510

COMMANDER
US ARMY MATERIEL DEVELOPMENT &
READINESS COMMAND
ATTN DRCLDC, JAMES BENDER
5001 EISENHOWER AVENUE
ALEXANDRIA, VA 22333

COMMANDER
US ARMY ARMAMENT MATERIEL
READINESS COMMAND
ATTN DRSAR-ASF, FUZE &
MUNITIONS SUPPORT DIV
ATTN DRSAR-RDF, SYS DEV DIV-FUZES
ATTN DRSAR-RDG-T, R. SPENCER
ATTN DRSAR-ASF
ATTN DRSAR-LEP-L, TECH LIBRARY
ROCK ISLAND, IL 61299

COMMANDER
US ARMY MISSILE & MUNITIONS
CENTER & SCHOOL
ATTN ATSK-CTD-F
REDSTONE ARSENAL, AL 35809

DIRECTOR
US ARMY MATERIEL SYSTEMS
ANALYSIS ACTIVITY
ATTN DRXSY-MP
ABERDEEN PROVING GROUND, MD 21005

DIRECTOR
US ARMY BALLISTIC RESEARCH LABORATORY
ATTN DRDAR-TSB-S (STINFO)
ABERDEEN PROVING GROUND, MD 21005

US ARMY ELECTRONICS TECHNOLOGY
& DEVICES LABORATORY
ATTN DELET-DD
FT MONMOUTH, NJ 07703

HQ, USAF/SAMI
WASHINGTON, DC 20330

TELEDYNE BROWN ENGINEERING
CUMMINGS RESEARCH PARK
ATTN MELVIN L. PRICE, MS-44
HUNTSVILLE, AL 35807

ENGINEERING SOCIETIES LIBRARY
ATTN ACQUISITIONS DEPARTMENT
345 EAST 47TH STREET
NEW YORK, NY 10017

COMMANDER IDDR&E
PENTAGON, ROOM 3D 1089
ATTN G. KOPCSAK
WASHINGTON, DC 20310

OFFICE OF THE DEPUTY CHIEF OF STAFF FOR
RESEARCH, DEVELOPMENT & ACQUISITION
DEPARTMENT OF THE ARMY
ATTN DAMA-ARP-P
ATTN DAMA-CSS-N
WASHINGTON, DC 20310

US ARMY R&D GROUP (EUROPE)
BOX 15
ATTN CHIEF, AERONAUTICS BRANCH
ATTN CHIEF, ENGINEERING SCIENCES
FPO NEW YORK 09510

US ARMY RESEARCH OFFICE
PO BOX 12211
ATTN R. SINGLETON
RESEARCH TRIANGLE PARK, NC 27709

BMD ADVANCED TECHNOLOGY CENTER
PO BOX 1500
ATTN J. PAPADOPOULOS
HUNTSVILLE, AL 35807

COMMANDER
US ARMY FOREIGN SCIENCE
& TECHNOLOGY CENTER
FEDERAL OFFICE BUILDING
ATTN DRXST-SD1
ATTN DRXST-IS3, C. R. MOORE
220 7TH STREET, NE
CHARLOTTESVILLE, VA 22901

DIRECTOR
APPLIED TECHNOLOGY LABORATORY
ATTN GEORGE W. FOSDICK, DAVDL-ATL-ASA
FT EUSTIS, VA 23604

COMMANDER
US ARMY MATERIEL & MECHANICS
RESEARCH CENTER
ATTN R. KATZ
WATERTOWN, MA 02172

COMMANDER
US ARMY MISSILE COMMAND
ATTN REDSTONE SCIENTIFIC INFORMATION
CENTER, DRSMI-RBD
ATTN DRSMI-RG, WILLIAM GRIFFITH
ATTN DRSMI-TGC, J. C. DUNAWAY
ATTN DRCPM-TOE, FRED J. CHEPLEN
REDSTONE ARSENAL, AL 35898

COMMANDER
US ARMY MOBILITY EQUIPMENT R&D CENTER
ATTN TECHNICAL LIBRARY (VAULT)
ATTN DRDME-EM, R. N. WARE
FT BELVOIR, VA 22060

COMMANDER
US ARMY ARRADCOM
ATTN SARPA-TS-S #59
ATTN DRDAR-LCN-C, A. E. SCHMIDLIN
ATTN DRDAR-LCW-E, J. CONNORS
ATTN DRDAR-SCF-IC, V. BAUMBARTH
ATTN PBM-DPM (TAGLAIRINO)
DOVER, NJ 07801

COMMANDER
WATERVLIET ARSENAL
ATTN SARWV-RDT-L
ATTN DRDAR-LCB-RA, R. RACICOT
WATERVLIET ARSENAL, NY 12189

COMMANDER
US ARMY TANK AUTOMOTIVE COMMAND
ARMOR & COMP DIV, DRDTA-RKT
BLDG 215
ATTN M. WHITMORE
WARREN, MI 48090

COMMANDER
ATTN STEWS-AD-L, TECHNICAL LIBRARY
WHITE SANDS MISSILE RANGE, NM 88002

COMMANDER/DIRECTOR
ATMOSPHERIC SCIENCES LABORATORY
USA ERADCOM
ATTN DELAS-AS (HOLT)
ATTN DELAS-AS-T (R. RUBIO)
WHITE SANDS MISSILE RANGE, NM 88002

OFFICE OF NAVAL RESEARCH
DEPARTMENT OF THE NAVY
ATTN STANLEY W. DOROFF, CODE 438
ATTN D. S. SIEGEL, CODE 211
ARLINGTON, VA 22217

DEPARTMENT OF THE NAVY
R&D PLANS DIVISION
ROOM 5D760, PENTAGON
ATTN BENJ R. PETRIE, JR.
OP-987P4
WASHINGTON, DC 20350

COMMANDANT
US NAVAL POSTGRADUATE SCHOOL
DEPARTMENT OF MECHANICAL ENGINEERING
ATTN CODE 69 Nn(NUNN)
MONTEREY, CA 93940

COMMANDER
NAVAL AIR DEVELOPMENT CENTER
ATTN R. MCGIBONEY, 60134

COMMANDER
NAVAL AIR DEVELOPMENT CENTER (Cont'd)
ATTN CODE 8134, LOIS GUISE
ATTN D. KEYSER, 60134
WARMINSTER, PA 18974

COMMANDING OFFICER
NAVAL AIR ENGINEERING CENTER
ATTN ESSD, CODE 9314, HAROLD OTT
LAKEHURST, NY 08733

NAVAL AIR SYSTEMS COMMAND
DEPARTMENT OF THE NAVY
ATTN CODE AIR-5162C1, J. BURNS
ATTN CODE AIR-5143J, D. HOUCK
WASHINGTON, DC 20361

COMMANDER
PACIFIC MISSILE TEST CENTER
ATTN CODE 3123, ABE J. GARRETT
ATTN CODE 1243, A. ANDERSON
POINT MUGU, CA 93042

COMMANDER
NAVAL SHIP ENGINEERING CENTER
PHILADELPHIA DIVISION
ATTN CODE 6772
PHILADELPHIA, PA 19112

COMMANDER
NAVAL SURFACE WEAPONS CENTER
ATTN CODE 413, CLAYTON MCKINDRA
WHITE OAK, MD 20910

COMMANDER
NAVAL ORDNANCE STATION
ATTN CODE 5123C, K. ENGLANDER
INDIANHEAD, MD 20640

NAVAL SHIP RES & DEV CENTER
CODE 1619, K. READER
BETHESDA, MD 20084

NAVAL RESEARCH LABORATORY
ATTN S. SEARLES, 117 BG A68
WASHINGTON, DC 20375

NAVAL SEA SYSTEMS COMMAND
SEA05R31
ATTN J. H. HARRISON
WASHINGTON, DC 20362

COMMANDER
NAVAL WEAPONS CENTER
ATTN CODE 533, LIBRARY DIVISION
ATTN CODE 3636, C. BURMEISTER
CHINA LAKE, CA 93555

COMMANDER
AF AERO PROPULSION LABORATORY, AFSC
ATTN LESTER SMALL, AFWAL/POTC
WRIGHT-PATTERSON AFB, OH 45433

COMMANDER
AIR FORCE AVIONICS LABORATORY
ATTN AARA-2, RICHARD JACOBS
WRIGHT-PATTERSON AFB, OH 45433

DIRECTOR
AF OFFICE OF SCIENTIFIC RESEARCH
ATTN NE
BOLLING AFB, DC 20332

COMMANDER
AIR FORCE FLIGHT DYNAMICS LABORATORY
ATTN AFWAL/FIGL, H. SNOWBALL
ATTN AFWAL/FIER, R. J. DOBBEK
WRIGHT-PATTERSON AFB, OH 45433

COMMANDER
AF WEAPONS LABORATORY, AFSC
ATTN SUL, TECHNICAL LIBRARY
KIRTLAND AFB, NM 87117

COMMANDER
ARMAMENT DEVELOPMENT & TEST CENTER
ATTN ADTC (DLOSL), TECH LIBRARY
ATTN DLMA, DAVID T. WILLIAMS
EGLIN AIR FORCE BASE, FL 32542

AIR FORCE FLIGHT TEST CENTER
6510 ABG/SSD
ATTN TECHNICAL LIBRARY
EDWARDS AFB, CA 93523

AF INSTITUTE OF TECHNOLOGY, AU
ATTN LIBRARY AFIT (LD),
BLDG 640, AREA B
ATTN AFIT (ENM), MILTON E. FRANKE
WRIGHT-PATTERSON AFB, OH 45433

HQ, AF SYSTEMS COMMAND
ATTN SGB, CPT GEORGE JAMES
ANDREWS AFB, DC 20334

ARGONNE NATIONAL LABORATORY
APPLIED PHYSICS DIV, BLDG 316
ATTN N. M. O'FALLAN
9700 S. CASS AVE
ARGONNE, IL 60439

OAK RIDGE NATIONAL LABORATORY
CENTRAL RES LIBRARY, BLDG 4500N, RM 175
PO BOX X
ATTN E. HOWARD
ATTN C. A. MOSSMAN
ATTN R. E. HARPER
OAK RIDGE, TN 37830

DEPARTMENT OF COMMERCE
NATIONAL BUREAU OF STANDARDS
ATTN JAMES SCHOOLEY, CHIEF,
TEMPERATURE SECTION
ATTN T. NEGAS, SOLID STATE
CHEMISTRY DIVISION
ATTN RAY DILS, RM B-254, BLDG 221
ATTN GEORGE BURNS, RM B-222, BLDG 221
WASHINGTON, DC 20230

DEPARTMENT OF COMMERCE
BUREAU OF EAST-WEST TRADE
OFFICE OF EXPORT ADMINISTRATION
ATTN WALTER J. RUSNACK
WASHINGTON, DC 20230

DEPARTMENT OF ENERGY
C-156, GTN (OART)
ATTN ROBERT ROBERTS
ATTN SANDY DAPKUNAS
WASHINGTON, DC 20545

DEPARTMENT OF ENERGY
FE-22
ATTN T. K. LAU
WASHINGTON, DC 20545

DEPARTMENT OF ENERGY
F-317, GTN (COAL GASIFICATION)
ATTN JIM CARR
WASHINGTON, DC 20545

FEDERAL BUREAU OF INVESTIGATION
J. EDGAR HOOVER BLDG
ATTN ROBERT WILLIS
WASHINGTON, DC 20535

DEPARTMENT OF JUSTICE
IMMIGRATION & NATURALIZATION SERVICE
425 "I" STREET, NW
ATTN NEILL MCKAY
WASHINGTON, DC 20536

SCIENTIFIC LIBRARY
US PATENT OFFICE
ATTN MRS. CURETON
WASHINGTON, DC 20231

NASA AMES RESEARCH CENTER
ATTN MS 244-13, DEAN CHISEL
MOFFETT FIELD, CA 94035

NASA LANGLEY RESEARCH CENTER
ATTN, MS 494, H. D. GARNER
ATTN MS 494, R. R. HELLBAUM
ATTN MS 185, TECHNICAL LIBRARY
HAMPTON, VA 23665

NASA SCIENTIFIC & TECH INFO FACILITY
PO BOX 8657
ATTN ACQUISITIONS BRANCH
BALTIMORE/WASHINGTON INTERNATIONAL
AIRPORT, MD 21240

UNIVERSITY OF ALABAMA
CIVIL & MINERAL ENGINEERING DEPT
PO BOX 1468
ATTN HAROLD R. HENRY
UNIVERSITY, AL 35486

UNIVERSITY OF ARKANSAS
TECHNOLOGY CAMPUS
PO BOX 3017
ATTN PAUL C. MCLEOD
LITTLE ROCK, AR 72203

UNIVERSITY OF ARKANSAS
MECHANICAL ENGINEERING
ATTN JACK H. COLE, ASSOC. PROF.
FAYETTEVILLE, AR 72701

CARNEGIE-MELLON UNIVERSITY
SCHENLEY PARK
ATTN PROF. W. T. ROULEAU,
MECH ENGR DEPT
PITTSBURGH, PA 15213

CASE WESTERN RESERVE UNIVERSITY
ATTN PROF. P. A. ORNER
ATTN PROF. B. HORTON
UNIVERSITY CIRCLE
CLEVELAND, OH 44106

THE CITY COLLEGE OF THE CITY
UNIVERSITY OF NY
DEPT OF MECH ENGR
ATTN PROF. L. JIJI
ATTN PROF. G. LOWEN
139TH ST. AT CONVENT AVE
NEW YORK, NY 10031

CLEVELAND STATE UNIVERSITY
FENN COLLEGE OF ENGINEERING
ATTN PROF. R. COMPARIN
CLEVELAND, OH 44115

DUKE UNIVERSITY
COLLEGE OF ENGINEERING
ATTN C. M. HARMAN
DURHAM, NC 27706

ENGINEERING SOCIETIES LIBRARY
ATTN HOWARD GORDON
ATTN ACQUISITIONS DEPARTMENT
345 EAST 47TH STREET
NEW YORK, NY 10017

FRANKLIN INSTITUTE OF THE STATE
OF PENNSYLVANIA
ATTN KA-CHEUNG TSUI, ELEC ENGR DIV
ATTN C. A. BELSTERLING
20TH STREET & PARKWAY
PHILADELPHIA, PA 19103

HUGHES HELICOPTERS
DIVISION OF SUMMA CORPORATION
CENTINELA & TEALE STREETS
ATTN LIBRARY 2/T2124
CULVER CITY, CA 90230

IIT RESEARCH INSTITUTE
ATTN K. E. MCKEE
10 WEST 35TH STREET
CHICAGO, IL 60616

JET PROPULSION LABORATORY
ATTN JOHN V. WALSH, MS 125-138
4800 OAK GROVE DRIVE
PASADENA, CA 91103

JOHNS HOPKINS UNIVERSITY
APPLIED PHYSICS LABORATORIES
ATTN MAYNARD HILL
ATTN THOMAS RANKIN
ATTN JOSEPH WALL
LAUREL, MD 20810

LEHIGH UNIVERSITY
DEPARTMENT OF MECHANICAL ENGINEERING
ATTN PROF. FORBES T. BROWN
BETHLEHEM, PA 18015

LINDA HALL LIBRARY
ATTN DOCUMENTS DIVISION
5109 CHERRY STREET
KANSAS CITY, MO 64110

LOS ALAMOS SCIENTIFIC LAB
PO BOX 1663
ATTN FRANK FINCH, MS 178
LOS ALAMOS, NM 87545

MASSACHUSETTS INSTITUTE OF TECHNOLOGY
ATTN ENGINEERING TECHNICAL REPORTS,
RM 10-408
ATTN DAVID WORMELY, MECH ENGR DEPT,
RM 3-146
77 MASSACHUSETTS AVENUE
CAMBRIDGE, MA 02139

MICHIGAN TECHNOLOGICAL UNIVERSITY
LIBRARY, DOCUMENTS DIVISION
ATTN J. HAWTHORNE
HOUGHTON, MI 49931

UNIVERSITY OF MISSISSIPPI
ATTN JOHN A. FOX
201 CARRIER HALL, DEPT OF MECH ENGR
UNIVERSITY, MS 38677

MISSISSIPPI STATE UNIVERSITY
DRAWER ME
ATTN C. J. BELL, MECH ENG DEPT
STATE COLLEGE, MS 39762

MISSISSIPPI STATE UNIVERSITY
DEPT OF AEROSPACE ENGINEERING
ATTN DAVID MURPHREE
MISSISSIPPI STATE, MS 39762

UNIVERSITY OF NEBRASKA LIBRARIES
ACQUISITIONS DEPT, SERIALS SECTIONS
ATTN ALAN GOULD
LINCOLN, NE 68508

UNIVERSITY OF NEW HAMPSHIRE
MECH ENGR DEPT, KINGSBURY HALL
ATTN PROF. CHARLES TAFT
ATTN PROF. DAVID LIMBERT
DURHAM, NH 03824

UNIVERSITY OF N. CAROLINA
INSTITUTE OF MARINE BIOMEDICAL RESEARCH
ATTN MICHAEL E. SHEEHAN
WILMINGTON, NC 28401

NEW JERSEY INSTITUTE OF TECHNOLOGY
DEPARTMENT OF MECHANICAL ENGINEERING
ATTN R. Y. CHEN
323 HIGH STREET
NEWARK, NJ 07102

OHIO STATE UNIVERSITY LIBRARIES
SERIAL DIVISION, MAIN LIBRARY
1858 NEIL AVENUE
COLUMBUS, OH 43210

OKLAHOMA STATE UNIVERSITY
SCHOOL OF MECH & AEROSPACE ENGR
ATTN PROF. KARL N. REID
STILLWATER, OK 74074

MIAMI UNIVERSITY
DEPT OF ENG TECH
SCHOOL OF APPLIED SCIENCE
ATTN PROF. S. B. FRIEDMAN
OXFORD, OH 45056

PENNSYLVANIA STATE UNIVERSITY
ATTN J. L. SHEARER
215 MECHANICAL ENGINEERING BUILDING
UNVERSITY PARK, PA 16802

PENNSYLVANIA STATE UNIVERSITY
ENGINEERING LIBRARY
ATTN M. BENNETT, ENGINEERING LIBRARIAN
201 HAMMOND BLDG
UNIVERSITY PARK, PA 16802

PORTLAND STATE UNIVERSITY
DEPT OF ENGINEERING &
APPLIED SCIENCE
PO BOX 751
ATTN PROF. P. I. CHEN
PORTLAND, OR 97207

PURDUE UNIVERSITY
SCHOOL OF MECHANICAL ENGINEERING
ATTN PROF. VICTOR W. GOLDSCHMIDT
ATTN PROF. ALAN T. MCDONALD
LAFAYETTE, IN 47907

ROCK VALLEY COLLEGE
ATTN KEN BARTON
3301 N. MULFORD ROAD
ROCKFORD, IL 61101

RUTGERS UNIVERSITY
LIBRARY OF SCIENCE & MEDICINE
ATTN GOVERNMENT DOCUMENTS DEPT
SANDRA R. LIVINGSTON
NEW BRUNSWICK, NJ 08903

SYRACUSE UNIVERSITY
DEPT OF MECH & AEROSPACE ENGINEERING
ATTN PROF. D. S. DOSANJH
139 E. A. LINK HALL
SYRACUSE, NY 13210

UNIVERSITY OF TENNESSEE
DEPT OF MECHANICAL ENGINEERING
ATTN PROF. G. V. SMITH
KNOXVILLE, TN 37916

UNIVERSITY OF TENNESSEE SPACE INST
ENERGY CONVERSION DIVISION
ATTN MARY ANN SCOTT
TULLAHOMA, TN 37388

UNIVERSITY OF TEXAS AT AUSTIN
DEPT OF MECHANICAL ENGINEERING
ATTN A. J. HEALEY
AUSTIN, TX 78712

THE UNIVERSITY OF TEXAS AT ARLINGTON
MECHANICAL ENGINEERING DEPARTMENT
ATTN ROBERT L. WOODS
ARLINGTON, TX 76019

TULANE UNIVERSITY
DEPT OF MECHANICAL ENGINEERING
ATTN H. F. HRUBECKY
NEW ORLEANS, LA 70118

UNION COLLEGE
MECHANICAL ENGINEERING
ATTN ASSOC. PROF. W. C. AUBREY
MECH ENGR DEPT, STEINMETZ HALL
SCHENECTADY, NY 12308

UNIVERSITY OF VIRGINIA
DEPT OF MECH & AEROSPACE ENGR
ATTN DAVID LEWIS
CHARLOTTESVILLE, VA 22090

VIRGINIA POLYTECHNIC INSTITUTE
OF STATE UNIV
MECHANICAL ENGINEERING DEPARTMENT
ATTN PROF. H. MOSES
BLACKSBURG, VA 24061

WASHINGTON UNIVERSITY
SCHOOL OF ENGINEERING
PO BOX 1185
ATTN W. M. SWANSON
ST LOUIS, MO 63130

WEST VIRGINIA UNIVERSITY
MECHANICAL ENGINEERING DEPARTMENT
ATTN RICHARD A. BAJURA
MORGANTOWN, WV 26505

WICHITA STATE UNIVERSITY
ATTN DEPT AERO ENGR, E. J. RODGERS
WICHITA, KS 67208

UNIVERSITY OF WISCONSIN
MECHANICAL ENGINEERING DEPARTMENT
ATTN FEDERAL REPORTS CENTER
ATTN NORMAN H. BEACHLEY, DIR
DESIGN ENGINEERING LABORATORIES
1513 UNIVERSITY AVENUE
MADISON, WI 53706

WORCESTER POLYTECHNIC INSTITUTE
ATTN GEORGE C. GORDON LIBRARY (TR)
ATTN TECHNICAL REPORTS
WORCESTER, MA 01609

AVCO SYSTEMS DIVISION
ATTN W. K. CLARK
201 LOWELL STREET
WILMINGTON, MA 01887

BARNES ENGINEERING CO
ATTN FRED SWEIBAUM
30 COMMERCE ROAD
STAMFORD, CT 06904

BELL HELICOPTER COMPANY
PO BOX 482
ATTN R. D. YEARY
FT WORTH, TX 76101

BENDIX CORPORATION
ELECTRODYNAMICS DIVISION
ATTN D. COOPER
11600 SHERMAN WAY
N. HOLLYWOOD, CA 90605

BENDIX CORPORATION
RESEARCH LABORATORIES DIV
BENDIX CENTER
ATTN C. J. AHERN
ATTN LAEL TAPLIN
SOUTHFIELD, MI 48075

BOEING COMPANY, THE
PO BOX 3707
ATTN HENRIK STRAUB
SEATTLE, WA 98124

BOWLES FLUIDICS CORPORATION
ATTN VICE PRES/ENGR
9347 FRASER AVENUE
SILVER SPRING, MD 20910

R. E. BOWLES
2105 SONDRA COURT
SILVER SPRING, MD 20904

CHAMBERLAIN MANUFACTURING CORP
EAST 4TH & ESTHER STS
PO BOX 2545
WATERLOO, IA 50705

CONTINENTAL CAN COMPANY
TECH CENTER
ATTN P. A. BAUER
1350 W. 76TH STREET
CHICAGO, IL 60620

CONTROL SYSTEMS INNOVATION
ATTN N. F. MACIA
517 EAST ORION STREET
TEMPE, AZ 85283

CORDIS CORPORATION
PO BOX 428
ATTN STEPHEN F. VADAS, K-2
MIAMI, FL 33137

CORNING GLASS WORKS
FLUIDIC PRODUCTS
ATTN R. H. BELLMAN
HOUGHTON PARK, B-2
CORNING, NY 14830

CHRYSLER CORPORATION
PO BOX 118
CIMS-418-33-22
ATTN L. GAU
DETROIT, MI 48231

JOHN DEERE PRODUCT ENGINEERING CENTER
ATTN V. S. KUMAR
WATERLOO, IA 50704

ELECTRIC POWER RESEARCH INSTITUTE
PO BOX 10412
ATTN MS. M. ANGWIN,
P. M. GEOTHERMAL ENERGY
3412 HILLVIEW AVE
PALO ALTO, CA 94303

FLUIDICS QUARTERLY
PO BOX 2989
ATTN D. H. TARUMOTO
STANFORD, CA 94305

FOXBORO COMPANY
CORPORATE
RESEARCH DIV
ATTN JAMES VIGNOS
ATTN J. DECARLO
ATTN JOHN CHANG
ATTN TOM KEGEL
38 NEPONSET AVE
FOXBORO, MA 02035

GARRETT PNEUMATIC SYSTEMS DIVISION
PO BOX 5217
ATTN GARY FREDERICK
ATTN TREVOR SUTTON
ATTN TOM TIPPETTS
ATTN C. ABBOTT
111 SOUTH 34TH STREET
PHOENIX, AZ 85010

GENERAL ELECTRIC COMPANY
SPACE/RES DIVISIONS
PO BOX 8555
ATTN MGR LIBRARIES, LARRY CHASEN
PHILADELPHIA, PA 19101

GENERAL ELECTRIC COMPANY
KNOLLS ATOMIC POWER LABORATORY
ATTN D. KROMMENHOEK
SCHENECTADY, NY 12301

GENERAL MOTORS CORPORATION
DELCO ELECTRONICS DIV
MANFRED G WRIGHT
NEW COMMERCIAL PRODUCTS
PO BOX 1104
ATTN R. E. SPARKS
KOKOMO, IN 46901

GRUMMAN AEROSPACE CORPORATION
TECHNICAL INFORMATION CENTER
ATTN C. W. TURNER, DOCUMENTS
LIBRARIAN
ATTN TED SORENSEN, MS B1535

GRUMMAN AEROSPACE CORPORATION (Cont'd)
ATTN JACK LEONARD, MS B1535
SOUTH OYSTER BAY ROAD
BETHPAGE, L. I., NY 11714

HAMILTON STANDARD
DIVISION OF UNITED AIRCRAFT CORPORATION
ATTN PHILIP BARNES
WINDSOR LOCKS, CT 06096

HONEYWELL, INC
ATTN J. HEDEEN
ATTN W. POSINGIES
1625 ZARTHAN AVE
MINNEAPOLIS, MN 55413

HONEYWELL, INC
ATTN RICHARD STEWART, MS 200
1100 VIRGINIA DRIVE
FT WASHINGTON, PA 19034

JOHNSON CONTROLS, INC
ATTN WARREN A. LEDERMAN
ATTN GEORGE JANU
507 E. MICHIGAN
MILWAUKEE, WI 53201

LEEDS & NORTHRUP CO
ATTN ERNEST VAN VALKENBURG
DICKERSON ROAD
NORTH WALES, PA 19454

MOORE PRODUCTS COMPANY
ATTN R. ADAMS
SPRING HOUSE, PA 19477

MARTIN MARIETTA CORPORATION
AEROSPACE DIVISION
ATTN R. K. BRODERSON, MP 326
PO BOX 5837
ORLANDO, FL 32805

MCDONNELL AIRCRAFT COMPANY
GUIDANCE & CONTROL MECHANICS DIVISION
ATTN LOYAL GUENTHER
ST LOUIS, MO 63166

MCDONNEL DOUGLAS ASTRONAUTICS CO
PROPULSION DEPARTMENT
ATTN V. E. HALOULAKOS (A3-226)
ATTN J. D. SCHWEIKLE (A3-226)
5301 BOLSA AVENUE
HUNTINGTON BEACH, CA 92647

NATIONAL FLUID POWER ASSOC.
ATTN JOHN R LUEKE
DIR OF TECH SERVICES
3333 NORTH MAYFAIR ROAD
MILWAUKEE, WI 53222

NEOS, INC
3711 AIR PARK RD
ATTN A. J. OSTDIEK
LINCOLN, NE 68524

NORTHRUP CORP, ELECTRONICS DIV
ATTN DESMOND NELSON,
SENOIR ENGINEER
ORGN C3133, W/C
2301 W. 120TH ST
HAWTHORNE, CA 90250

PATSCENTER INTERNATIONAL
ATTN MR. JOHN CLINE
707 ALEXANDER ROAD
PRINCETON, NJ 08540

PLESSEY AEROSPACE LTD
ATTN A. ROSENBERG
1700 OLD MEADOW ROAD
MCLEAN, VA 22102

PROCON, INC
ATTN HERB MARCH
OUP PLAZA
DES PLAINES, IL 60016

PROPULSION DYNAMICS
ATTN T. HOULIHAN
2200 SOMERVILLE R
ANNAPOLIS, MD 21401

ROCKWELL INTERNATIONAL CORPORATION
COLUMBUS AIRCRAFT DIVISION, PO BOX 1259
ATTN MARVIN SCHWEIGER
ATTN LOUIS BIAFORE
4300 E. 5TH AVENUE
COLUMBUS, OH 43216

SANDIA LABORATORIES
ATTN WILLIAM R. LEUENBERGER, DIV 2323
ATTN JERRY HOOD
ATTN NED KELTNER
ATTN ANTHONY VENERUSO, DIV 4742
ALBUQUERQUE, NM 87185

SCIENCE APPLICATIONS, INC.
ATTN J. ISEMAN
8400 WESTPARK DR
MCLEAN, VA 22102

SCIENCE & TECHNOLOGY ASSOCIATES, INC
ATTN DR. T. DRZEWIECKI
1700 N. MOORE ST., SUITE 1920
ARLINGTON, VA 22209

SIKORSKY AIRCRAFT
ATTN J. R. SOEHNLEIN
NORTH MAIN STREET
STRATFORD, CT 06602

STEIN ENGINEERING SERVICES, INC
5602 E MONTEROSA
PHOENIX, AX 85018

TRANS-TECH, INC
ATTN L. DOMINGUES
12 MEEM AVE
GAITHERSBURG, MD 20760

TRITEC, INC
ATTN L. SIERACKI (2 COPIES)
PO BOX 56
COLUMBIA, MD 21045

UNITED TECHNOLOGIES RESEARCH CENTER
ATTN R. E. OLSON, MGR FLUID
DYNAMICS LABORATORY
400 MAIN STREET
E. HARTFORD, CT 06108

VOUGHT CORP
PO BOX 225907
ATTN KELLEY FLING
DALLAS, TX 75265

US ARMY ELECTRONICS RESEARCH
& DEVELOPMENT COMMAND
ATTN TECHNICAL DIRECTOR, DRDEL-CT
ATTN PUBLIC AFFAIRS OFFICE, DRDEL-IN

HARRY DIAMOND LABORATORIES
ATTN CO/TD/TSO/DIVISION DIRECTORS
ATTN RECORD COPY, 81200
ATTN HDL LIBRARY , 81100 (3 COPIES)
ATTN HDL LIBRARY (WOODBRIDGE), 81100
ATTN TECHNICAL REPORTS BRANCH, 81300
ATTN LEGAL OFFICE, 97000
ATTN CHAIRMAN, EDITORIAL COMMITTEE
ATTN CORRIGAN, J., 20240
ATTN CHIEF, 13000
ATTN CHIEF, 13400 (20 COPIES)